WHEAT RIBOSOMAL PROTEIN S4 IS A CYSTEINE PROTEASE THAT CAN ABROGATE PROTEIN SYNTHESIS

A Thesis
Submitted for the Degree of

DOCTOR OF PHILOSOPHY

by

M. YADAIAH

SCHOOL OF CHEMISTRY
UNIVERSITY OF HYDERABAD
HYDERABAD 500 046
INDIA

December 2007

మాతృదేవోభవ
పితృదేవోభవ
ఆచార్యదేవోభవ

CONTENTS

School of Chemistry
University of Hyderabad
Central University P. O.,
Hyderabad 500 046
India

STATEMENT

I hereby declare that the work embodied in this dissertation is the result of the investigation carried out by me in the School of Chemistry, University of Hyderabad, Hyderabad, under the supervision of **Prof. Abani K. Bhuyan.**

YADAIAH M.

December 2007

STATEMENT VERIFIED

(PROF. ABANI K. BHUYAN)
PROJECT SUPERVISOR

School of Chemistry
University of Hyderabad
Central University P. O.,
Hyderabad 500 046
India

CERTIFICATE

Certified that the work embodied in this thesis entitled **'WHEAT RIBOSOMAL PROTEIN S4 IS A CYSTEINE PROTEASE THAT CAN ABROGATE PROTEIN SYNTHESIS'** has been carried out by Mr. M.Yadaiah, under my supervision and the same has not been submitted elsewhere for a Degree.

Prof. Abani K. Bhuyan
(THESIS SUPERVISOR)

Dean
School of Chemistry

ACKNOWLEDGEMENTS

– కృషితో నాస్తి దుర్భిక్షం

I express my deep sense of gratitude and profound thanks to **Prof. Abani K. Bhuyan** who fearlessly accepted me as a PhD student for his project and was the main creator of the great ideas, techniques, and whole background of this thesis. We experienced together all the ups and downs of routine work, the shared happiness of success, and the depression of failure when (sometimes) everything went wrong. He managed to teach me how to work independently (which is very important), but at any time, his useful advice was available to me. It is a real pleasure to work and communicate with such a polite, honest and open-minded person. I would also like to acknowledge his language abilities which were extremely useful, particularly in the beginning of my work.

I wish to express my sincere gratitude to Prof. E. D. Jemmis (Former Dean) and Prof. M. Periasamy (Dean, School of Chemistry) for providing all necessary facilities to work in this School, and to other faculty members for direct and indirect help.

It has been a pleasure to work with such a fine group of people over the years: Dr. Rajesh, Prakash, Krishna, Nageswar, Harish, and Umakar. I am extremely thankful to all of them for stimulating discussions, timely help, and morale support. I am very thankful to all members of our school: research scholars, M.Sc. students, and non-teaching staff. I like to thank the University authorities for providing necessary facilities. Research fellowships and financial support from CSIR, DST and DBT Government of India, are gratefully acknowledged.

I thank Prof. K.V.A. Ramaiah for the excellent discussions, opportunity to use the facilities in his lab and learn modern biochemical techniques. I would like to thank the following people from his lab, Dr. Rajashekar, Hussain, Rajesh, Pushpa, Aarti, Anu, Murthy, and Satyam for their help and constant discussions.

I acknowledge the timely help of Mr. C. S. Murthy, Mr. Suresh, and the staff of CIL, UOH. I thank all the non teaching staff of Life Sciences, especially Mr. Jagan, and Mr. Lalanji.

I also thank Dr. Apurva Sarin, NCBS, Bangalore for kindly providing the wild type Bcl-x_L gene and Professor J. C. Martinou, University of Geneva, Switzerland for the kind gift of purified tBid protein.

I thank my friends and classmates: Reddanna, Buchi, KK, Narahari, Anwar, Mallu, Veerendar, Kavitha, JP, Ravi, LK, Chitta, Subbu, MVSRN Murthy, Shivaiah, and Srinadh with whom I enjoyed the M.Sc. days. I also thank my senior Jagan who had helped me by sending the reference journals promptly.

I thank all my teachers who taught and impressed me at all stages of my carrier especially Mr. Narsi Reddy who turned my attention toward science. I also thank my childhood friends: Jangaiah , Eadaiah, Shankar, Gouni, Singotam, Bakka Seenu, Chandra shekar, Sriram, Venkat, and Prasanna.

Thanks to Dr. Satish, Dr. Narsi Reddy, Shyamraj, Dr. Suresh, Swati, Hema, Jimmi, Roy who made my stay in the campus a memorable one.

Last but not the least I would like to thank my wife Latha for her patience and constant support during the research work. I cannot find words to say how much I appreciate the love and affection showered on me by my parents, grand parents, sister Aliveni, brother Srinivas, his wife Sureka, and their daughter Sravalika, and my nieces Akanksha, and Pranathi, and nephew Pranay. Thank you, mom and dad, for your unending support and always believing in me, I could never have come this far without you. It is impossible to remember all who, in one way or another, helped me to reach this stage in my life. I apologize to anyone whose contribution toward my achievement has been inadvertently overlooked. Lastly, I thank them all.

There is no word to thank people who dedicated their lives to research. I salute them, without their intense work and inherent wisdom I could not indeed make this thesis.

1. ABSTRACT

To uncover a proteolysis phenomenon detected in translationally active wheat germ lysate, a series of studies were conducted using classical biochemical methods in conjunction with mass spectrometry and immunochemistry. The investigations reveal that the protein S4 from cytosolic ribosome of wheat is an endoprotease exhibiting all characteristics of a cysteine protease. Addition of S4 to a cell-free translation system abrogates BMV RNA-coded protein synthesis by cleaving several eukaryotic translation initiation factors and kinases. Incorporation of cysteine protease inhibitors, including Zn^{2+} and leupeptin, in the translation system restores protein synthesis to the normal level. Indeed, the recombinant wheat S4, overexpressed in *E. coli*, shows the same hydrolysis reaction, which initially identified in the wheat germ lysate had led to this search. Interestingly, the recombinant S4 copurifies with a sizable piece of RNA, and the two appears to exist tightly bound to each other. Further, S4 shows proteolytic activity both in the presence and absence of RNA. These unexpected characters of S4 not only raise questions about the significance of its proteolytic role, but also points to the complexity of ribosomal function at molecular level.

2. INTRODUCTION

A protein can often have more than one related or unrelated function. An instructive case is the role of cytochrome *c*, which normally functions to transfer electrons in the mitochondrial respiratory chain[1], but at times turns to activate the initiator caspase-9 in the cytosol of cells already programmed to die[2]. Other widely studied examples of multifunctional proteins include the p53 gene product[3,4,5], human CD38[6], RTX toxin of *Vibrio cholerae*[7], the heat shock protein Hsp70[8,9], and translation initiation factor eIF-2[10]. From a rapidly growing list of such proteins, it appears that the cell harbors many more of them, and alternative functions of some remain unknown. While studying BMV RNA-coded protein synthesis in wheat cell-free translation system, a cysteine protease activity was encountered serendipitously. By using this protease activity as both the marker guide and the assay method in follow up studies, the origin of the endoproteolytic activity was unexpectedly traced to the S4 protein of the 40S ribosomal subunit.

This surprising observation is emerging at a time when enormous efforts are underway to unravel the molecular details of the ribosomal protein synthesis process. "Synthesis of ribosomal proteins" or "synthesis of proteins by (poly) ribosomes". Work on the complexity and regulation of ribosomal mechanism began several decades ago[11,12], and they have provided the foundation for recent atomic-level structural data for the prokaryotic subunits and individual protein and RNA components[13-19]. Ribosomes of plants and animals are more highly regulated than those of prokaryotes, although similarities between many components exist[16], and a large majority of available information has come from elegant experiments using the latter. Thus, functions for certain ribosomal proteins have been described[20,21], and attributes for others are being steadily found[22,23].

The protein S4 has attracted attention of many for a long time for a variety of its functional qualities. It binds to rRNA[20,24,25] and plays a pivotal role in the core assembly of the smaller ribosomal subunit[26]. Classic work of Nomura and associates[27-29] have shown that S4 in *E. coli* feedback-inhibits self-synthesis, and in the process blocks synthesis of those ribosomal proteins that are coded by the same polycistronic mRNA. Furthermore, S4 is an antitermination transcription factor with properties similar to NusA[30]. In humans, S4 deficiency has been associated with Turner syndrome[31,32]. In spite of such progress, not much is known about the role of plant S4 from cytosolic ribosome, but it is expected to share at least some of the basic functional attributes listed above. In this perspective, wheat S4 is now found to be an endoprotease that can inhibit protein synthesis by non-specific proteolysis of initiation factors and kinases, and perhaps other proteins in the milieu.

3. MATERIALS AND METHODS

Wheat germ was obtained from Sigma, Ac-DEVD-AFC from Calbiochem, DEAE cellulose from Whatman, gel filtration media and materials from General Electric, in-vitro wheat germ lysate translation kit from Promega, and S^{35} Methionine from Bhabha Atomic Research Center, India. The recombinant proteins used were overexpressed and purified in the laboratory. Antibodies were from Santacruz. Other reagents and chemicals were obtained from Sigma and Merck.

3.1 Preparation of Wheat Germ Lysate and Identification of S4

Wheat germ lysate was prepared as described earlier[33]. The lysate in buffer A (40 mM HEPES-KOH, 100 mM potassium acetate, 5 mM magnesium acetate, 1 mM DTT, 100 μM PMSF, pH 7.6) was passed through a Sephadex G-25 column, the

eluted fractions were brought to 40% saturation of $(NH_4)_2SO_4$, and the salted out pellet was dissolved in buffer B (20 mM HEPES-KOH, 1 mM DTT, 1 mM EDTA, 20 mM NaCl, 0.05% CHAPS, 5% sucrose) at pH 7.6. The solution was chromatographed on a Sephadex G-75 or G-150 column using buffer B, and the higher molecular weight pool of proteins was collected. The protein mixture was then loaded onto a DEAE cellulose column equilibrated in buffer B at pH 7.6, washed, and eluted by a continuous gradient obtained by mixing 125 mL each of 0.020 and 0.7 M NaCl in buffer B. Fractions that hydrolyzed Ac-DEVD-AFC were combined, concentrated using centricon tubes, flash- frozen, and stored at -70°C until further use. The presence of S4 was identified by combining SDS gel electrophoresis and Ac-DEVD-AFC hydrolysis carried out with different fractions. The active fraction (labeled E in Fig. 1C, also referred to as S4 preparation henceforth) was used for all biochemical experiments. All chromatography procedures were performed in the cold (4-8°C).

3.2 Assay for Protease Activity

Typically, ~10 μg of Ac-DEVD-AFC substrate was added to 500 μl of fraction E described above (~100 μg protein) in Buffer B, and following a very brief incubation period either static emission spectrum or time-base fluorescence emission or both was measured using a FluoroMax 3 instrument (Jobin-Yvon) at 490 nm (slit width: 8 nm) with excitation at 400 nm (slit width: 1.5 nm). The time dependence of fluorescence emission was recorded up to 40 min or 1 hr. In most cases, the protein substrate mixture was incubated at ~37°C.

3.3 Determination of the Effects of pH, Temperature, NaCl, $ZnCl_2$, and $MgCl_2$ on the S4 Activity

These experiments required finding the rate of hydrolysis of Ac-DEVD-AFC by S4 as a function of the variables. For measurement of pH effect, a buffer consisting of 20 mM HEPES, 20 mM PIPES, 1 mM DTT, 1mM EDTA, 20 mM NaCl, 0.05% CHAPS and 5% sucrose was used. The pH of the buffer was adjusted to values in the 5.9-8.0 range. This buffer (at pH 7) was also used for measurement of temperature and NaCl dependences. The buffer for experiments involving $ZnCl_2$ and $MgCl_2$ consisted of 20 mM HEPES, 0.05% CHAPS, 5% sucrose,20 mM NaCl, and 15 mM β-mercaptoethanol, pH 6.8. Hydrolysis of Ac-DEVD-AFC was monitored using the procedure for activity assay described above. However, incubation of the enzyme-substrate mixture was not allowed. Time-base fluorescence emission was measured immediately after mixing the substrate with the protein preparation at 37°C. Each trace was recorded up to ~30 min, the slope of the initial linear portion of which yielded the rate of Ac-DEVD-AFC hydrolysis.

3.4 Inhibition of S4 Activity by Various Enzyme Inhibitors

The S4 preparation along with Ac-DEVD-AFC was mixed separately with various enzyme inhibitors so as to obtain uniform concentrations of S4 and substrate in all mixtures. Final concentrations of the inhibitors were 3 μM Ac-DEVD-CHO, 3 μM PMSF, 100 μM leupeptin, 0.5 μM aprotinin, 1 μM pepstatin, and 1 mM iodoacetic acid. Samples were incubated at 37°C for 1 hr, and steady-state fluorescence spectra at 400-nm excitation were taken. The peak intensity at 495 nm was noted for various enzyme inhibitors. To determine the inhibition by leupeptin and PMSF, the rate of hydrolysis of Ac-DEVD-AFC by the S4 preparation was titrated

out by each inhibitor. As detailed above, the hydrolysis rates were determined from the slope of fluorescence with time for the initial linear portion of the kinetic trace.

3.5 Western blot Analysis

10 μg of the S4 protein preparation was incubated separately with and without 4 μg Ac-DEVD-CHO for 30 minutes. 5 μg recombinant PKR or PERK protein was added to each tube, and incubated overnight at 37°C. For controls, S4, PKR, and PERK taken individually were also incubated. The samples were subjected to 12% SDS-PAGE, transferred to PVDF membrane, and probed with anti PKR and anti PERK followed by respective alkaline phosphatase-conjugated 2° antibodies. The bands were detected with NBT/BCIP.

3.6 Tryptic Digestion of S4 and Mass Spectrometry

Cut silver-stained gel bands were destained (×2) in 200 μL of the destaining solution (100 μL of 100 mM NH_4HCO_3, pH 8, mixed with 100 μL acetonitrile) for 45 min at 37°C. The gel slices were dried, reduced with 100 μL of 10 mM DTT, 25 mM NH_4HCO_3, pH 8, for 15 min at 37°C, alkylated by adding 100 μL of 20 mM iodoacetamide in 25 mM NH_4HCO_3, pH 8, and incubated at 37°C in dark. Gel bands were then washed (×3) with 200 μL of 2 mM NH_4HCO_3 for 15 min, dried, and rehydrated in 20 μL of 0.02 μg/μL trypsin in acetonitrile, NH_4HCO_3, pH 8, for 1 hr at room temperature. After removing the unabsorbed trysin-containing liquid, gel slices were covered with 50 μL of 10% acetonitrile, 40 mM NH_4HCO_3, pH 8, incubated for ~16 hours at 37°C, and the supernatant was extracted and discarded. Gel pieces were then incubated with 50 μL of 0.1% TFA for 1 hr at 37°C, and the supernatant was extracted. The two extracts were combined, and dried repeatedly (×3) after

suspending in 200 μL H_2O. The final resuspension volume was 10 μL.

For MALDI-TOF/TOF measurement, 2 μL of the peptide mixture was mixed with 2 μL of 2% TFA and 2 μL of the matrix solution (2, 5 di-hydroxy acetophenone with 10 mM di-ammonium acetate). 1 μL of the mixture was pipetted onto a MALDI sample plate. The mass spectra from the digests were recorded in the positive, reflectron mode using the smart beam TM laser at 200 Hz repetition rate. About 1000 single spectra were added to a sum spectrum. The peptide masses were then fed into MASCOT database, and searched against the wheat database for identification. Homology sequence analysis was performed by a BLAST search, and the sequence alignment was done by ClustalW.

3.7 Preparation of Ribosomes and Fractionation

The wheat germ lysate obtained from the Sephadex G-25 column in buffer (40 mM HEPES-KOH, 25 mM potassium acetate, 2 mM magnesium acetate, 1 mM DTT, 100 μM PMSF, pH 7.6) was spun at 15000 rpm for 15 min, and the top three-fourth of the fraction was passed through a Sephadex G-25 column, the eluted fractions were used to isolate ribosome. 3 mL of the lysate layered over 0.8 mL of the cushion buffer (10 mM Tris-HCl pH 7.7, 25 mM KCl, 5 mM NaCl, 2 mM magnesium acetate, 50% glycerol) contained in a swinging bucket Beckman SW-60 rotor tube was spun at 40,000 rpm for 5 hrs in a Beckman centrifuge. The ribosome pellet was resuspended in a buffer containing 20 mM HEPES-KOH, pH 6.8, 1 mM EDTA, 1 mM DTT, frozen in small volumes in liquid nitrogen, and stored at -70°C.

Ribosomes were fractionated using 10-40% linear sucrose gradient. In the control run, intact (80S) ribosomes were fractionated in a buffer containing 50 mM Tris-HCl pH 7.7, 50 mM KCl, 3 mM $Mg(CH_3COO)_2$ and 1 mM DTT. For

fractionation into 40S and 60S sub-units, the same buffer was used but with 300 mM KCl and 10 mM $Mg(CH_3COO)_2$. Approximately 100 μg of protein was added to the gradient and spun at 40,000 rpm for 2 hrs. The fractionation profile was generated using density gradient fractionator (ISCO) with 50% sucrose.

3.8 Protein Synthesis

A typical 50 μL in-vitro translation reaction mix contained 25 μL wheat germ lysate (Promega) 130 mM potassium acetate, 25 μM amino acid mix minus methionine, 5 μCi S^{35} methionine, and 1 μg Brome Mosaic Virus RNA. The reaction was carried out at 25°C for 1 hr, and terminated by the addition of SDS-PAGE sample buffer. Immediately the samples were boiled for 3-5 mins, and separated electrophoretically on 10% SDS-PAGE, the gel was later coomassie-stained and dried. The dried gel was exposed to phosphor imager screen and scanned using a Typhoon phosphorimager (Amersham Pharmacia) to detect the S^{35} methionine incorporated proteins. Prestained protein molecular weight markers obtained from Fischer was used as molecular weight standard. To assess the effect of the S4 proteinase on in vitro translation, protein synthesis was carried out in the presence and absence of S4 (2 μg) and its physiologic inhibitors like leupeptin (10 μM), Ac-DEVD-CHO (1 μM), Zn^{2+} (2.5 mM), and also in the presence of analogues like recombinant human caspase-3 (100 ng). In protein synthesis studies involving the inhibitors of the S4 protein, the protein-inhibitor mixture was pre-incubated prior to addition to the in-vitro translation mix.

3.9 Cleavage of Eukaryotic Translation Initiation Factors (eIF) by S4

4 μg protein from the S4 preparation was incubated separately with purified

recombinant human eIF2α, eIF2β (10 μg each), and rat liver tissue extract for 1hr at 37ºC. For positive control, another set of the reaction mixtures (Volume ~ 25 μL) was prepared for which the S4 preparation used was preincubated for 15 min at 37ºC with 10 μM leupeptin or 1 μg Ac-DEVD-CHO. The cleavage was stopped by the addition of SDS-PAGE sample buffer, the proteins were separated on 12% SDS-PAGE, transferred to PVDF membrane, probed with polyclonal anti-eIF2α (Santacruz), monoclonal anti-eIF2β (Santacruz), polyclonal anti-eIF–4E (Cell signaling) and polyclonal anti-eIF5 (Santacruz) antibodies respectively. For negative controls for this experiment, the S4 preparation, eIF2α, eIF2β, and the tissue extract individually and in amounts equal to those used in cleavage reaction above, were subjected to electrophoresis. After incubating with respective alkaline phosphotase- conjugated secondary antibody, the bands were detected with substrates NBT and BCIP.

3.10 cDNA Synthesis, Cloning, and Generation of Expression Construct for Wheat S4 Protein

Total RNA from 10-days old wheat seedlings was isolated using TRI Reagent (Sigma), chloroform, and isopropanol. The RNA was washed with 75% ethanol, dissolved in nuclease-free water, and checked for integrity by agarose gel electrophoresis. cDNA synthesis was performed using single-step cDNA synthesis kit (Abgene single step RT-PCR, USA) essentially by manufacturer's instructions. To a mixture of 25 μL 2X Master mix (Fermentas), 1 μL RT Blend enzyme, and 5 μL total RNA, 1 μL each of forward and reverse primers were added. The primers (10 picomolar each) synthesized by Sigma were

*Nde*1

S4-F: 5′ GCCATATGGCGAGGGGTTTGAAGAA 3′

S4-R: 5′ CCCTCGAGTCAGGCCTTGGCAGCTGCCT 3′.

*Xho*1

The total volume of the reaction mixture was made up to 50 μL by adding nuclease free water. The RT-PCR program involved an initial 30-sec denaturation at 95°C, 30-sec annealing at 54°C, and 1-min polymerization at 72°C; to be repeated from step two for 25 cycles. Long polymerization was carried out for 10 minutes, and the final temperature was set at 4 °C. The amplified cDNA separated on 1% agarose gel was eluted by using the gel elution kit from Qiagen. The purified cDNA was inserted into TA (pTZ57R/T) vector using Bateriphage T4 DNA ligase (Fermentas) for 16 hr at 22°C. The cDNA was sequenced, translated into protein sequence using expasy tools, and compared by alignment with the original protein sequence using clustalW.

The TA plasmid was transformed into XL1 Blue *E. coli*, and grown on ampicilin- containing (100 μg ml^{-1}) LB-agar plate by streaking. To confirm the positive colonies, the recombinant vector-containing white colonies were subjected to colony PCR. The recombinant TA vector was subjected to restriction digestion between Nde1 and Xhol (Fermentas). The cleaved cDNA, isolated by agarose gel electrophoresis and elution, was re-inserted into pET28a (+) vector (Novagen) using bacteriophage T4 DNA ligase. The recombinant pET28a (+) vector was transformed into XL1 Blue *E. coli* cells, and grown on kanamycin (Calbiochem)-containing (50 μg ml^{-1}) LB-agar plate. The positive white colonies, confirmed by colony PCR, were inoculated into kanamycin-containing (50 μg ml^{-1}) LB medium at 37ºC. The plasmid was isolated from the overnight mini culture, and transformed into BL21 (DE3) RIL *E. coli*.

3.11 Protein Expression and Purification

A starter culture was grown by inoculating a single colony from the petri plate containing pET28a (+) S4 vector in BL21 (DE3) RIL cells into 50 μg ml^{-1} kanamycin-containing LB media. Growth was allowed overnight at 37ºC with 180 rpm shaking. A secondary culture was made in 50 μg ml^{-1} kanamycin-containing LB media from the starter culture in a 1:25 ratio. Cells were grown at 37 ºC in LB media to a A_{600} of 0.5, and protein expression was induced with 0.5 mM IPTG at 30ºC and 180 rpm shaking speed. After two hours of induction, cells were harvested at 10,000 rpm for 10 min. The cell pellet (~1.89 g wet weight per litre of culture) was washed with PBS, and resuspended in 1:5 W/V buffer A (50 mM Tris, pH 8.0, 0.2 M NaCl, 5 mM β-mercaptoethanol, 5 mM imidazole, and 1% Glycerol), and stirred for 15 min at 4 ºC. Cells were disrupted by pulsed sonication, and the lysate was spun at 15000 rpm for 15 min. The soluble fraction was loaded onto a Ni-NTA-His bind column (Novagen) equilibrated with buffer A. The column was washed with 300 mL of a buffer containing 50 mM Tris, pH 8.0, 0.2 M NaCl, and 50 mM imidazole until the A_{280} reached 0.001. The second wash was done with 50 ml of 50 mM Tris, pH 8.0, and the protein was eluted with 150 mM imidazole in 50 mM Tris, pH 8.0. The protein-containing fractions were pooled and dialyzed against 1000 ml of 50 mM Tris, pH 8.0. The protein concentration was estimated with Bradford method, and the purity was checked by SDS gel electrophoresis.

3.12 Mass Spectrometry of Purified Recombinant S4 Protein

2 μL of the purified protein solution (~0.21 μg) was mixed with 2 μL of 2% TFA and 2 μL of the matrix solution (2,5 dihydroxyacetophenone with 10 mM di-ammonium citrate). Mass measurements were performed on Autoflex III TOF/TOF

spectrometer (Bruker) in the positive linear mode of operation. ~1000 single spectra were added. Spectra were processed using 10 Da Gauss filter smoothing and baseline subtraction.

3.13 Fluorescence and CD Measurements

Fluorescence and CD spectra of recombinant S4 protein were recorded with 3 μM protein in 50 mM Tris, pH 7.0, 25°C. For fluorescence, a photon counting instrument (FluoroMax-3, Jobin-Yvon) was used (excitation: 280 nm, 1.5 nm slit). CD spectra were taken in a JASCO J715 spectropolarimeter with the protein solution contained in 2 mm path length cylindrical cell. Sixteen scans were averaged.

3.14 Assay for the Proteolytic Cleavage of Ac-DEVD-AFC Substrate by Recombinant S4

150 μg purified S4 protein was taken in 500 μL of 50 mM Tris, pH 7.0 and 10 μg of Ac-DEVD-AFC (Calbiochem) substrate was added, and following a very brief incubation period either static emission spectrum or time-base fluorescence emission or both was measured using a FluoroMax 3 instrument (Jobin-Yvon) emission at 490 nm (slit width: 8 nm) with excitation at 400 nm (slit width: 1.5 nm). The time dependence of fluorescence emission was recorded up to 40 min or 1 hr. In most cases, the protein substrate mixture was incubated at ~37°C.

3.15 Electrophoresis and Western blot Analysis for Recombinant S4-induced Cleavage of PKR, PERK, Bcl-X_L and eIF2α

Typically, 2-5 μM S4 protein was incubated with 6-10 μM PKR or PERK with or without inhibitors (1 μM Ac-DEVD-CHO and 10 μM leupeptin) for 4-5 hours

at 37°C. Another set of experiments were conducted by incubating with S4 (5 μg), Bcl-X_L (15 μg), eIF2α (10μg) and with an inhibitor leupeptin (10 μM). Samples were subjected to 10% SDS-PAGE, and coomassie-stained or transferred to PVDF membrane for Western blotting. For the latter, bands were probed with anti-PKR and anti-PERK followed by the respective alkaline phosphotase-conjugated 2° antibodies.

3.16 Homologous Structure Alignment Database (HOMSTRAD)

Sequence structure homology was done using fugue tool. Compared a query sequence or sequence alignment against each structural profile in its profile library derived from HOMSTRAD. Three dimensional structure of S4 protein was built in Insight II.

4. RESULTS

4A. THE INITIAL LANDMARK

The isolation and purification of the proteinase factor from innumerable proteins in the wheat germ lysate is obviously an arduous task. Hence, the eventual goal of cloning and overexpression was set right at the initial stage of the study, and to achieve this, the identification of the protein and the minimal sequence was a prerequisite. In this section, the results of the initial long search relevant for the detection of the enzyme are presented.

4A.1 Partial Purification and Identification of the Wheat Enzyme

The detection of caspase-like activity in translationally active wheat germ lysate was fortuitous. Figure 1A shows fluorescence-detected hydrolysis of the

caspase-3 substrate Ac-DEVD-AFC by wheat germ lysate, and the inhibition of the activity in the presence of the synthetic inhibitor Ac-DEVD-CHO. It was this observation that led to search for the protease using the same Ac-DEVD-AFC hydrolysis as the marker assay.

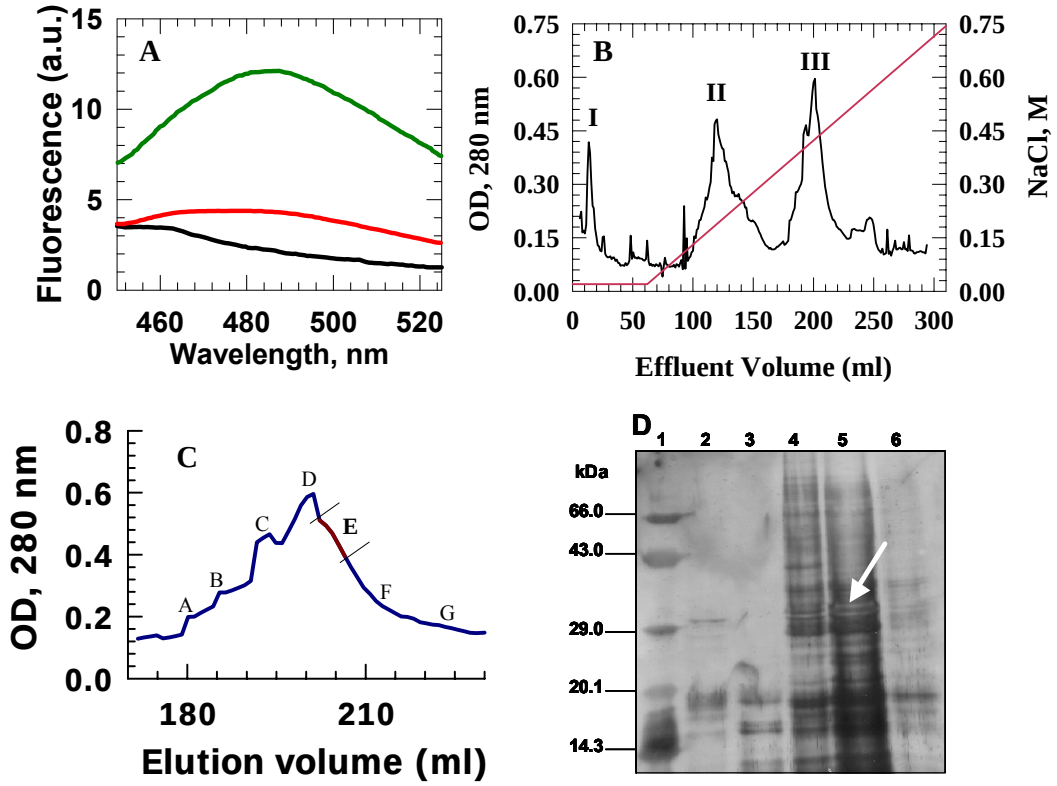

Figure 1. Identification and partial purification of the wheat enzyme. (A). Normal translationally active wheat germ extract in the absence (-), and in the presence of Ac-DEVD-AFC (-). The fluorescence emission due to the cleavage of the AFC group is quenched when the inhibitor Ac-DEVD-CHO is added (-), indicating the inhibition of enzyme activity. (B). DEAE cellulose

chromatography of the wheat germ lysate initially gel-filtered on a Sephadex G-150 column. The NaCl gradient for elution is shown, and the three major peaks are labeled. (C). Resolution of peak III of the ion-exchange chromatogram by partitioning the peak fractions into groups A to G. Each group was checked for fluorescence-monitored Ac-DEVD-AFC hydrolysis; only group E fractions exhibited high-level of hydrolytic activity. (D). Silver-stained SDS-PAGE analysis of various group fractions. The marker proteins are in lane 1, and lanes 2 to 6 correspond to fractions from group B, C, D, E, and F, respectively. A significant protein band in lane 5 (group E fractions) pointed out by an arrow is not observed in other lanes. The protein corresponds to a molecular mass of ~30 kDa. Because only group E fractions show Ac-DEVD-AFC hydrolysis, this protein must be the putative protease.

For separation of the putative protease, several column chromatography procedures under a variety of conditions were tried out, and the anion-exchange chromatography was found the best. Wheat germ lysate, initially gel-filtered on a Sephadex G-150 column, was loaded on a DEAE cellulose column equilibrated in buffer B (20 mM HEPES, 2 mM DTT, 1 mM EDTA, 20 mM NaCl, 0.05% CHAPS, 5% sucrose) at pH 7.6, and eluted by using a linear salt gradient generated by mixing 125 mL each of 0.02 M and 0.75 M NaCl (Figure 1B). Elution peaks were expectedly not homogeneous. Fractions from peaks I and II did not show Ac-DEVD-AFC hydrolysis activity. We then concentrated on peak III, and divided the fractions into seven groups (A to G) as shown in Figure 1C. High-level Ac-DEVD-AFC hydrolysis was found for group E fractions, with traces for group F. Proteins from different groups were separated on 12% SDS-PAGE and silver-stained. Figure 1D shows that a significant protein band corresponding to a molecular mass of ~30 kDa due to group E fractions (arrow-pointed in lane 5) stands out, and is not detected in other lanes to any considerable extent. This band must be due to the putative protease, since only

group E proteins showed Ac-DEVD-AFC hydrolysis.

4A.2 Biochemical Characteristics of the Enzyme are Similar to those of Cysteine Proteases

At this point, we set to determine the influence of common environmental parameters on the Ac-DEVD-AFC hydrolysis rate, so as to optimize solution conditions under which the assay would be more sensitive, and to learn something about the active site residue(s) of the enzyme. The hydrolysis rate, ΔF (s^{-1}), was extracted from the slope of the initial linear increase of fluorescence due to the release of AFC as a function time. The same time regime was used consistently for all traces.

The substrate hydrolysis rate, measured as a function of pH for fixed concentrations of enzyme and Ac-DEVD-AFC (Figure 2A) shows that the enzyme is maximally active at pH 6.6, indicating its functional activity within the pH range normally found in active cells. The bell-shaped profile suggests a single active form of the enzyme. The fit of the data to the equation.

$$v = \frac{c \times 10^{(pH - pK_{a1})}}{1 + 10^{(2\,pH - pK_{a1} - pK_{a2})} + 10^{(pH - pK_{a1})}} \qquad (1)$$

Where c is a constant, yields two ionizing groups with pK_{a1}=6.1, and pK_{a2}=6.6. The observed pH dependence is quite similar to pH profiles described earlier for certain cysteine proteases[34,35], especially with regard to the pK_{a1} values reported for caspases-3, -7, and -8[35]. Since Ac-DEVD-AFC also serves as a substrate for caspase-3, there appeared a basis, although insufficient by itself, to assume that the wheat germ enzyme being investigated here is a cysteine protease having caspase-like activity.

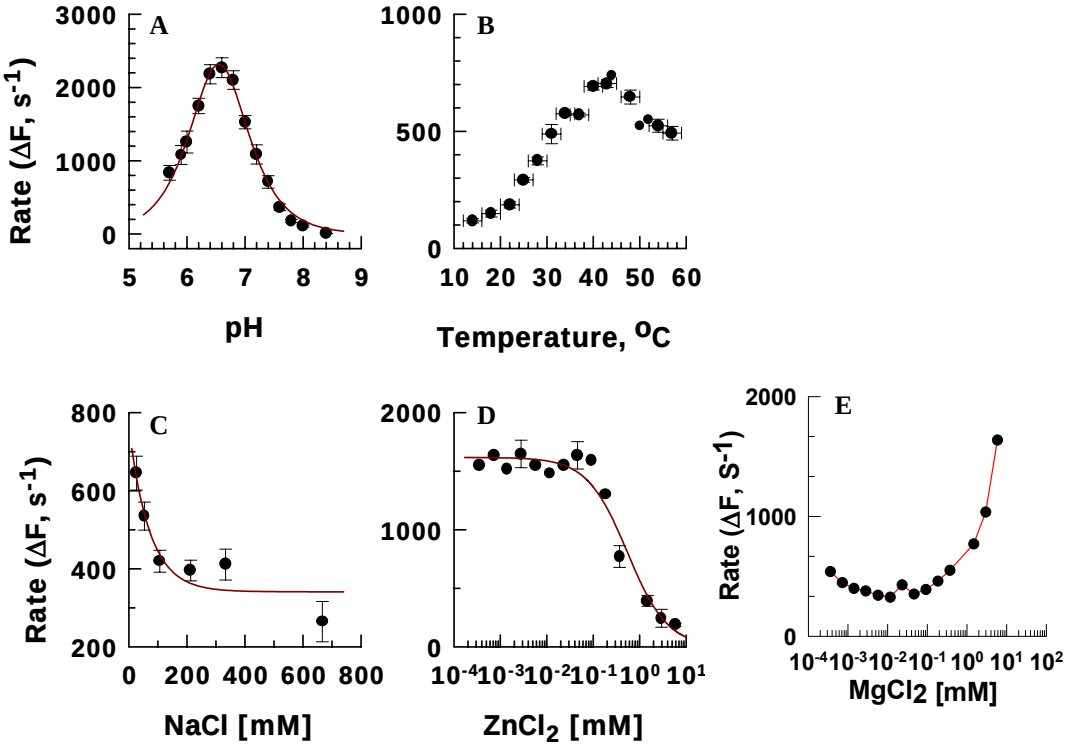

Figure 2. Some biochemical characteristics of the wheat protease. Rates of hydrolysis of Ac-DEVD-AFC as a function of variables and buffer conditions (described in the text) are plotted. (A). the optimum pH value for hydrolytic activity is ~6.8. (B). Temperature effect. The enzyme is maximally active at ~40°C. (C). the enzyme activity is highly sensitive to NaCl concentration. (D). Inhibition by $ZnCl_2$. The apparent binding constant, K_{Zn}^{app} =0.31 mM. (E). Effect of Mg^{2+} ion. The activity passes through a minimum centered at ~0.1 mM $MgCl_2$.

The temperature optimum for the hydrolytic activity is ~40°C (Figure 2B), suggesting respectable thermal stability of the enzyme. The activity is, however,

highly sensitive to the ionic strength of the medium. The rate of substrate hydrolysis declines drastically as the NaCl concentration is increased to ~100 mM, and remains nearly the same thereafter (Figure 2C). The extreme salt response distinguishes this enzyme from other cysteine proteases, especially from the family of animal caspases[35].

The activities of cysteine and serine proteases are generally influenced by transition metal ions[36,37]. With hints obtained so far that the wheat enzyme under observation is a cysteine protease, the influence of Zn^{2+} ions was examined by titrating the enzyme activity with increments of $ZnCl_2$ (Figure 2D). The buffer used for this set of experiment excluded EDTA, and DTT was substituted by 15 mM β-mercaptoethanol in order to prevent zinc chelating by DTT. However, since Zn^{2+} can also react with the SH group of mercaptoethanol, the $ZnCl_2$ titration data can provide only an apparent binding constant for Zn^{2+}. The zinc dependence of proteolytic activity was analyzed by assuming simple competitive inhibition expressed by

$$v = \frac{V_{max}}{1 + \left(\frac{K_s}{[S]}\right)\left(1 + \frac{[Zn^{2+}]}{K_{Zn}^{app}}\right)} \qquad (2)$$

Where, V_{max} is the maximum initial velocity (proportional to the total enzyme concentration), K_s is the steady-state constant, [S] is substrate concentration, and K_{Zn}^{app} is the apparent binding constant. The fit through the data yields K_{Zn}^{app} =0.31 mM. It is also apparent that ~10 mM $ZnCl_2$ is required for complete inhibition of the enzyme. The observed zinc sensitivity provides another hint that the wheat enzyme could be a cysteine protease. Comparison of these results with those published for caspases[35] indicates that the affinity of the wheat enzyme for Zn^{2+} is at least 30-fold

lower, suggesting different structures and conformations.

Because the wheat enzyme was extracted from translationally active germ lysate, and protein synthesis is sensitive to magnesium, checking the effect of Mg^{2+} ion on the hydrolytic activity was contemplated. The data in Figure 2E shows that initial increments of $MgCl_2$ somewhat diminishes the Ac-DEVD-AFC hydrolysis activity, but large increments (>0.1 mM $MgCl_2$) are activating. Concentrations of $MgCl_2$ higher than ~6 mM caused turbidity and precipitation of the enzyme. The results indicate that the physiological concentration of Mg^{2+} (1-2 mM) required for maintaining the integrity of ribosomes also supports the activity of the enzyme.

4A.3 Effects of Protease Inhibitors on the Hydrolytic Activity of the Wheat Enzyme: Implication for a Cysteine Protease

To gather further information about the type of protease based on the active site residue, the effects of several inhibitors on the Ac-DEVD-AFC hydrolytic activity of the partially purified wheat protease was examined (Figure 3B). While Ac-DEVD-CHO inhibits the protease significantly as observed routinely in assays, iodoacetic acid (IAA) almost completely diminished the activity (compare bars 1 and 8 in Figure 3B). The same concentration of IAA also knocks out the activity of caspase-3 completely (Figure 3C), suggesting that the wheat protein is a cysteine protease. Consistent with this, leupeptin, specific for cysteine proteases, influences the activity to some extent (bar 5), and the sign of inhibition is also apparent in the presence of PMSF, an inhibitor of both cysteine and serine proteases (bar 4). Concentration dependent profiles show that the leupeptin effect reaches the saturation level (30% inhibition) at ~25 μM (Figure 3D), while PMSF effect is marginal (~10% inhibition) even at 1 mM concentration (Figure 3E). It is concluded that the wheat

enzyme is a cysteine protease.

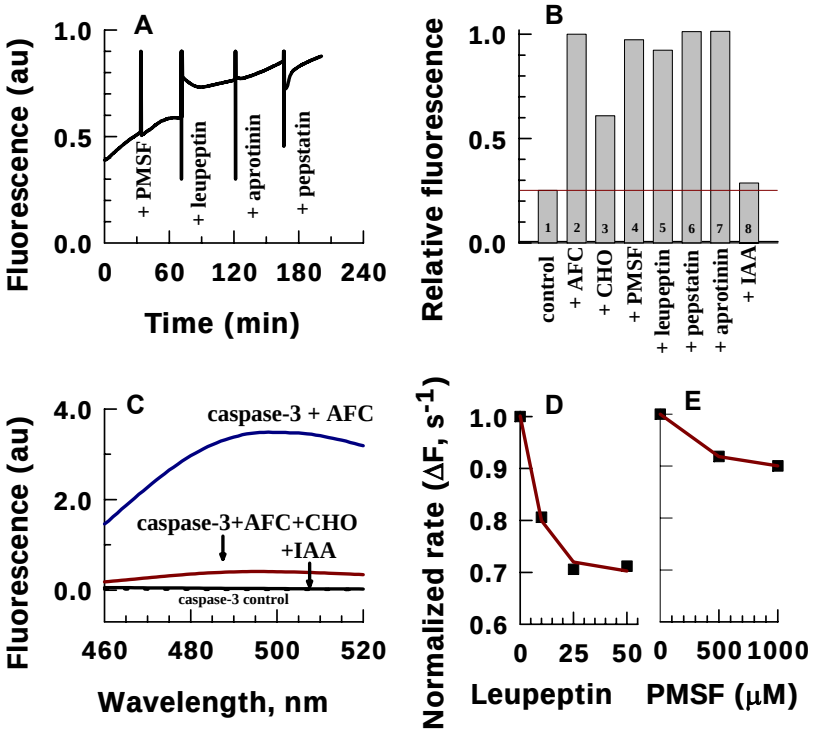

Figure 3. The wheat enzyme is a cysteine protease. The assay was conducted as in legend to Figure 1. (A). Effect of various enzyme inhibitors on Ac-DEVD-AFC hydrolysis was measured in time base fluorescence spectra. (B). Effect of various enzyme inhibitors on Ac-DEVD-AFC hydrolysis indicates that the enzyme could be a cysteine protease. Iodoacetic acid (IAA) completely inhibits the activity. (C). Matching concentration of IAA completely abolishes the activity of purified caspase-3, a cysteine protease whose Ac-DEVD-AFC hydrolysis activity is competitively inhibited by the synthetic inhibitor Ac-DEVD-CHO, suggesting that the wheat protein is a cysteine protease. (D). the wheat protease

activity in the presence leupeptin, a cysteine protease-specific inhibitor. (E). PMSF, less specific for cysteine proteases, inhibits the activity only marginally, and that too requires ~1 mM of inhibitor concentration.

4A.4 Proteolytic Activity of the Cysteine Protease

To demonstrate its proteolytic activity toward real proteins, cleavages of recombinant human PKR (double-stranded RNA-activated protein kinase) and PERK (pancreatic endoplasmic-resident eIF2α kinase) were checked. These two proteins were chosen simply because of their ready availability in our laboratories. The partially purified wheat protease was incubated separately with the test proteins in the presence and absence of the synthetic inhibitor Ac-DEVD-CHO, and the reaction products were immunoblotted using human anti-PKR or anti-PERK (Figure 4). The wheat protease cleaved both proteins (lane 2 in Figure 4A, B), but proteolysis was blocked by the CHO inhibitor (lane 1 in each case).

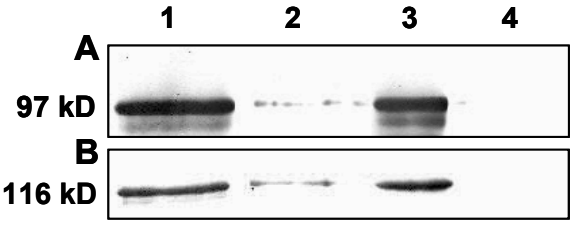

Figure 4. Endoproteolysis by the wheat cysteine protease shown by Western analysis of cleavage products of substrate proteins. The protease was incubated with the test protein in the presence and absence of the synthetic inhibitor Ac-DEVD-CHO, and the reaction product was immunoblotted using antibody for the test protein. The figure is Western blot. (A) and (B) Cleavage of human recombinant PKR and PERK, respectively. Both proteins are cleaved by the wheat cysteine protease (lane 2), but the cleavage is blocked by the inhibitor Ac-DEVD-CHO (lane 1). In controls, PKR and PERK (lane 3) were individually incubated in buffer. The wheat enzyme alone was also run in each case (lane 4).

4A.5 Identification of the Wheat Cysteine Protease as the Ribosomal Protein S4

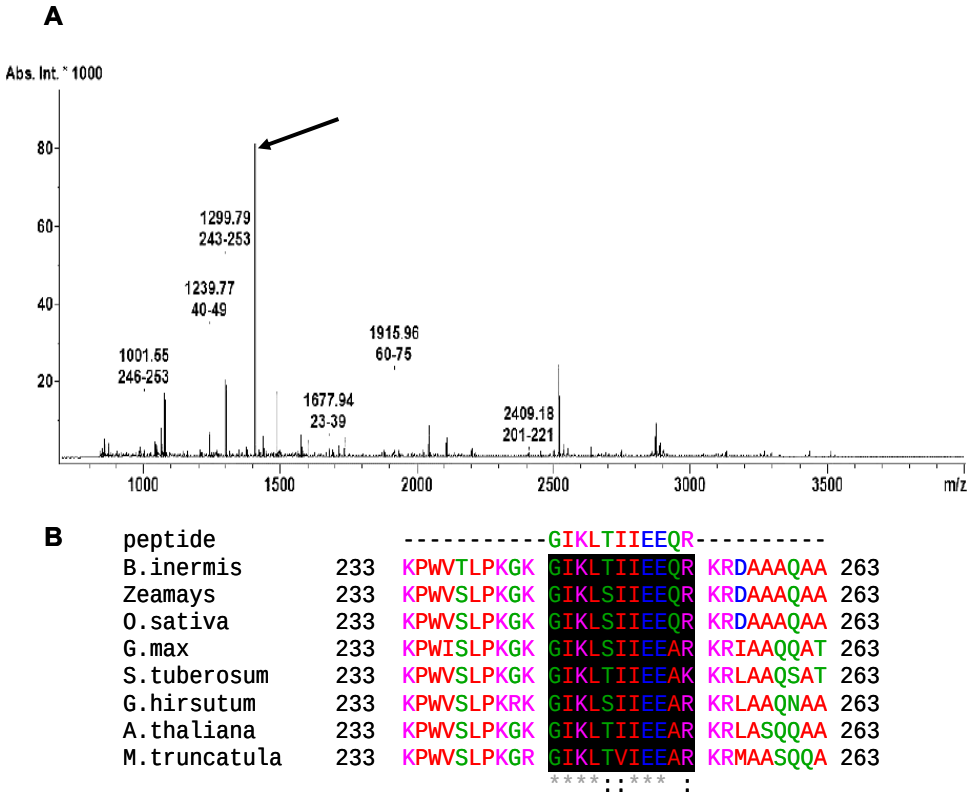

Figure 5. Mass spectrometry and sequence similarity analysis identify the wheat cysteine protease as ribosomal protein S4. (A). MALDI TOF/TOF profile of a tryptic digest of the wheat enzyme was recorded by a Bruker Autoflex III spectrometer. One of the peptide fingerprints used for further analysis is shown by an arrow. (B). Alignment of an 11-amino acid length fragment of the wheat ribosomal S4 endopeptidase with a highly conserved region of several plant ribosomal S4 proteins. Sequence similarity was determined with the BLAST program (NCBI). Amino acids identical to the

wheat sequence are boxed in black. Accession numbers are: *Bromus inermis* BAD22763, *Zea mays* AAS48726, *Oryza sativa* BAD52963, *Glycine max* AAM93434, *Solanum tuberosum* ABB72798, *Gossypium hirsutum* CAA55882, *Arabidopsis thaliana* BAB11167, and *Medicago truncatula* ABE91098. The numbers in the sequences refer to amino acid positions in the full-length sequences.

The protein band corresponding to the active enzyme, shown by the arrowhead in Figure 1D, was carefully excised from the SDS gel, and processed for mass spectrometric analysis. To generate peptide map, MALDI TOF/TOF spectra were taken on a tryptic digest of the protease (Figure 5A). Analyses using the most intense peak with a mass of 1299.79 (indicated by arrowhead) identified homology to the putative 40S ribosomal protein S4. Figure 5B shows the sequences producing significant alignment with an Expect (E) Value of 0.27 in each case. Localization of the protease in the ribosome is gratifying, since our initial observations were made invariably on translationally active wheat germ lysate.

4A.6 Ac-DEVD-AFC Hydrolytic Activity Detected in the 40S Fraction of Wheat Germ Ribosome

If the cysteine protease is indeed the putative S4, then the hydrolytic activity should be detected in the 40S ribosomal fraction. Ribosomes isolated from wheat germ were fractionated into 40S and 60S subunits in the presence of 300 mM KCl and 10 mM $Mg(CH_3COO)_2$ using a 10-40% linear sucrose gradient (Figure 6B). The control profile (Figure 6A) was generated by reducing the KCl and $Mg(CH_3COO)_2$ concentrations to 50 and 3 mM, respectively. The 40S and 60S fractions were tested for their hydrolytic activities. The time-base fluorescence at the emission maximum of hydrolyzed Ac-DEVD-AFC (Figure 6C and the *inset*) clearly shows the activity of the 40S and inactivity of the 60S fractions, reinforcing the homology analysis result

that the protease under scrutiny is the S4 protein.

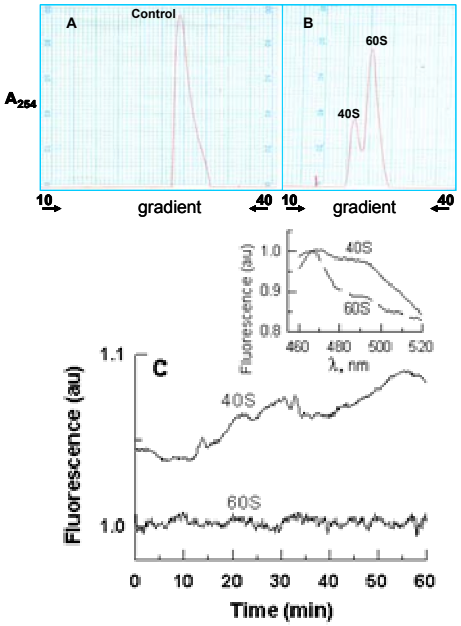

Figure 6. Fractionation of ribosome into 40S and 60S subunits in a 10-40% linear sucrose gradient, and detection of hydrolysis activity in the 40S subunit. (A). The control was run in the presence of 50 mM KCl and 3 mM $Mg(CH_3COO)_2$. As the profile shows, the subunits remain associated under these conditions. (B). The dissociation and fractionation of subunits are achieved in 300 mM KCl and 10 mM $Mg(CH_3COO)_2$. (C). Ac-DEVD-AFC is hydrolyzed by the 40S fraction only. The steady-state fluorescence spectra displayed *inset* show the same result that only the 40S fraction is active.

4A.7 S4 Acts to inhibit in vitro Protein Synthesis

A question arises- what role S4 plays in the ribosomal function? One of the basic approaches is to check the effect of extrinsically added S4 on ribosomal protein synthesis. So, in vitro translation of BMV-RNA (Brome Mosaic Virus RNA) in wheat germ lysate was performed with necessary controls. In Figure 7a,b, lane 1 shows the level of protein synthesis in actively translating control lysate. Interestingly, translation is very significantly diminished in the presence of S4 (lanes

4 and 5 in Figure 7a, and lane 2 in Figure 7b). This action of S4 is abolished, and

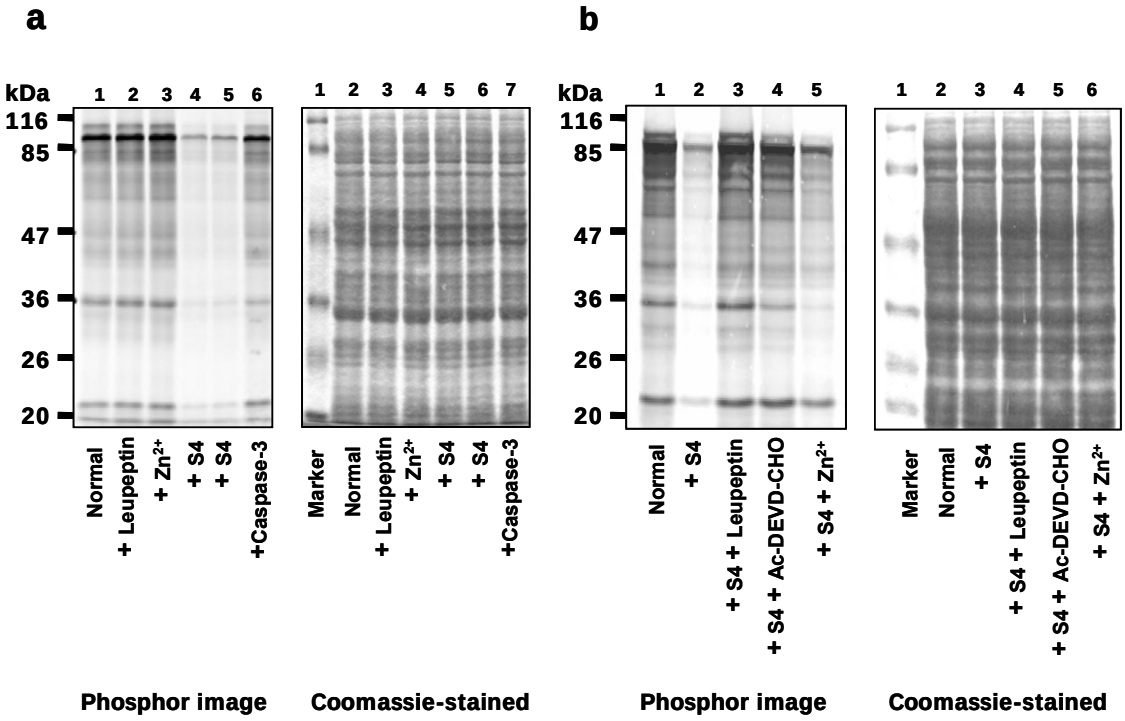

Figure 7. *In vitro* translation of BMV-RNA in wheat germ lysate (WGL) to analyze the effects of S4 and its inhibitors on protein synthesis. The experiment was performed as described under Methods, and the results are detailed in the text. Molecular weight markers are indicated at the left of each panel. (a).Hence, lanes 1-6 of the image correspond sequentially to lanes 2-7 of the coomassie-stained gel. The normal activity of protein synthesis (lane 1) is marginally affected by leupeptin (lane 2) or Zn^{2+} (lane 3), but S4 suppresses protein synthesis dramatically (lanes 4,5). Human caspase-3, another cysteine protease, also reduces the level of translation. This effect, although relatively less (lane 6), is likely due to caspase-3-mediated proteolysis of key translational regulatory protein(s), suggesting that S4 may arrest translation by its proteolytic activity. (b), Normal translation (lane 1) is suppressed by S4

(lane 2). However, translation is restored when leupeptin or Ac-DEVD-CHO or Zn^{2+} is incorporated into the medium in order to block the suppressive action of S4 (lanes 3-5).

protein synthesis is restored when translation is allowed in the presence of the S4 inhibitors- leupeptin, Ac-DEVD-CHO, and Zn^{2+} (lanes 3, 4, and 5, respectively, in Figure 7B). The restoration in the presence of Zn^{2+} is relatively less, perhaps due to chelation of a part of it by traces of DTT in the lysate. As illustrated with leupeptin and Zn^{2+} in lanes 2 and 3, respectively (Figure 7A), the inhibitors of S4 do not affect protein synthesis when translation is carried out in the absence of extrinsic S4, suggesting that the intrinsic ribosome-bound S4 may not be accessible to the inhibitors. Translation in the presence of recombinant human caspase-3 provides a positive control for this set of experiment (lane 6, Figure 7A). The reduction in protein synthesis, albeit less relative to the effect observed with S4 alone (lanes 4, 5), is likely due to the cleavage action of caspase 3 on the eIF family of translation initiation proteins[38]. Overall, protein synthesis results demonstrate that the S4 protein, when soluble or disintegrated from the ribosome assembly, acts to diminish or even terminate translation, and since S4 is a cysteine protease, it exerts the suppressive effect by proteolysis of one or more key proteins.

4A.8 Translation Initiation Factors are indeed Proteolysed by S4

The conjecture made above on the basis of the protein synthesis results that S4 may suppress translation by acting on the initiation factors, was verified by a set of direct immmunoblotting experiments with bacterially expressed human eIF2-α and eIF2-β, and endogenous eIF4E and eIF5 in rat liver tissue extract. The partially purified S4 (fraction E in Figure 1C) was incubated for 1 hr separately with purified

eIF2-α, eIF2-β, and rat liver extract in the presence and the absence of inhibitors, leupeptin and Ac-DEVD-CHO.

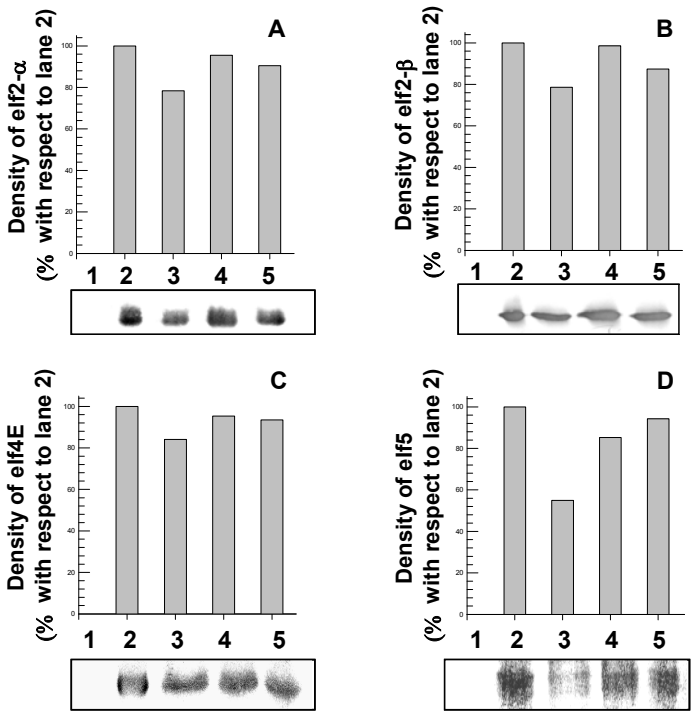

Figure 8. Western analysis of cleavage of eukaryotic translation initiation factors (eIF) by S4. In each experiment, the S4 fraction was incubated with eIfF (recombinant purified or endogenously available in rat liver extract) in the presence and absence of inhibitors. Reaction products were analyzed by immunoblotting with the relevant eIF antibody. In each panel, the bars represent the band intensities (presented below the corresponding graph) normalized to the intensity of the control run where S4 was not included (bar 2). Other bars are: 1, S4 protein alone; 3, eIF+S4; 4, eIF+S4+leupeptin; eIF+S4+Ac-DEVD-CHO. (A) eIF2-α (recombinant human). (B) eIF2-β (recombinant human). (C) eIf4E (endogenous from rat liver).(D) eIF5 (endogenous from rat liver).

The reaction products were analyzed by immunoblotting with corresponding initiation factor antibodies. Figure 8 shows densitometric band intensities of the Western blots normalized with respect to the intensity of the control run that did not include S4 (lane 2 in each panel). Proteolysis in the 20-50% range occurred for all the

four initiation factors considered (lane 3 in each panel). This extent of cleavage should be regarded as considerable, because the proteolysis reactions were carried out using a partially purified S4 preparation, due to which the actual ratio of S4 to initiation factor concentrations could be rather lower than what cellular conditions would employ. But proteolysis is blocked by leupeptin (lane 4) and Ac-DEVD-CHO (lane 5) due to their inhibitory action on S4. These results suggest that S4 suppresses translation by proteolytic cleavage of the eukaryotic initiation factors.

4B. CLONING, OVEREXPRESSION, AND SOME PROPERTIES OF S4

The functional activities and description of S4 provided above are based on results obtained with the partially pure preparation. To confirm that these attributes are bona fide and solely due to S4, it was necessary to obtain the protein in purest form. Further, the availability of the pure protein would facilitate future studies of its atomic structure, conformation, and physiological properties.

4B.1 Cloning of Ribosomal Protein S4

To clone the S4 gene (NCBI accession number AB 181482) containing the N-terminal 1-265 amino acids, RNA from 10-day old wheat seedlings was used. Using two synthetic oligonucleotides as primers, the total RNA, and the cDNA library as a template, the complete coding sequence (798bp) of the S4 protein was obtained by RT-PCR (Figure 9A). The sequence of the PCR product (Figure 9B) was exactly similar to the cDNA library template. The PCR fragment was inserted into a pET28a (+) vector using NdeI and Xho1 restriction sites. Transformation of the recombinant plasmid into *E. coli* BL21 (DE3) RIL cells, led to overexpression of the protein in soluble form (Figure 9C). No expression was observed in BL21 (DE3) cells. The

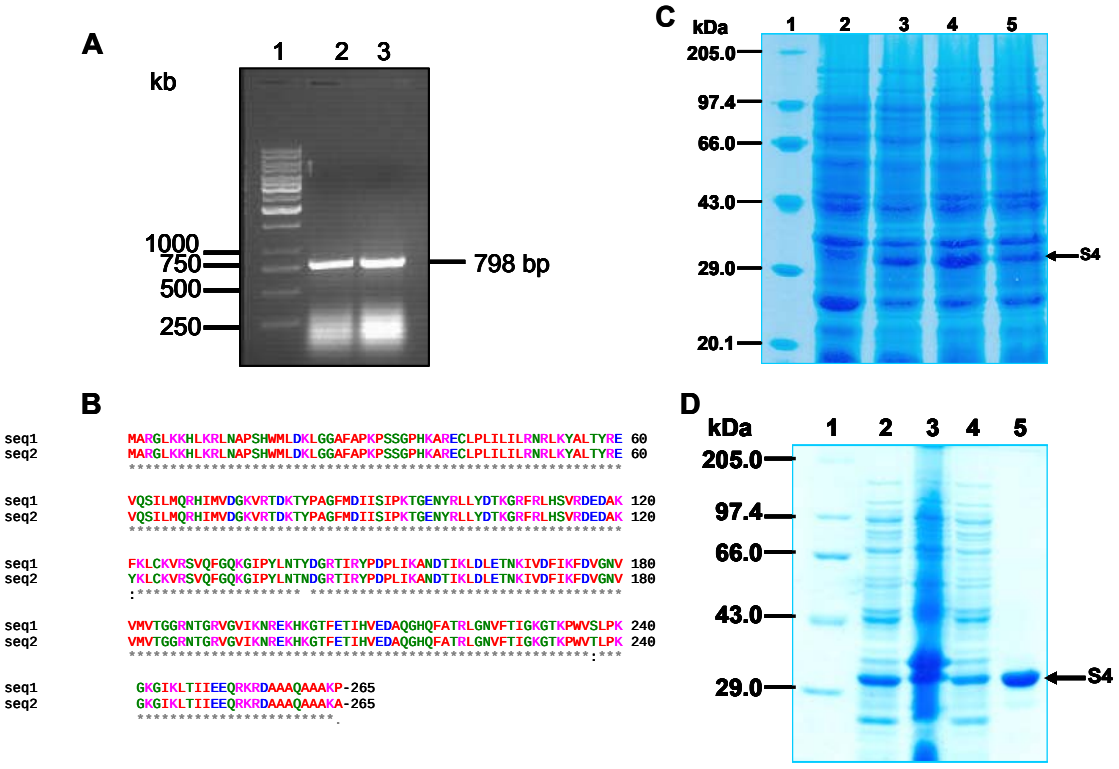

Figure 9. Cloning, expression and purification of wheat S4 protein. (A). Agarose gel electrophoresis of PCR amplified S4 (1-798): DNA ladder (lane 1), and PCR products (lanes 2-3). (B). the amino acid sequence of the cloned protein (seq 1) and aligned with the library S4 protein sequence (seq 2). (C). shows the expression with time, Molecular weight marker (lane1), uninduced (lane2), 1 hr, 2 hr , 3hr are corresponds to lanes 3,4,5 respectively. (D). His_6-tagged wheat S4 overexpressed in *E. coli* was purified to homogeneity by Ni^{2+}-nitrilotriacetate-His bind column. Shown is a coomassie-stained 10% SDS-polyacrylamide gel. The lanes corresponding are marker, Extract, cell debris, unbound and elution fraction.

culture grown for 3 hrs at 30 ºC and 0.4 mM IPTG produces the protein in the soluble form. In cultures grown at 37 ºC, the protein was localized in the inclusion body fraction.

The actual length of the S4 protein is 265 residues. The expression vector added an additional 20 residues, including the His_6 tag, to the N-terminus of the protein. The purification of the protein simply involved Ni-NTA column chromatography of the *E. coli* extract. In the elution employing 200 mM imidazole, the eluted fractions turned turbid and the protein precipitated. Therefore, protein elution was carried out with low concentrations of imidazole (~150 mm). The protein was dialyzed and stored at -80ºC in aliquots of low concentration (~10 μM). The expression and purification procedures described here are reproducible, and yield about 98% pure protein. Approximately 6 mg of the pure enzyme can be obtained from 1 liter of culture. The purified enzyme was homogeneous, as shown by SDS-PAGE (Fig. 9D**).** A molecular weight of ~30,000 was estimated by SDS-PAGE. The extinction coefficient at 280 nm was calculated to be ~82600 $M^{-1}cm^{-1}$.

4B.2 Mass and Basic Conformational Characterization

Figure 10A shows the Gauss filter-smoothed mass spectrum (TOF/TOF) of S4 protein. The singly charged [$M+1H^+$] fundamental peak corresponds to a mass of 31,981.24 Da. The molecular weight calculated for the 265-amino acid S4 is 29930.83. The calculated molecular weight of the actual 285-amino acid (20 residues in the N-terminus, including the six histidines, are due to the vector) polypeptide is 32009.05 Da at pH 7, consistent with the mass data.

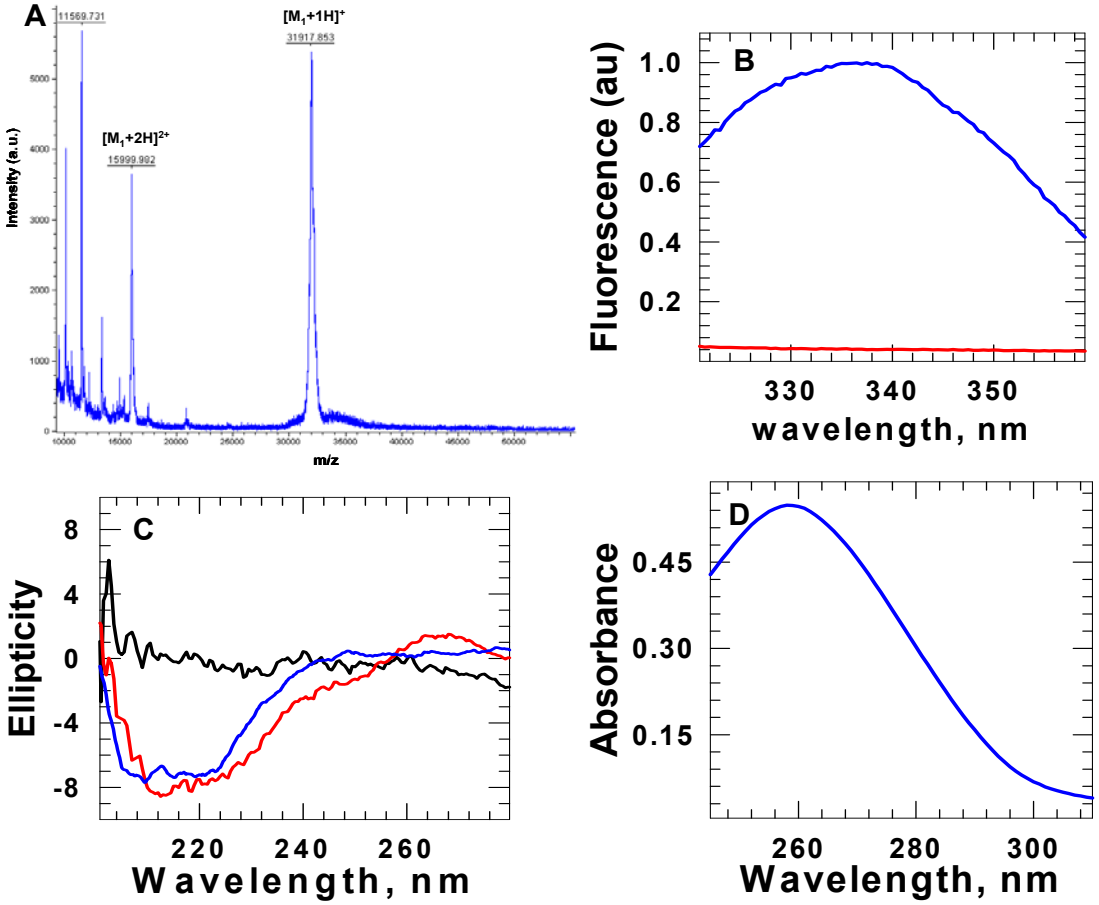

Figure 10. Basic conformational characterization of recombinant S4 protein. (A). Molecular mass of the His_6-tagged S4 is 31,981.243 Da as indicated by mass spectrometry. (B). Fluorescence spectra of the native protein (N) with a peak wavelength of 336 nm. (C) The far-UV CD spectrum of the native protein S4 (-), Buffer (-), and recombinant human Bcl-X_L (-) indicates the presence of native-state secondary structures. (D). absorption spectrum of S4 protein.

Figure 10B shows the 280-nm excited fluorescence spectrum of the native protein (N). The emission maximum of the native-state spectrum is centered at 335.5 nm. The far-UV CD spectrum of purified S4 ((Figure 10C) attracts special attention. The overall band shape in the 200-225 nm region of the spectrum (red) indicates a substantial content of protein secondary structure. In the region longer than 225 nm, the band appears broad, and the ellipticity becomes positive in the 260-276 nm region. These are atypical features of a pure protein CD spectrum. For comparison, the CD spectrum of monomeric Bcl-X_L, an antiapoptotic protein cloned and purified in this laboratory, is also shown (plotted in blue). These features are most likely due to the content of some nucleic acid, perhaps bound to S4. This conjecture is supported by the UV absorption spectrum of purified S4 shown in Figure 10D, where the absorption maximum appears at 258 nm instead of 280 nm.

4B.3 S4 is Bound to RNA: a Ribonucleoprotein Complex

Since S4 interacts extensively with rRNA[20,24,25], the conjecture that the *E. coli*-overexpressed S4 purifies as a complex with RNA needs scrutiny. To examine the possibility, the recombinant S4 initially eluted from Ni-NTA column was digested with RNase for ~6 hours, and chromatographed again on Ni-NTA column to isolate the protein. Figure 11A distinguishes the UV absorption spectra of S4 before (blue) and after (red) RNAse digestion. Clearly, the spectra are significantly different-RNase digestion resulted in a decrease in the band area, and a 258-to-267 nm shift in the λ_{max}. Ideally, the UV-absorption spectrum of a purified protein, even if His_6-tagged, should display a λ_{max} of 280 nm as shown for recombinant His_6-tagged Bcl-x_L (the black spectrum in Figure 11A). The observed λ_{max} of 267 nm for S4 after RNase

digestion may be due to the presence of cut pieces of RNA either in the solution or still bound to the protein. Nevertheless, the result does demonstrate that the recombinant S4 purifies with RNA bound to it.

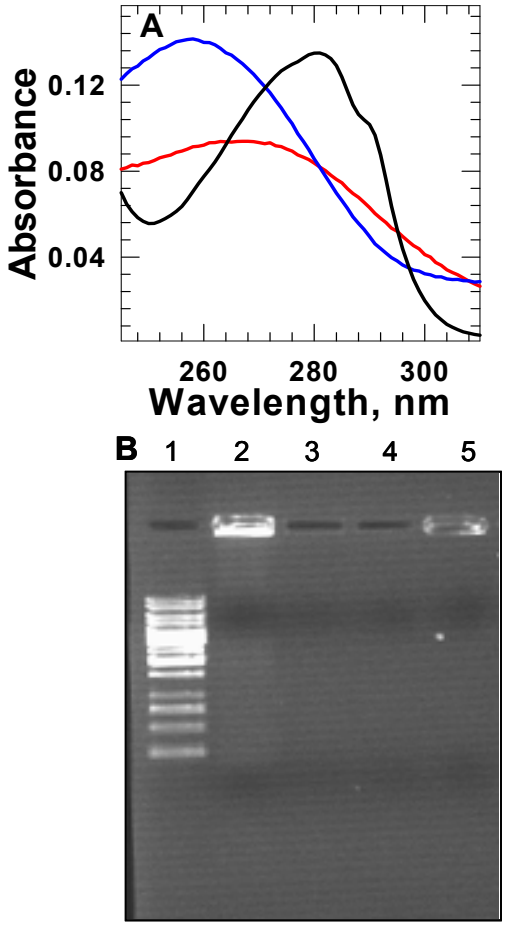

Figure 11. S4 is bound to RNA. (A) The spectrum of the His_6-tagged recombinant S4 (blue, λ_{max}=258 nm) changes dramatically when the protein solution is incubated with RNAse, and rechromatographed on a nickel column in order to remove most of the digested RNA. The spectrum now (red) shows a λ_{max} of 267 nm. Ideally the λ_{max} should have shifted to 280 nm. Persistence of some RNA in the sample even after RNAse digestion may be responsible for the shift less than expected. To show that the His_6 tag is not associated with the unusual appearance of the spectrum of recombinant S4, the spectrum of His_6-tagged Bcl-x_L (black) is also presented. (B) The association of S4 and RNA is analyzed by RNAse digestion and agarose gel electrophoresis. Lane labels are: 1, marker; 2, the ethanol-precipitated RNA from purified S4; 3, the S4 protein sample after RNAse digection; 4, recombinant Bcl-x_L; 5, the S4 protein as such without RNAse digestion or any other treatment.

Figure 11B shows agarose gel electrophoresis detection of RNA bound to

purified S4. The S4-bound RNA precipitated by ethanol does not enter into agarose gel (lane 2), suggesting its large size. The RNAse-digested S4-bound RNA is shown in Lane 3. Absence of bands in the lane suggests that the digestion must have fragmented the RNA into small pieces that ran out of the gel. Lane 4 presents a control where recombinant Bcl-x_L was loaded, clearly shows that there is no RNA present in the recombinant purified Bcl-x_L protein. Lane 5 again shows the RNA bound to RNAse-untreated S4.

Evidences are thus compelling that the recombinant S4 is bound to a sizable piece of RNA. It appears that at a post-translational stage, the wheat S4 binds *E. coli* RNA, and the ribonucleoprotein complex copurifies. The mass spectrometric result seems to argue against though. The MALDI spectrum (Figure 10A) should have detected the association. This point will have to be checked, perhaps by using other matrix used for MALDI mode of mass spectrometric measurement. Even so, the available biochemical results weigh in rather heavily for a persistent association between S4 and RNA. The exact nature and structure of this RNA has not been established at this stage of the work, although it is likely to be one of the rRNA molecules of *E. coli*.

4B.4 Purified Recombinant S4 Shows Ac-DEVD-AFC Hydrolytic Activity

Figure 12A shows the fluorescence-detected hydrolysis of Ac-DEVD-AFC by the recombinant protein as obtained from nickel column chromatography. Steady-state spectra of the protein-substrate mixture initially and 12 hours later are shown in the *inset*. To note, RNA is still bound to the protein at this stage. Figure 12B presents the activity of the protein that was obtained after digesting the bound RNA by employing RNAse A. These results indicate that S4 can hydrolyze substrates in the

presence or absence of RNA. $K_{M,}$ V_{max} values were found by keeping the protein concentration constant and varying the substrate concentrations from 2.5, 5.0, 7.5, 10.0 μg. The calculated K_M and V_{max} values are 6.99 μM^{-1} and 36.36 μM min^{-1}, respectively.

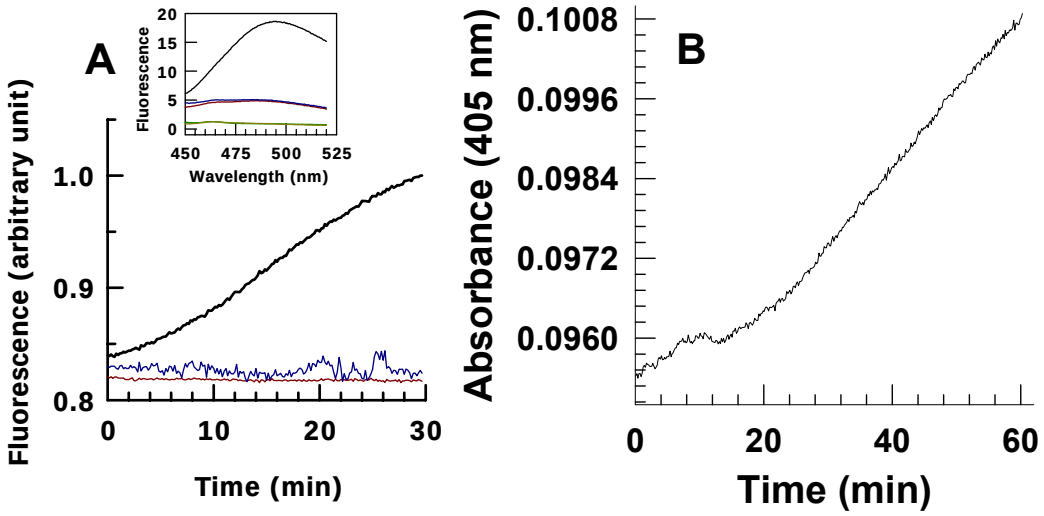

Figure 12. Recombinant S4 can hydrolyze substrates in the presence or absence of RNA. (A) Overproduced and Ni-NTA column purified S4 (5 μM) cleaves the cysteine protease substrate analogue Ac-DEVD-AFC (10 μM) to release the fluorescent AFC group whose emission at 490 nm upon excitation at 400 nm can be followed as a function of time in the absence (black) and presence (blue) of the synthetic inhibitor Ac-DEVD-CHO (10 μM). The protein does not contribute to the 490-nm fluorescence (red). The qualitative extent of cleavage can also be monitored by steady state spectrum (inset). The spectrum in green is for the buffer (20 mM Tris, pH 7.4, 37°C). (B) S4 separated out from the initially bound RNA by employing RNAse A is also capable of hydrolyzing substrate. In this case, the hydrolysis of 5 μg of Ac-DEVD-pNA (Acetyl-Asp-Glu-Val-Asp-p-nitroanilide) added to 500 μL of the reaction mixture is measured at 405 nm.

4B.5 Proteolytic activity of Recombinant S4 Protein

Since S4 is a cysteine protease, its suppressive effect on translation should

arise from proteolysis of possibly one or more translation regulatory proteins. Here, S4-mediated cleavage of four recombinant proteins are shown. Presented first are results for two kinases, PKR (double-stranded RNA-activated inhibitor) and PERK (endoplasmic reticulum stress-activated protein kinase), both known to phosphorylate

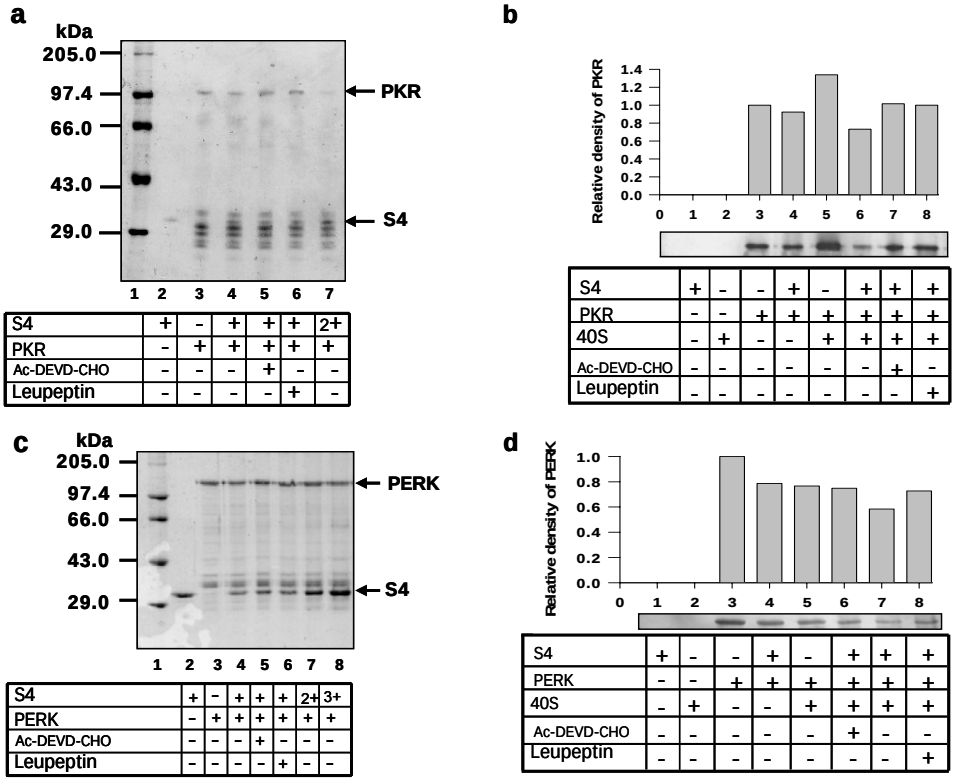

the α-subunit of eIF2 (eukaryotic translation initiation factor 2) and, thereby,

Figure 13. S4 cleaves the two kinases that phosphorylate eIF2-α. (a) Proteolysis of PKR by S4 (lanes 4, 7) diminishes when the cleavage reaction medium contains the S4 inhibitors Ac-DEVD-CHO and leupeptin (lanes 5, 6). (b) These results are verified by Western analysis using monoclonal anti-PKR

(lanes 4,6-8). To determine if the integral S4 is also capable of acting on PKR, the 40S ribosomal subunit prepared by sucrose density gradient ultracentrifugation of 80S was also incubated with PKR in the presence and absence of S4. However, the anomalous band intensity (lane 5), likely due to ribosome-binding property of PKR (see Fig. 3d also), obscures the view. In the presence of both S4 and 40S, the PKR band intensity is not as intense (lane 6), suggesting that the action of free S4 reduces the PKR population available for binding to the surface of 40S. (c). Cleavage of PERK by S4 in the absence (lane 4,7,8) and the presence of Ac-DEVD-CHO (lane 5) and leupeptin (lane 6). (d). The Western analysis with polyclonal anti-PERK also provides evidence for S4-mediated PERK proteolysis. Here, incubation of PERK with the isolated 40S ribosomal subunit has produced detectable cleavage (lane 5), apparently suggesting that the integral S4 is capable of carrying out proteolysis. However, it is more likely that a small fraction of S4 dissociated from the 40S subunit during sample handling causes this.

attenuate the rate of translation initiation[32]. In a 1:2 incubation mixture (by gram weight) of wheat S4 and human PKR proteins, the latter is proteolysed, and the proteolysis is alleviated when cysteine protease inhibitors such as Ac-DEVD-CHO and leupeptin are included in the reaction mixture (Fig. 13a, lanes 4,5,6). Also noted is increased proportion of PKR cleavage when the amount of S4 in the reaction mixture is increased (Fig. 13a, lane 7). Similar observations are made for mouse PERK cleavage (Fig. 13c), and both results are substantiated by Western blot assays employing monoclonal anti-PKR (Fig. 13B) and polyclonal anti-PERK (Fig. 13d).

The S4-mediated cleavages of recombinant human Bcl-x_L and human eIF2α are shown in Figure 14. Due to non-availability of monoclonal antibodies for these proteins, simple SDS page analysis is presented. Clearly, S4 proteolyzes both proteins (lanes 4 and 7 for Bcl-x_L and eIF2α, respectively), and the proteolysis is blocked by the cysteine protease inhibitor leupeptin (lanes 5 and 8 for Bcl-x_L and

eIF2α, respectively). The cleavage products appear to be small peptide fragments as can be visualized from intensities of dye fronts of the gel.

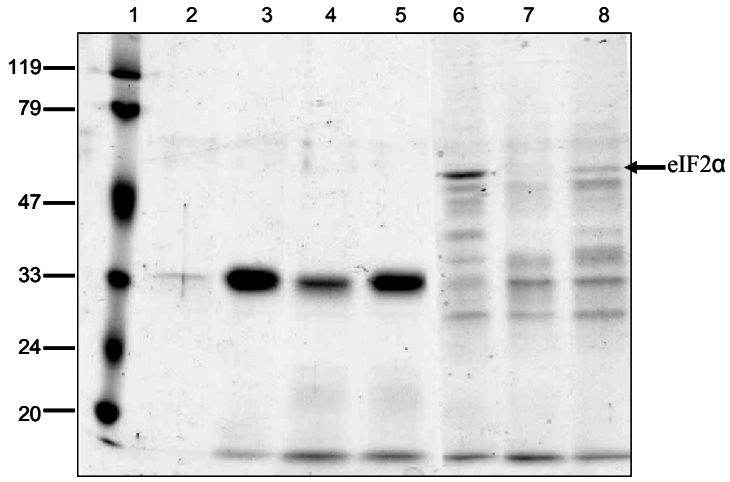

Figure 14. Coomassie-stained 10% SDS page analysis of S4-mediated proteolysis of Bcl-x_L and eIF2α. Lane labels are: 1, prestained marker proteins; 2, recombinant S4 alone (5 μg); 3, recombinant human Bcl-x_L alone (15 μg); 4, S4 (5 μg) incubated overnight with Bcl-x_L (15 μg); 5, S4+Bcl-x_L+leupetin (5:15:10 μM); 6, recombinant human eIF2α alone (10 μg); 7, S4 (5 μg) incubated overnight with eIF2α (10 μg); 8, S4+eIF2α+leupetin (5:10:10 μM). To note, since eletrophoretic mobilities of S4 and Bcl-x_L are quite comparable, the band appearing in the 33 kDa region in lanes 3-5 is due to both proteins.

4B.6 S4 Sequence Structural Homology Prediction

As the primary structural analysis carried out using SMART search showed that the S4 protein contains a RNA binding domain (residue 42-106), attempt was made to identify higher order structural homologs of S4 using the FUGUE program[39]. FUGUE identifies one "likely" match (Z SCORE = 5.04 = 95% confidence): Bacillus stearothermophilus ribosomal protein S4 (PDB id: 1c06, 159 residues), but it is not similar in length and primary sequence homology to wheat S4. Based on this similarity, a 3D structural model was built for wheat S4 by threading in Insight II

(figure 15). The 3D structure contains six α-helixes (α1=6-13, α2=23-27, α3=38-41, α4=43-47, α5=58-67, α6= 139-142) and four β-sheets (β1=112-116, β2= 120-124, β3= 88-92, β4= 71-73).

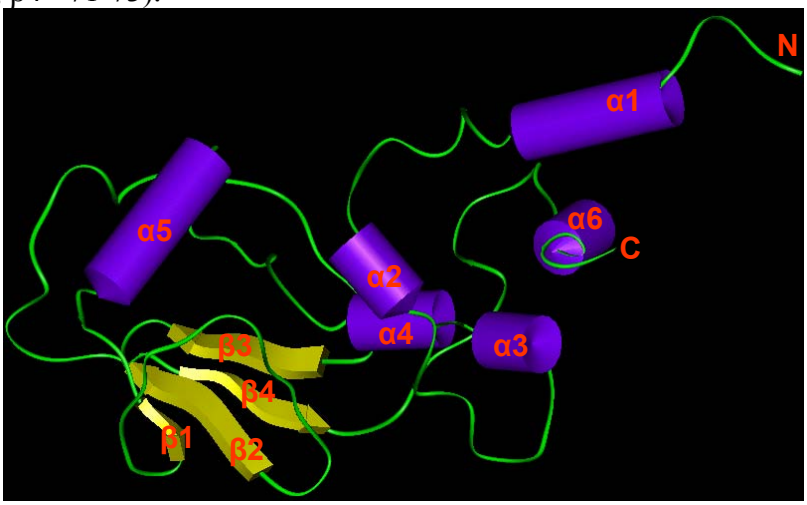

Figure 15. FUGUE search for S4 protein. The model was built by threading with Bacillus tearothermophilus ribosomal protein S4 (PDB id: 1c06, 159 residues 1C06) in Insight II.

5. DISCUSSION

This study identifies the wheat 40S ribosomal subunit protein S4 as a cysteine endoprotease, and shows that protein synthesis is indiscriminately blocked when a S4 preparation is added to the cell-free translation system. The biochemical experiments have provided much new information fundamental to the understanding of the complex regulatory mechanism of eukaryotic ribosome. The current knowledge of the role of S4 in the ribosome assembly, function, and regulation has come vastly from years of genetic, biochemical, NMR and X-ray work on the prokaryotic system[11,13-

[19,28, 40-44]. Regarding plant and animal S4, not much information is available except for some detailed analyses of genetic structure and consequences of expression level of human S4 encoded by sex-linked genes[31,32,40,45]. Nevertheless, structural similarities of corresponding proteins, including S4, from different organisms have been suggested[16,46]. The following discourse is, therefore, presented in the light of the current description of prokaryotic ribosome, even though the mechanisms for prokaryotes and eukaryotes, especially the modes of action of S4, may not be identical.

5.1 Wheat S4 is a Cysteine Endoprotease

The rationale for this inference is drawn from the range of functional and inhibitor studies presented. S4 is a non-specific endoprotease, because the hydrolyzed products analyzed by SDS electrophoresis and Western blotting did not show sizably large fragments. Certain structural attributes of S4 also appear to qualify it for the class of cysteine proteases. First, the sequence of wheat S4 features two cysteines, C41 and C124, one of which could orchestrate the characteristic catalytic triad of cysteine proteases, and carry out the nucleophilic attack on the substrate carbonyl carbon. Second, the crystal and NMR solution structures of prokaryotic S4 consist of two distinct structural domains, a common feature for cysteine proteases. The fissure at the interface of the two domains of S4 serves as the center of the protein surface that interacts with RNA. That such a ribonucleoprotein can also act as a cysteine protease is exemplified by the structure and function of bleomycin hydrolase, an enzyme that binds RNA, single-stranded DNA, and nicked double stranded DNA[47,48]. It is a highly conserved and ubiquitous cysteine protease[49] having a hexameric structure, where each monomer has the characteristic fold of two-domain

structure[50,51] similar to that for S4. Bleomycin hydrolase can proteolyze substrates in the presence or absence of nucleic acids[48]. Strikingly enough, the recombinant S4 is also bound to RNA, and the complex is highly proteolytic. It is unlikely, suggesting non-compulsory involvement of the nucleic acid for the proteolytic activity of S4. However, whether S4 complexed with RNA can still function as the peptidase is an important issue to be addressed in future studies.

5.2 Association of Zinc and S4

Zinc inhibits the proteolytic activity of wheat S4 and restores protein synthesis in cell-free translation system (Figures 2D and 7), presumably by binding to the catalytic cysteine. But, because S4 is a RNA-binding protein[20,24,25,52], it is also expected to carry a zinc finger structure. A N-terminal Zn finger has indeed been observed for the S4 protein in the *Thermus thermophilus* 30S crystal structure[14], and this motif is probably preserved up to plants and animals. To note, the zinc binding cysteines are not conserved[14], and unlike *Thermus* S4 that has four of them to support a zinc finger structure, other sequences, including that of *E. coli*, may not have the required number. I encounter a similar situation in the case of wheat S4. Simultaneous accommodation of two novelties, a catalytic site and a classic zinc finger structure, with the two available cysteines that are separated in the sequence by 82 amino acids poses a difficulty. In the absence of the zinc finger structure, one of the two cysteines could act as the catalytic center. The apparent zinc-binding constant, K_{Zn}^{app} =0.31 mM, derived from zinc-inhibited (competitive) proteolytic activity of S4 (Figure 2D) suggests a low affinity, and should represent binding of zinc to the catalytic site.

5.3 Role of S4 as a Cysteine Protease

An important insight into the regulation of synthesis of ribosomal proteins in *E. coli* was provided by a series of studies in Nomura's laboratory[28,52]. Induction of certain ribosomal proteins, including S4, leads to inhibited synthesis of those ribosomal proteins that are coded by the polycistronic mRNA containing the cistron of the induced protein[27]. This feedback regulation is also reproduced in cell-free translation system of *E. coli* when purified S4 is added[28,29,52]. More recently, have found that *E. coli* S4 is a general transcription antitermination factor that associates with RNA polymerase during normal transcription and is also involved in rRNA operon antitermination[30]. Thus, S4 presumably fine-tunes and coordinates the production of ribosomal proteins and RNA.

In this study, wheat S4 blocked *in vitro* translation of BMV-RNA in cell-free translation system by cleaving the initiation factors (Figures 7, 8, and 14) and kinases like PKR and PERK (Figures 4 and 13). S4 also cleaves Bcl-x_L (Figure 14), and proteolysis of certain monomeric eukaryotic proteins including casein has been observed in preliminary experiments (data not shown). Possibility of proteolysis of other proteins, including those that participate in the translational apparatus[53] is not excluded. The available evidences suggest a rather broad substrate spectrum for S4. The fact that translation of BMV-RNA is restored in the presence of inhibitors of S4 (Figure 7) implies that the phenomenon reported in this thesis is solely due to the proteolytic activity of S4. However, the occurrence of the S4-induced translational control of the α-operon[28,54] and transcription antitermination activities[30] described for *E.coli.* cannot be excluded in the case of wheat until synthesis of ribosomal proteins encoded by the appropriate wheat genes and the transcription terminator

read-through are examined.

The role for proteolytic activity of S4 is puzzling. S4 presumably does not occur in the free form in the cytoplasm, because of its role both in the assembly of the core of functional ribosomes and in binding to rRNA. Its proteolytic activity should remain masked except under conditions yet unknown where the ribosomal proteins are disassembled and released into the cytoplasm. Alternatively, S4 may be activated by a sort of mechanism akin to that of phosphorylation of ribosomal protein S6 by a death-associated protein kinase (DAPK) leading to a reduction of protein synthesis[55]. These enigmatic issues will be reported in future.

6. SUMMARY AND CONCLUSION

S4 is one of the integral proteins of the smaller subunit of the cytosolic ribosome. In prokaryotes, it serves as one of the core proteins that can independently interact with the 16S RNA [25,26,56]. Two functional roles of S4 have been identified in *Escherichia coli*. It regulates the synthesis of ribosomal proteins by feedback inhibition of the expression of α operon genes[27,29], and facilitates synthesis of ribosomal RNA by direct binding to RNA polymerase thereby acting as a transcription antiterminator[30]. However, functional roles and regulatory actions of S4 in eukaryotes are little known, although its deficiency in humans has been associated with Turner syndrome[31,32]. This work has shown that wheat S4 is a cysteine protease that can abrogate protein synthesis in an actively translating cell-free system. Recombinant S4 is shown to proteolyze *in vitro* at least three key translational regulatory proteins, PKR, PERK, and eIF2α. Cysteine protease inhibitors such as leupeptin counter this action of S4. Thus, the study has demonstrated a third functional role for S4 arising solely from its proteolytic action and operating at the

translational level in eukaryotes. The significance and the underlying signaling mechanism for this apparently destructive role of S4, and the stage of the cell cycle where this mechanism is operative are key questions emanating.

7. REFERENCES

1. Lehninger, A.L., Nelson, D.L., and Cox, M.M. (1993). Principles of Biochemistry, 2nd edition. (Worth Publishers, New York).

2. Liu, X., Kim, C.N., Yang, J., Jemmerson, R., and Wang, X. (1996). Induction of apoptotic program in cell-free extracts: requirement for dATP and cytochrome *c*. Cell **86**, 147-157.

3. Long, X., Wu, G., Gaa, S.T., and Rogers, T.B. (2002). Inhibition of protein phosphatase-1 is linked to phosphorylation of p53 and apoptosis. Apoptosis **7**, 31039.

4. Moll, U.M., Wolff, S., Speidel, D., and Deppert, W. (2005). Transcription-independent pro-apoptotic function of p53. Curr. Opin. Struct. Biol. **17**, 631-636.

5. Jacobs, S.B., Kaplan, D.R., and Miller, F.D. (2006). The p53 family un nervous system development and disease. J. Neurochem. **97**, 1571-1584.

6. Mehta, K., Shahid, U., and Malavasi, F. (1996). Human CD38, a cell-surface protein with multiple functions. FASEB J. **10**, 1408-1417.

7. Sheahan, K.L., Cordero, C.L., and Satchell, K.J. (2007). Autoprocessing of the Vibrio cholerae RTX toxin by the cysteine protease domain. EMBO J. **26**, 2552-2561.

8. Rassow, J., Voos, W., and Pfanner, N. (1995). Partner proteins determine multiple functions of Hsp70. Trends Cell Biol. **5**, 207-212.

9. Vickery, L.E., and Cupp-Vickery, J. R. (2007). Molecular chaperones HscA/Ssq1 and HscB/Jac1 and their roles in iron-sulfur protein maturation. Crit. Rev. Biochem. Mol. Biol. **42**, 95-111.

10. Gaspar, N.J., Kinzy, T.G., Scherer, B.J., Hümbelin, M., Hershey, J.W.B., and Merrick, W.C. (1994). Translation initiation factor eIF-2: cloning and expression of the human cDNA encoding the γ-subunit. J. Biol. Chem. **269**, 3415-3422.
11. Spirin, A.S. (1986). Ribosome Structure and Protein Biosynthesis (California: Benjamin/Cummings Publishing Company, Inc.).
12. Kresge, N., Simoni, R.D., and Hill, R.L. (2007). Purification of the components of the ribosome and reconstitution of active ribosomes: the work of Masayasu Nomura. J. Bio. Chem. **282**, e9-e10.
13. Sayers, E.W., Gerstner, R.B., Draper, D.E., and Torchia, D.A. (2000). Structural preordering in the N-terminal region of ribosomal protein S4 revealed by heteronuclear NMR spectroscopy. Biochemistry **39**, 13602-13613.
14. Wimberly, B.T., Brodersen, D.E., Clemons, W.M., Morgan-Warren, R.J., Carter, A. P., Vonrhein, C., Hartsch, T., and Ramakrsihnan, V. (2000). Structure of the 30S ribosomal subunit. Nature **407**, 327-339.
15. Spahn, C.M., Beckmann, R., Eswar, N., Penczek, P.A., Sali, A., Blobel, G., and Frank, J. (2001). Structure of the 80S ribosome from Saccharomyces cerevisiae-tRNA-ribosome and subunit-subunit interactions. Cell **107**, 373-386.
16. Doudna, J., and Rath, V.L. (2002). Structure and function of the eukaryotic ribosome: the next frontier. Cell **109**, 153-156.
17. Moore, P.B., and Steitz, T.A. (2003). The structural basis of large ribosomal subunit function. Annu. Rev. Biochem. **72**, 813-850.
18. Selmer, M., Dunham, C.M., Murphy, F.V., Weixlbaumer, A., Petry, S., Kelley, A.C., Weir, J.R., and Ramakrishnan, V. (2006). Structure of the 70S ribosome complexed with mRNA and tRNA. Science **313**, 1935-1942.
19. Grela, P., Helgstrand, M., Krokowski, D., Boguszewska, A., Svergun, D., Liljas,

A., Bernado, P., Grankowski, N., Akke, M., and Tchorzeqski, M. (2007). Structural characterization of the ribosomal P1A-P2B protein dimer by small-angle X-ray scattering and NMR spectroscopy. Biochemistry **46**, 1988-1998.

20. Vartikar, J.V., and Draper, D.E. (1989). S4-16S ribosomal RNA complex. Binding constant measurements and specific recognition of a 460-nucleotide region. J. Mol. Biol. **209**, 221-234.

21. Wool, I.G. (1996). Extra ribosomal functions of ribosomal proteins. Trends. Bichem. Sci. **21**, 164-165.

22. Flygare, J., Aspesi, A., Bailey, J.C., Miyake, K., Caffrey, J.M., Karlsson, S., and Ellis, S.R. (2007). Human RPS19, the gene mutated in Diamond-Blackfan anemia, encodes a ribosomal protein required for the maturation of 40S ribosomal subunits. Blood **109**, 980-986.

23. Maisnier_patin, S., Paulander, W., Pennhag, A., and Andersson, D.I. (2007). Compensatory evolution reveals functional interactions between ribosomal proteins. J. Mol. Biol. **366**, 207-215.

24. Schaup, H.W., Sogin, M., and Woese, C. (1971). Characterization of an RNA "binding site" for a specific ribosomal protein of Escherichia coli. Mol. Gen. Genet. **114**, 1-8.

25. Stern, S., Wilson, R.C., and Noller, H.F. (1986). Localization of the binding site for S4 as 16S ribosomal RNA by chemical and enzymatic probing and primer extension. J. Mol. Biol. **192**, 101-110.

26. Nowotny, V., and Nierhaus, K.H. (1988). Assembly of the 30S subunit from Escherichia coli ribosomes occurs via two assembly domains which are initiated by S4 and S7. Biochemistry **27**, 7051-7055.

27. Dean, D., and Nomura, M. (1980). Feedback regulation of r-protein gene

expression in *Escherichia coli*. Proc. Natl. Acad. Sci. USA **77**, 3590-3594.
28. Yates, J.L., and Nomura, M. (1980). E. coli ribosomal protein L4 is a feedback regulatory protein. Cell **21**, 517-522.
29. Yates, J.L., Arfsten, A.E., and Nomura, M. (1980). In vitro expression of Escherichia coli ribosomal protein genes: autogenous inhibition of translation. Proc. Natl. Acad. Sci. USA **77**, 1837-1841.
30. Torres, M., Condon, C., Balada, J., Squires, C., and Squires, C.L. (2001). Ribosomal protein S4 is a transcription factor with properties remarkably similar to NusA, a protein involved in both non-ribosomal and ribosomal RNA antitermination. EMBO J. **20**, 3811-3820.
31. Fisher, E.M., Beer-Romero, P., Brown, L.G., Ridley, A., McNeil, J.A. Lawrence, J.B., Willard, H.F., Bieber, F.R., and Page, D.C. (1990). Homologous ribosomal protein genes on the human X and Y chromosomes: escape from X inactivation and possible implications for Turner syndrome. Cell **63**, 1205-1218.
32. Zinn, A.R., Alagappan, R.K., Brown, L.G., Wool, I., and Page, D.C. (1994). Structure and function of ribosomal protein S4 genes on the human and mouse sex chromosomes. Mol. Cell. Biol. **14**, 2485-2492.
33. Janaki, N., Krishna, V.M., and Ramaiah, K.V.A. (1995). Phosphorylation of wheat germ initiation factor 2 (eIF-2) by N-ethylmaleimide-treated wheat germ lysate and by purified casein kinase II does not affect guanine nucleotide exchange on eIF-2. Arch. Biochem. Biophys. **324**, 1-8.
34. Lewis, E.R., Johnson, F.A., and Shafer, J.A. (1981). Effect of cysteine-25 on the ionization of histidine-159 in papain as determined by proton nuclear magnetic resonance spectroscopy. Evidence for a his-159-cys25 ion pair and its possible role in catalysis. Biochemistry **20**, 48-51.

35. Stennicke, H.R., and Salvesen, G.S. (1997). Biochemical characteristics of caspases-3, -6, -7, and-8. J. Biol. Chem. **272**, 25719-25723.
36. Sluyterman, L.A., and Wijdenes, J. (1976). Proton equilibria in the binding of Zn^{2+} and of methyl mercuric iodide to papain. Eur. J. Biochem. **71**, 383-391.
37. Coffeen, W.C., and Wolpert, T.J. (2004). Purification and characterization of serine proteases that exhibit caspase-like activity and are associated with programmed cell death in Avena sativa. Plant Cell **16**, 857-873.
38. Saelens, X., Kalai, M., and Vandenabeele, P. (2001). Translation inhibition in apoptosis. Caspase-dependent PKR activation and eIF2-α phosphorylation. J. Biol. Chem. **276**, 41620-41628.
39. Shi, J., Blundell, T.L., and Mizuguchi, K., (2001). Fugue: sequence-structure homology recognition using environment-specific substitution tables and structure-dependent gap penalties. *J. Mol. Biol.* **310**, 243–257.
40. Omoe, K., and Endo, A. (1996). Relationship between the monosomy X phenotype and Y-linked ribosomal protein S4 (Rps4) in several species of mammals: a molecular evolutionary analysis of Rps4 homologs. Genomics **31**, 44-50.
41. Cate, J.H., Yusupov, M.M., Yusupova, G.Z., Earnest, T.N., and Noller, H.F. (1999). X-ray crystal structure of 70S ribosome functional complexes. Science **285**, 2095-2104.
42. Maguire, B.A., and Zimmermann, R.A. (2001). The ribosome in focus. Cell **104**, 813-816.
43. Ramakrishnan, V., and Moore, P.B. (2001). Atomic structures at last: the ribosome in 2000. Curr. Opin. Struct. Biol. **11**, 144-154.
44. Yusupov, M.M., Yusupova, G.Z., Baucom, A., Lieberman, K., Earnest, T.N., Cate, J.H., and Noller, H.F. (2001). Crystal structure of the ribosome at 5.5Å

resolution. Science 292, 883-896.
45. Geerkens, C., Just, W., Held, K.R., and Vogel, W. (1996). Ulrich-Turner syndrome is not caused by haploinsufficiency of RPS4X. Hum. Genet. **97**, 39-44.
46. Braun, H.P., Emmermann, M., Mentzel, H., and Schmitz, U.K. (1994). Primary structure and expression of a gene encoding the cytosolic ribosomal protein S4 from potato. Biochim. Biophys. Acta **1218**, 435-438.
47. Takeda, A., Masuda, Y., Yamamoto, T., Hirabayashi, T., Nakamura, Y., and Nakaya, K. (1996). Cloning and analysis of cDNA encoding rat bleomycin hydrolase, a DNA-binding cysteine protease. J. Biochem. (Tokyo) **120**, 353-359.
48. Zheng, W., and Johnston, S.A. (1998). The nucleic acid binding activity of bleomycin hydrolase is involved in bleomycin detoxification. Mol. Cell. Biol. **18**, 3580-3585.
49. Schwartz, D.R., Homanics, G.E., Hoyt, D.G., Klein, E., Abernethy, J., and Lazo, J.S. (1999). The neutral cysteine protease bleomycin hydrolase is essential for epidermal integrity and bleomycin resistance. Proc. Natl. Acad. Sci. USA **96**, 4680-4685.
50. Joshua-Tor, L., Xu, E.H., Johnston, S.A., and Rees, D.C. (1995). Crystal structure of a conserved protease that binds DNA: the bleomycin hydrolase, Gal6. Science **269**, 945-950.
51. O'Farrell, P.A., Gonzalez, F., Zheng, W., Johnston, S.A., and Joshua-Tor., L. (1999). Crystal structure of human bleomycin hydrolase, a self-compartmentalizing cysteine protease. Structure **7**, 619-627.
52. Noller, H.F., and Nomura, M. (1996). Ribosomes. In Escherichia coli and Salmonella typhimurium: cellular and molecular biology, F.C. Neidhardt et al., eds. (Washington, DC: ASM Press), pp. 167-186.

53. Browning, K.S. (1996). The plant translational apparatus. Plant Mol. Biol. **32**, 107-144.

54. Keener, J., and Nomura, M. (1996). Regulation of ribosome synthesis. In Escherichia coli and Salmonella typhimurium: cellular and molecular biology, F.C. Neidhardt et al., eds. (Washington, DC: ASM Press), pp. 1417-1428.

55. Schumacher, A.M., Velentza, A.V., Watterson, D.M., and Dresios, J. (2006). Death-associated protein kinase phosphorylates mammalian ribosomal protein S6 and reduces protein synthesis. Biochemistry **45**, 13614-13621.

56. Mizushima, S. and Nomura, M. Assembly mapping of 30S ribosomal proteins from *E. coli*. *Nature* **226**, 1214-1218 (1970).

8. LIST OF PUBLICATIONS

1. **Yadaiah, M.,** Rao, P.N., Harish, P. and Bhuyan, A. K. (2007). High Affinity Binding of Bcl-x_L to Cytochrome *c*: Implication for a Possible Interception of Translocated Cytochrome *c* in Apoptosis. Biochim. Biophys. Acta. **1774**, 1370-1379.
2. Rao, N.P., **Yadaiah, M**., Roy, K.R., Potu, H. and Bhuyan, A.K. (2007).Cloning, *E. coli* expression, refolding, and ATP-binding properties of a WD40-deleted Apaf-1 isoform. Protein expression and purification **56**, 220-228.
3. **Yadaiah, M.**, Kumar, R. and Bhuyan, A. K. (2007). Glass transition in the folding landscape of cytochrome c detected by laser flash photolysis. Biochemistry **46**, 25445-2551.
4. Rao, D. K., Kumar, R**., Yadaiah, M.** and Bhuyan, A. K. (2006). The Alkali Molten Globule State of Ferrocytochrome *c*: Extraordinary Stability, Persistent Structure, and Constrained Overall Dynamics. Biochemistry **45**, 3412-3420.
5. Kumar, R., Prabhu, N. P., **Yadaiah, M.** and Bhuyan, A. K. (2004). Protein stiffening and entropic stabilization in the sub denaturing limit of guanidine hydrochloride. Biophysical Journal **87**, 2656-2662.
6. **Yadaiah, M.**, Hussain, G.S., Ramaiah, K.V.A. and Bhuyan, A. K. (2008). Eukaryotic ribosomal protein S4 is a cysteine protease that can abrogate protein synthesis. (Being Communicated).
7. **Yadaiah M.,** Reddy, U.S. and Bhuyan A.K. (2008). Cloning, Expression, Purification and characterization of S4 protein from wheat (Being Communicated).

8. **Yadaiah M.,** Reddy, U.S. and Bhuyan A.K. (2008). Biochemical and enzymatic properties of the wheat ribosomal protein S4. (Being Communicated).

---

9. APPENDIX

Available online at www.sciencedirect.com
ScienceDirect
Biochimica et Biophysica Acta 1774 (2007) 1370–1379
BBA
www.elsevier.com/locate/bbapap

High affinity binding of Bcl-x_L to cytochrome *c*: Possible relevance for interception of translocated cytochrome *c* in apoptosis

M. Yadaiah [a], P. Nageswara Rao [a], P. Harish [a], Abani K. Bhuyan [a,b,*]

[a] *Schools of Chemistry, University of Hyderabad, Hyderabad 500046, India*
[b] *Life Sciences, University of Hyderabad, Hyderabad 500046, India*

Received 29 March 2007; received in revised form 28 July 2007
Available online 14 August 2007

Abstract

The release of cytochrome *c* from mitochondria and apoptosis relies on several preferential and selective interactions involving the Bcl-2 family of proteins. There is, however, no direct evidence for the interaction of cytochrome *c* with these proteins at any stage of apoptosis. To investigate if any pro-survival protein from the Bcl-2 family could intercept cytochrome *c* after its translocation from mitochondria, the interaction of cytochrome *c* with bacterially expressed human Bcl-x_L was studied at pH 7. In size-exclusion chromatography, purified full-length His_6-tagged Bcl-x_L migrated as both dimer and monomer, of which the monomeric fractions were used for experiments. Coimmunoprecipitation studies show that cytochrome *c* interacts with Bcl-x_L. The extent of caspase activity in cell lysate elicited by externally added cytochrome *c* is reduced when a preincubated mixture of Bcl-x_L and cytochrome *c* is used instead. Equilibrium binding monitored by optical absorption of cytochrome *c* as a function of titrating concentrations of Bcl-x_L yields the association constant, $K_{ass} = 8.4(\pm 4) \times 10^6\ M^{-1}$ (binding affinity, $K_{diss} = 1/K_{ass} \approx 120$ nM) which decreases at high ionic strength. The rates for binding of Bcl-x_L to cytochrome *c*, studied by stopped-flow kinetics at pH 7, show that the bimolecular rate constant for binding, $k_{bi} = 0.24 \times 10^6\ M^{-1}\ s^{-1}$. Values of the thermodynamic and kinetic parameters for Bcl-x_L–cytochrome *c* interaction are very similar to those known for regulatory protein–protein interactions in apoptosis.

Keywords: Apoptosis; Bcl-2 protein; Bcl-x_L; Cytochrome *c*

In the intrinsic apoptotic pathway, cytochrome *c* translocated from mitochondria assists in the assembly of an apoptosome required for activation of caspase-9 and subsequent activation of other caspases [1–3]. The rapid release of cytochrome *c* from mitochondria is believed to arise from effects of pro-apoptotic proteins of the Bcl-2 family, including Bax, Bak, and Bad, which form pores on the outer mitochondrial membrane to facilitate release of cytochrome *c* [4–9]. Alternatively, these proteins may function to cause a loss of mitochondrial membrane potential that can lead to membrane permeabilization [10–14].

The pro-survival members of the Bcl-2 family proteins, including Bcl-x_L, Bcl-2, and Bcl-w, counter the release of cytochrome *c* from mitochondria by less understood mechanisms. Numerous studies have established that Bcl-x_L participates in a number of protein–protein interactions to exert its pro-survival effect. In the intrinsic apoptotic pathway, Bcl-x_L blocks cytochrome *c* release by preventing Bax from disrupting the integrity of the outer mitochondrial membrane [15,16], and in the extrinsic apoptotic pathway initiated by death ligands, Bcl-x_L can prevent death by blocking Bid redistribution downstream of caspase-8 [17]. In hypoxia/reoxygenation-induced apoptosis, Bcl-x_L has been found to interfere with the assembly of death-inducing signal complex (DISC), block the translocation of both Bax and Bid to mitochondria, and inhibit the activation of caspase-8 [18].

Thus, Bcl-x_L appears to prevent cell death through diverse protein–protein interactions, seemingly in a case specific manner. However, there is no known mechanism by which cytochrome *c* translocated to cytosol can be intercepted, such that the apoptosome is not assembled. There have been reports that Bcl-x_L can block the formation of the apoptosome by

* Corresponding author. Schools of Chemistry, University of Hyderabad, Hyderabad 500046, India. Tel.: +91 40 23134810; fax: +91 40 23012460.
E-mail address: akbsc@uohyd.ernet.in (A.K. Bhuyan).

1570-9639/$ - see front matter © 2007 Elsevier B.V. All rights reserved.
doi:10.1016/j.bbapap.2007.08.005

associating itself with Apaf-1 and caspase-9 to produce an antiapoptotic ternary complex [19,20]. In another earlier immunoprecipitation study, cytochrome *c* was found to interact specifically with Bcl-x_L as a cellular response to ionizing radiation and genotoxic stress [21]. The present study is basically aimed at providing quantitative data on the interaction between the two proteins. To characterize the affinity of this interaction so that Bcl-x_L could possibly be implicated for arresting cell death by inhibiting the cytosolic cytochrome *c*, we have investigated the interaction between bacterially over-expressed full-length human Bcl-x_L and horse cytochrome *c* using coimmunoprecipitation and classical biochemical methods. We report that cytochrome *c* displays very high binding affinity for Bcl-x_L, which closely matches the reported affinities of BH3 peptides/domains for Bcl-x_L. The bimolecular binding rate of Bcl-x_L to cytochrome *c* is also within the range set by dimerization of Bcl-2 family proteins, and by BH3–Bcl-2 protein interactions. Possible significance and relevance of these binding characteristics to the regulation of the intrinsic pathway for apoptosis is discussed.

1. Materials and methods

1.1. Production and purification of Bcl-x_L

A pET-16b (Novagen) vector coding for full length human Bcl-x_L with N-terminal His_6 tag was kindly provided by Dr. Apurva Sarin, and the plasmid was transformed into *E. coli* BL21(DE3) cells. The cells were grown in LB media to a A_{600} of 0.5. Protein expression was induced with 0.8 mM IPTG at 30 °C and 180 rpm. Cells were harvested at 10000 rpm for 10 min. The cell pellet, washed with PBS, was resuspended in 1:5 W/V buffer A (50 mM Tris, pH 8.0, 0.2 M NaCl, 0.2 mM PMSF, 5 mM β-mercaptoethanol, 5 mM imidazole, and 1% glycerol), and stirred for 15 min at 4 °C. The cells were disrupted by pulsed sonication, and the lysate was spun at 15000 rpm for 30 min. The soluble fraction was loaded onto a Ni-NTA-His bind column (Novagen) equilibrated with buffer A. The column was washed with 45 mM imidazole in buffer A until the A_{280} reached 0.001, and the protein was eluted with 200 mM imidazole in the same buffer. The protein fractions were pooled, concentrated, and loaded onto a Sephadex G-75 (Amersham) gel filtration column preequilibrated with buffer B (50 mM Tris, pH 8.0, 50 mM NaCl, 1 mM DTT, 2 mM EDTA, and 0.2 mM PMSF) at 4 °C. Of the two major peaks, the one corresponding to the monomeric protein was collected and loaded onto an anion-exchange DEAE-cellulose column (Whatman) equilibrated with buffer B. The column was washed with 10-volumes of buffer B, and the protein was eluted with a 50–400 mM NaCl gradient applied linearly. The protein-containing fractions were pooled and dialyzed extensively against 1× PBS at 4 °C. Protein purity was determined to be >99% by SDS/PAGE silver staining. The protein concentration was determined spectrophotometrically using ε_{280}=41940 M^{-1} cm^{-1} in 6 M guanidine hydrochloride.

1.2. Coimmunoprecipitation

A mixture of 50 μg each of horse heart cytochrome *c* and the purified human Bcl-x_L was incubated with constant shaking. 1 μg monoclonal anti cytochrome *c* (Novagen) was added to the mixture, and incubated for another 3 h at 4 °C. To this mixture, 100 μl of 50% protein-A slurry was added, and incubated with shaking at 4 °C for 3 h. The beads were separated by centrifuging the mixture at 2000 rpm for 1 min, and the pellet was washed 3 times with 0.5× PBS. To the washed beads, 60 μl of 2× sample-loading dye was added, boiled for 5 min to dissociate the immuno complex, and the beads were collected by centrifugation. The protein-containing supernatant was separated by 15% SDS/PAGE, and transferred onto a PVDF membrane. One set of membranes was probed with anti bcl-x_L (Promega) and the other with anti cytochrome *c*. The bands were detected with corresponding ALP conjugate 2° antibodies and NBT/BCIP.

1.3. Coimmunoprecipitation using Ca^{2+}-induced release of cytochrome *c* from purified healthy mitochondria

Wistar rats (12 to 14 weeks old) were decapitated and the liver was taken in ice cold 0.9% NaCl. The liver was washed thoroughly with 0.9% NaCl to remove the blood, transferred to MSH buffer (220 mM mannitol, 70 mM Sucrose, 2 mM HEPES, pH 7.4, 0.2 mM EDTA, 6 μM BSA), washed twice in the same buffer, and cut into small cubes. The cubes were taken in MSH buffer the volume of which was ~10% of the body weight. The liver was homogenated using dounce homogenizer and Teflon pestle, and centrifuged at 2000×*g* for 10 min at 4 °C. The supernatant, collected after removing the white lipid layer using cotton shrubs, was centrifuged again at 12000×*g* for 15 min. The pellet was resuspended in 20 ml of a washing medium containing 220 mM mannitol, 70 mM sucrose, 2 mM HEPES, and 0.2 mM EDTA, pH 7.4, and centrifuged again at 12000×*g* for 10 min at 4 °C. This pellet-washing step was repeated one more time. 0.5 mL of the resuspended pellet was layered over preformed discontinuous Percoll gradient consisting of a bottom layer of 2 mL of 40% Percoll, and a top layer of 2 mL of 26% Percoll in the washing medium. The gradient was spun at 31,000×*g* for 28 min in a Beckman SW-60 rotor. The mitochondrial fraction appearing in the interface between the two Percoll layers was transferred into a fresh tube, diluted 1:5 with the same (washing) medium, and centrifuged at 31,000×*g* for 20 min. The pellet was then resuspended in 0.5 mL of 0.25 M sucrose and kept on ice. Mitochondrial protein was determined by the Bradford method using BSA as a standard.

0.6 mg mitochondria contained in an eppendorf tube was incubated with 1.4 μmol Ca^{2+} per mg of protein for 2 h at 4 °C. Controls were generated by incubating under identical conditions the same quantity of mitochondria with 125 mM KCl (in Buffer A) in one tube, and 250 mM sucrose (in Buffer B) in another. After incubation, mitochondria were pelleted by centrifugation at 12,000×*g* for 10 min. 50 μg purified Bcl-x_L was added to the supernatant, and incubated for 2 h at room temperature by constant shaking. The mixture was then divided into two halves; one half was treated with 1.0 μg of monoclonal anti-cytochrome *c* (Novagen), and the other half with 1.0 μg monoclonal anti-caspase-9 (Santa Cruz) as a negative control antibody. After incubating at room temperature for 3 h, the mixture was combined with 50 μl of 50% protein-A slurry, and incubated further for 1 h at room temperature. The beads were separated by centrifuging the mixture at 2000 rpm for 1 min, and the pellet was washed 3 times with 0.5× PBS. To the washed beads, 60 μl of 2× sample-loading dye was added, boiled for 5 min to dissociate the immunocomplex, and the beads were collected by centrifugation. The protein-containing supernatant was separated by 15% SDS/PAGE, and transferred onto a PVDF membrane. The first set of membranes was probed with anti bcl-x_L (Promega), the second with anti-His (Santa Cruz), and the third with anti cytochrome *c*. The bands were detected with corresponding ALP conjugate 2° antibodies and NBT/BCIP.

1.4. Coimmunoprecipitation using HeLa cell stimulated to release cytochrome *c*

Cells were maintained at 37 °C in Dulbecco's modified eagle medium (DMEM, Gibco) supplemented with 10% FCS, 2 mM L-glutamine, 200 μg ml^{-1} penicillin, and 100 μg ml^{-1} streptomycin sulfate in a humidified atmosphere (5% CO_2 / 95% air). At the 70% confluent stage, apoptosis was induced with 10 ng ml^{-1} human TNF together with 10 μg ml^{-1} cycloheximide, and the cells were incubated for 6 h at 37 °C. The media was then replaced by 0.1% trypsin-EDTA (TE), and the flask was incubated at 37 °C for 30 min. The detached cells were rinsed out with 5 ml of the fresh medium, pelleted at 1000 rpm for 5 min, and washed with 1× PBS. Cytosolic extracts were prepared as described earlier by Bossy-Wetzel et al. [22]. Cells (24×10^6) were incubated for 30 min on ice in the lysis buffer (68 mM sucrose, 200 mM mannitol, 50 mM PIPES–KOH, pH 7.4, 50 mM KCl, 1 mM EGTA, 1 mM EDTA, 1 mM DTT, protease inhibitors), lysed with 80 strokes of a dounce eppendorf homogenizer, and centrifuged at 14,000×*g* for 15 min at 4 °C. To the supernatant (cytosolic extract), 50 μg of Bcl-x_L was added, and incubated on a rocker for 3 h at room temperature. 10 μg of monoclonal anti-cytochrome *c* was added to the mixture and incubated for 1 h. The immunocomplex was precipitated with protein-A agarose beads, and blots were developed using monoclonal anti-Bcl-x_L, anti-cytochrome *c*, and anti-His tag. Later, the blots were probed with ALP conjugated 2° anti mouse and detected by NBT/BCIP.

1.5. Induction of caspase-like activity by cytochrome c and the Bcl-x_L–cytochrome c complex

These experiments were conducted using *Spodoptera frugiperda* (*Sf*9) ovarian cells. Four million healthy cells pelleted by centrifugation at 3000 rpm for 5 min, were suspended in 1× PBS, and centrifuged at 1000×*g* for 15 s. The pellet was resuspended in a buffer consisting of 50 mM PIPES–KOH, pH 7.0, 0.2 mM EDTA, 0.2 mM EGTA, 1 mM DTT, 10 μg ml^{-1} pepstatin, 10 μg ml^{-1} aprotinin, and 10 μg ml^{-1} PMSF (400 μL for 10 ml culture), and the cells were allowed to swell on ice for 15 min. Cells were then disrupted with 0.01% NP40 detergent (optimized), vortexed gently, and spun at 1600 rpm for 30 min. The supernatant was spun again at 13000 rpm for 30 min. This final supernatant is the cytosolic extract (CE) required for this set of experiments. The pellet is the nuclear fraction containing the organelles including mitochondria, and was discarded. For measurement of caspase activity, 23 μL CE (~50 μg protein) was combined with 20 μl of the dilution buffer (10 mM PIPES, pH 7.0, 5 mM EGTA, 2 mM $MgCl_2$, 2 mM ATP, 10 mM phosphocreatine, 50 μg/ml creatine kinase), 2 mM dATP, and one of the following: 1 μM cytochrome *c*, 2 μM Bcl-x_L, and a preincubated mixture (1:1 and 1:2) of the two proteins. The control mixture contained none of these; the final volume of each reaction mixture was however made constant to 50 μl. The mixtures were incubated at 37 °C for 1 h, made up to 500 μl with caspase assay buffer (50 mM PIPES, pH 7.0, 0.1 mM EDTA, 10% glycerol, 1 mM DTT), and incubated for another hour after addition of 5 μg Ac-DEVD-AFC substrate. AFC hydrolysis was measured by 490-nm emission (excitation: 400 nm) using a FluoroMax-3 instrument (Jobin-Yvon, Horiba).

1.6. Determination of equilibrium constant for the binding of Bcl-x_L to cytochrome c

Titration experiments were carried out holding cytochrome *c* constant at one of the concentrations in the 1–4 μM range. A set of samples containing a fixed concentration of cytochrome *c* and variable concentration of Bcl-x_L (0–8 μM) was prepared in a pH 7 buffer composed of 50 mM phosphate, 4 mM DTT, and a given concentration of NaCl. This procedure of equilibrium titration annulled dilution effects. Samples were incubated for ~4 h at 22 °C before recording baseline-corrected optical absorption spectra in the 600–400 nm wavelength region using a Cary 100 (Varian) spectrophotometer.

Absorbance at 415 nm, which is the Soret maximum for DTT-reduced cytochrome *c*, was used for binding analysis. The concentration of free Bcl-x_L in the titration mixture is given by

$$[\text{Bcl}-x_L]\text{free} = \frac{[\text{cyt } c] \times \Delta A}{\Delta A_{\infty}} \quad (1)$$

in which, $\Delta A = A_x - A_0$, and $\Delta A_{\infty} = A_{\infty} - A_0$, where A_0, A_x, and A_{∞} are 415-nm absorbances of solutions containing cytochrome *c* alone, cytochrome *c* in the presence of *x* concentration of Bcl-x_L, and cytochrome *c* in the presence of infinite or saturating concentration of Bcl-x_L, respectively. The association constant, K_{ass}, was extracted from the equation

$$\log\left[\frac{\Delta A}{A_{\infty} - A_x}\right] = \log K_{\text{ass}} + \log[\text{Bcl}-x_L]\text{free} \quad (2)$$

The *x*-intercept of the plot of log [$\Delta A/(A_{\infty} - A_x)$] vs. log [Bcl-$x_L$] gives the value of pK_a for cytochrome *c*–Bcl-x_L interaction.

1.7. Equilibrium binding of the Bad BH3 domain to cytochrome c

In this set of experiment, 475 nM cytochrome *c* was titrated out by a fluorescein-labeled Bad BH3 peptide (Calbiochem). The titration was followed by both Soret optical absorbance due to cytochrome *c* as described above, and 535-nm fluorescence emission due to the BH3 peptide (excitation: 485 nm). Absorbance data were analyzed using Eqs. (1) and (2). The binding parameters from the fluorescence data were extracted from the equation

$$y(x) = \frac{c}{1 + 10^{n(x - K_{\text{diss}})}} \quad (3)$$

where, *n* is the number of peptides bound to cytochrome *c*, K_{diss} is apparent dissociation constant, and *c* is the total change in fluorescence normalized to unity. In the concentration range of the peptide (0–7 μM) used for the titration experiment, there was no inner filter effect on the fluorescence emission, since the optical absorbance of the peptide at the excitation wavelength was less than 0.32 in this range of concentrations.

1.8. Stopped-flow kinetics of interaction of Bcl-x_L with cytochrome c

All solutions for kinetic experiments were prepared in 50 mM phosphate, 4 mM DTT, and 50 mM NaCl, pH 7. In a two-syringe mixing procedure, a solution of 24 μM cytochrome *c* was mixed with Bcl-x_L solutions of variable concentration in the 2–12 μM range. The mixing ratio was 1:7. These experiments were done in a Bio-Logic SFM 400 instrument. The temperature was regulated at 22 °C using an external circulating water bath. The traces were analyzed using a single-exponential function: $y(t) = A_{\infty} + A\exp(-kt)$, where *A* is the amplitude, A_{∞} denotes the baseline signal at long times, and *k* is the observed rate constant. The bimolecular binding rate was calculated from the slope of the plot of the observed rate constant as a function of Bcl-x_L concentration.

2. Results

Fig. 1a shows that the nickel column-eluted protein migrates as equal fractions of dimer (D) and monomer (M) on the Sephadex G75 size-exclusion column, consistent with recent reports of homodimers of cytosolic Bcl-x_L [23]. The result indicates that purified Bcl-x_L exists in a slow dynamic equilibrium between the two forms. The monomeric fractions were further chromatographed on a DEAE anion-exchange

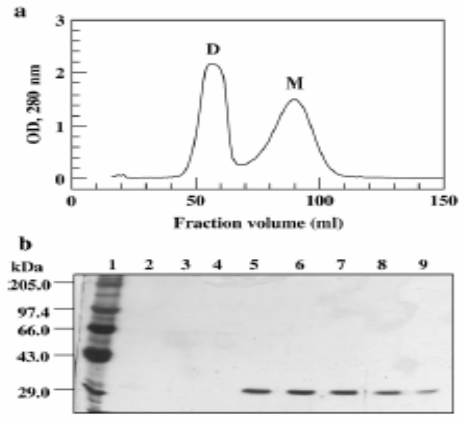

Fig. 1. (a) Sephadex G75 chromatography of the nickel column-eluted fractions show a slow equilibrium of monomeric and dimeric forms. SDS electrophoresis shows that the monomeric fractions also contain smaller molecular weight proteins eluted from the nickel column. Therefore, the monomeric fraction was rechromatographed on an anion-exchange column, and eluted with a linear NaCl gradient. (b) Silver-stained SDS electrophoresis of different fractions from the peak corresponding to Bcl-x_L (0.23 M NaCl) shows >99% purity of the protein. Lane 1 shows the marker proteins.

column, and more than 99% pure protein was obtained, as confirmed by silver-stained SDS/PAGE (Fig. 1b).

To check for the functional activity and binding specificity of the purified human Bcl-x_L, we performed coimmunoprecipitation and immunoblot analyses using anti-cytochrome *c* and anti-Bcl-x_L antibodies. Mitochondria fractionated in a discontinuous Percoll gradient was stimulated to release cytochrome *c* by the use of Ca^{2+} in the wash buffer that contained 70 mM sucrose but no NaCl. We also generated two controls by simply incubating mitochondria in Buffer A containing 125 mM KCl, and in Buffer B containing 250 mM sucrose. Various buffer compositions are detailed under Materials and methods. As determined from the visible absorption spectrum of the supernatants (not shown), only Ca^{2+} induced the release of cytochrome *c*, and the released cytochrome *c* accounted for ~0.12% of the mitochondrial preparation (in terms of protein content) that was subjected to Ca^{2+} induction. We then carried out immunoprecipitation using all three supernatants, each with monoclonal anti-cytochrome *c* as the positive control, and monoclonal anti-capsase-9 as the negative control, and developed each blot with anti-Bcl-x_L, anti-His-tag, and anti-cytochrome *c*. Fig. 2 shows the Western blots. In each, lane 7 shows the pure protein blotted by the corresponding antibody. The supernatant obtained in buffer B that contained no calcium show no trace of cytochrome *c* and Bcl-x_L in both positive (lane 1) and negative (lane 2) immunoprecipitations. Similarly, buffer A did not produce any effect (lanes 3 and 4, corresponding to positive and negative controls, respectively). Lane 5 shows the Ca^{2+}-induced release of cytochrome *c*. Interestingly, this lane also exhibits a relatively faint band for Bcl-x_L detected by anti-Bcl-xL, but not by anti-His-tag, suggesting that traces of endogenous Bcl-x_L residing in mitochondrial membrane may have translocated and precipitated with cytochrome *c*. We notice that the proteins in this lane (lane 5) were immunoprecipitated by using anti-cytochrome *c*. Here, anti-His-tag does not blot Bcl-x_L because the precipitated Bcl-x_L is endogenous. The Ca^{2+}-induced supernatant immunoprecipitated by the use

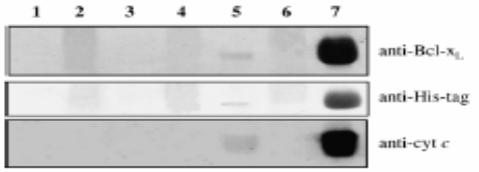

Fig. 2. Effects of buffer A, buffer B, and Ca^{2+} on the translocation of cytochrome *c* from Percoll gradient fractionated healthy mitochondria, and coimmunoprecipitation of Bcl-x_L and cytochrome *c*. Immunoprecipitations from the supernatant were carried out using anti-cytochrome *c* (positive, +) or anti-caspase-9 (negative, −), and developed using anti-Bcl-x_L (upper panel), anti-His-tag (middle panel), and anti-cytochrome *c* (lower panel). Lane descriptions are: 1, buffer B treated (+); 2, buffer B treated (−); 3, buffer A treated (+); 4, buffer A treated (−); 5, Ca^{2+}-induced (+); 6, Ca^{2+}-induced (−); and 7, recombinant Bcl-x_L simply developed with anti-Bcl-x_L (upper panel) and anti-His-tag (middle panel), and cytochrome *c* developed with anti-cytochrome *c* a (lower panel). Further details are given in the text.

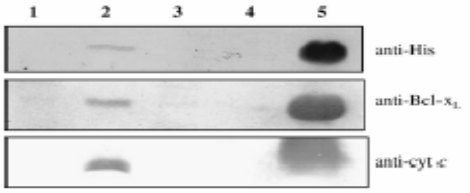

Fig. 3. Western blot showing complex formation between purified human Bcl-x_L and intrinsic HeLa cell cytochrome *c* stimulated to release to the cytosol by treatment with TNF plus cycloheximide. Unstimulated cells were used to perform control experiments. For complexation, 50 μg of purified Bcl-x_L was added to the cytosolic extract, and immunoprecipitated by adding 10 μg of monoclonal anti-cytochrome *c* (positive, +) or anti-caspase-9 (negative, −). Blots were developed using anti-His-tag (upper panel), anti-Bcl-x_L (middle panel), and anti-cytochrome *c* (lower panel). Lane descriptions are: 1, stimulated to apoptose by TNF and cycloheximide (−); 2, stimulated to apoptose by TNF and cycloheximide (+); 3, unstimulated (−); 4, unstimulated (+); and 5, recombinant Bcl-x_L simply developed with anti-His-tag (upper panel) and anti-Bcl-x_L (middle panel), and cytochrome *c* developed with anti-cytochrome *c* a (lower panel).

of anti-caspase-9 (negative control) does not report any protein band (lane 6). These results suggest that cytochrome *c* does bind to Bcl-x_L, whatever may be the mechanism by which the latter is made available in the medium. The His-tagged recombinant protein is detected by both anti-Bcl-x_L and anti-His-tag, and the endogenous form is blotted only by the protein antibody.

To show that Bcl-x_L indeed arrests cytosolic cytochrome *c* in apoptosed cells, we stimulated HeLa cells by using human TNF together with cycloheximide [3], and checked for precipitation of Bcl-x_L with endogenous cytochrome *c* released from mitochondria of the induced cells. About 0.2 μg cytochrome *c* (determined from the visible region absorption spectrum; λ_{max}=415 nm) was released per million of apoptosed cells. Blots were developed using all three antibodies: anti-cytochrome *c*, anti-Bcl-x_L, and anti-His-tag (Fig. 3). In the extract of the apoptosed cells immunoprecipitated by anti-caspase-9 (treated negative) none of the three antibodies detect a band (lane 1). But, as lane 2 shows, all three antibodies detect the corresponding proteins in the immunoprecipitate obtained from the apoptosed cell extract by the use of anti-cytochrome *c* (treated positive). Here also, both anti-His-tag and anti-Bcl-x_L blot the band, because the cell extract was presented with exogenous recombinant Bcl-x_L. Lanes 3 and 4 correspond to negative and positive controls, respectively, of the extract from healthy uninduced cells. Lane 5 presents the bands due to recombinant Bcl-x_L and commercial horse cytochrome *c*; the former blotted by both anti-His-tag and anti-Bcl-x_L, and the latter by anti-cytochrome *c*. These results again demonstrate that Bcl-x_L specifically interacts with cytochrome *c* whenever the latter appears in the medium. Such immunochemical studies of Bcl-x_L–cytochrome *c* interaction have already been reported for human leukemia cells challenged with γ-irradiation [21]. Our results elucidate the phenomenon with more examples by incorporating necessary controls. We conclude that the

cytochrome *c* translocated to cytosol from mitochondria in response to apoptotic stimuli is vulnerable to arrest by Bcl-x_L.

Yet, the major objective of this study is to quantify the binding parameters for Bcl-x_L–cytochrome *c* interaction. To study equilibrium binding in titration experiments, we initially attempted to use the intrinsic fluorescence of Bcl-x_L. Full-length Bcl-x_L is highly fluorescent due to the content of six tryptophan residues, but cytochrome *c* does not fluoresce due to intramolecular excitation energy transfer from its lone tryptophan (W59) to the heme. Therefore, the fluorescence of Bcl-x_L can, in principle, be used to monitor its titration with cytochrome *c*. However, the concentration of cytochrome *c* in the solution (>1.5 μM) needed to achieve a complete titration titrate was found to quench the intrinsic fluorescence of Bcl-x_L. The quenching of Bcl-x_L fluorescence due to cytochrome *c* in the bulk solution obscures the actual change in fluorescence due to the interaction of the two proteins. A control experiment where a lysozyme solution was titrated with cytochrome *c* showed exactly the same behavior, suggesting that fluorescence is not preferred to probe the Bcl-x_L–cytochrome *c* interaction.

We then turned to the measurement of optical absorption of a fixed concentration of cytochrome *c* in the Soret heme region as a function of variable concentration of Bcl-x_L. Fig. 4a shows that the absorbance due to cytochrome *c* increases with increments of Bcl-x_L; for the 3 μM solution of cytochrome *c*, the change in absorbance across the complete titration is 33 milliOD. The difference spectra generated by subtracting the spectrum of cytochrome *c* alone from spectra in the presence of Bcl-x_L (Fig. 4a, inset) show that Bcl-x_L binding causes the absorption peak to shift from 415 to 413.2 nm. These observations suggested that heme optical absorption of cytochrome *c* could be used as a reliable marker to follow its interaction with Bcl-x_L. Fig. 4b shows the plot used for binding analysis as described under Materials and methods. The *x*-intercept of the linear fit of the data yields the association constant, K_{ass}=8.4(±4)×10^6 M^{-1}, indicating tight affinity of cytochrome *c* for Bcl-x_L. The slope of the plot (n=0.6) indicates a 1:1 interaction. The Gibbs free energy for Bcl-x_L–cytochrome *c* interaction ($\Delta G^\circ = -RT \ln K_{ass}$) calculated by using this value of K_{ass} is ~9.3 kcal mol^{-1} at 22°C.

Cytochrome *c* is lysine-rich, and hence highly basic. It is therefore desirable to address as to how its interaction with Bcl-x_L varies with ionic strength and pH. Fig. 4c shows that K_{ass} is maximum at ~80 mM NaCl, and declines by nearly 12-fold in the presence of 600 mM NaCl, suggesting that the physiological ionic strength supports the tightest interaction between the two proteins. The dependence of K_{ass} on pH could not be studied in detail due to alkaline isomerization of cytochrome *c* in basic medium (pH>8), and heme spin change in acid solutions (pH<5). In the accessible range of pH, K_{ass} was found to change little.

The kinetics of protein–protein interactions are of special significance since rates of such interactions often play important regulatory roles. To determine the rate of binding of Bcl-x_L to cytochrome *c* we performed stopped-flow experiments where the time dependence of the change in 415-nm absorbance due to cytochrome *c* was monitored after mixing the two protein solutions. The representative traces labeled 1, 2, and 3 in Fig. 5a show the time dependence of the change in absorbance after mixing 3 μM cytochrome *c* with 6, 4, and 2 μM Bcl-x_L, respectively. The solid lines through the data are single-

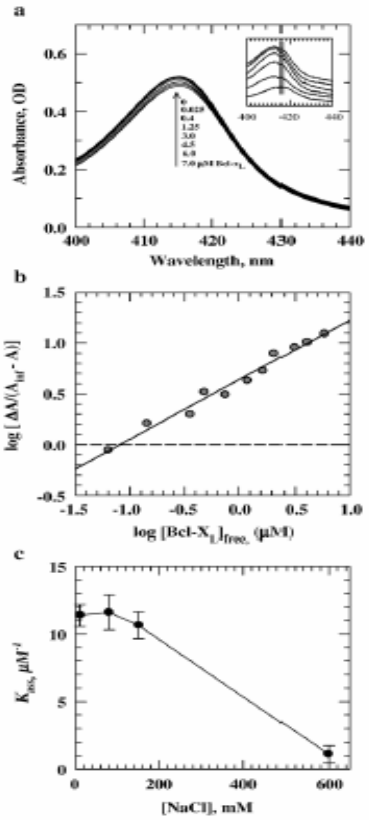

Fig. 4. (a) Absorption spectra of cytochrome *c* in the presence of different concentrations of Bcl-x_L, pH 7, 22 °C, 3.5 mM DTT, 100 mM NaCl. The inset shows difference absorption spectra obtained by subtracting the spectrum of cytochrome *c* alone from the spectra of cytochrome *c* in the presence of different concentrations of Bcl-x_L. (b) The final plot for analysis of binding data, as described under Materials and methods (Eqs. (1) and (2)). The equilibrium association constant, K_{ass} (8.4(±4) μM^{-1}, is calculated from the *x*-intercept of the straight line (pK_{ass}). The slope of the line (n=0.6) indicates a 1:1 binding interaction. (c) The variation of K_{ass} as a function of NaCl concentration in 50 mM phosphate buffer, pH 7, 4 mM DTT, 22 °C. Mixtures of Bcl-x_L and cytochrome *c* were incubated for 2–8 h. Optical absorption spectra were analyzed as described under Materials and methods.

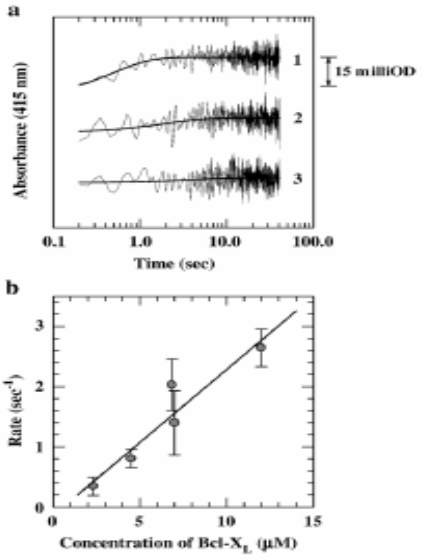

Fig. 5. Kinetics of binding of Bcl-x_L to cytochrome *c* in 50 mM phosphate buffer, pH 7, 4 mM DTT, 22 °C. The concentration of cytochrome *c* was held constant at 3 μM. (a) Representative kinetic traces: labels 1 to 3 correspond to 6, 4, and 2 μM Bcl-x_L, respectively. The solid lines through the data represent single-exponential fits. (b) The rate obtained is proportional to the concentration of Bcl-x_L. The slope of the linear fit through the data yields the bimolecular rate constant for binding, k_{bi}=0.24 μM^{-1} s^{-1}. The error bars represent standard deviations of the rate constants measured with different preparations of Bcl-x_L.

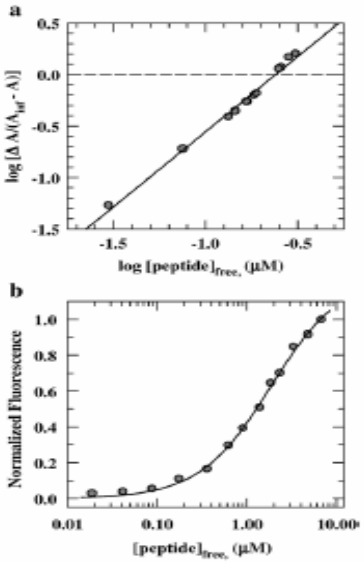

Fig. 6. (a) Analysis of horse cytochrome *c* and Bad BH3 peptide binding (equation 1,2) monitored by the optical absorbance of cytochrome *c*, pH 7, 22 °C, 3.5 mM DTT, 100 mM NaCl. Values of K_{ass} and *n* are 4.1(±1) μM^{-1} and 0.91, respectively. (b) The same binding monitored by fluorescence of the fluorescein-labeled Bad BH3 peptide (Eq. (3)). Values of K_{ass} and *n* extracted from this analysis are 1.2(±0.2) μM^{-1} and 1.3, respectively.

exponential fits, showing clearly that the rate of interaction changes with the concentration of Bcl-x_L. The dependence of the observed rate on the concentration of Bcl-x_L is shown in Fig. 5b, the slope of the linear fit of which yields the bimolecular association rate constant, k_{bi}=0.24×10^6 M^{-1} s^{-1}.

Incorporation of a control experiment is necessary to show that cytochrome *c* does not interact with other proteins indiscriminately. As a negative control, we checked for interaction of Bcl-x_L with myoglobin (the latter was chosen because it resembles cytochrome *c* in containing a heme group and a fairly sizable number of positively charged amino acids), but did not detect any binding. As a positive control, we set to look into the interaction of cytochrome *c* with Bad BH3. Since the BH3 domain is involved in a number of interactions amongst the Bcl-2 family proteins and Bcl-x_L is found to interact with cytochrome *c*, one naively expects binding of the BH3 peptide to cytochrome *c*. We used the optical absorbance of cytochrome *c* (λ_{max} ≈415 nm) to assess this interaction. We also took advantage of the fluorescence emission of the fluorescein-labeled Bad BH3 peptide (λ_{max} ≈496 nm) to monitor the titration of 475 nM cytochrome *c* with increments of the peptide up to 7 μM. In this range of concentration of the peptide, no inner filter effect in the fluorescence of the peptide was detected. The analysis of the titration monitored by the absorbance of cytochrome *c* (Eqs. (1) and (2)) yields K_{ass}=4.1 (±1)×10^6 M^{-1}, indicating rather tight affinity of the BH3 peptide for cytochrome *c* (Fig. 6a), and the slope of 0.91 suggests 1:1 interaction. Values of K_{ass} and *n* extracted from the peptide fluorescence-monitored data (Eq. (3) and Fig. 6b) are 1.2(±0.2)×10^6 M^{-1} and 1.3(±0.1), respectively, fairly consistent with the values obtained from the optical absorbance data.

In another control experiment, we studied the equilibrium binding of Bid with cytochrome *c*. The working rationale was the same as mentioned above in the context of interaction of Bad BH3 peptide with cytochrome *c*. Since the Bid protein

Table 1
K_{ass} values for interactions amongst horse cytochrome *c*, human His_6-tagged Bcl-x_L, and Bad BH3 peptide

Binding interactions	K_{ass} (μM^{-1})	Reference
Bcl-x_L–cytochrome *c*	8.4 (±4)	This work
Bcl-x_L–Bad BH3	46.5	[37]
Bad BH3–cytochrome *c*	2.65 (±1.45)	This work

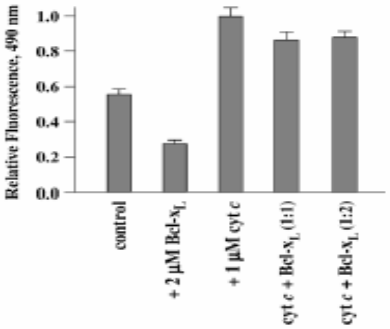

Fig. 7. DEVD-AFC hydrolysis observed in *Sf*9 cell extract after addition of purified human Bcl-x_L, horse cytochrome *c*, and preincubated mixtures of the two. The bars are normalized with reference to the maximum hydrolysis (fluorescence) observed after addition of 1 μM cytochrome *c* (bar 3 from left).

binds both pro- and antiapoptotic proteins, including Bcl-x_L, one expects its interaction with cytochrome *c* as well. Indeed, by titrating 300 nM cytochrome *c* with increments of Bid, we obtained $K_{ass}=4.05(\pm 2.25)\times 10^6$ M^{-1} for this interaction (Table 1). These results suggest that in addition to Bcl-x_L certain pro- and antiapoptotic Bcl-2 proteins may bind to the cytosolic pool of cytochrome *c* in apoptosed cells.

To establish the functional consequence of the interaction of Bcl-x_L and cytochrome *c* in the cytosol we looked at caspase activity promoted by cytochrome *c*. If Bcl-x_L interacts with cytochrome *c*, then caspase activity in response to extrinsically added cytochrome *c* would be diminished when cytochrome *c* and Bcl-x_L are coadded to elicit the activity in cell lysates. Healthy *Sf*9 cell lysate was used to measure caspase activity by monitoring fluorescence of DEVD-AFC (Fig. 7). In the control run (bar 1), no cytochrome *c* was added; the basal caspase activity observed is due to traces of intrinsic cytochrome *c* that leaks out of mitochondria during the lysate preparation. In the presence of 2 μM purified human Bcl-x_L (bar 2), the caspase activity reduces to nearly half of the basal value, suggesting that Bcl-x_L somehow arrests the traces of intrinsic cytochrome *c*. In the presence of 1 μM horse cytochrome *c*, the fluorescence increases two-fold (bar 3) when compared to the control run, indicating that the added cytochrome *c* elicits caspase activity. The use of a preincubated 1:1 or 1:2 mixture of horse cytochrome *c* and human Bcl-x_L also induces DEVD-AFC cleavage; however, compared to the case of cytochrome *c* alone (bar 3), the activity decreases by ~15% (bars 4 and 5), a weak indication of complexation of Bcl-x_L and cytochrome *c*. Although merely 15%, we could not dismiss the decrease by considering the fact that the cell lysate already contains traces of intrinsic cytochrome *c*. Rest of the observed activity is due to a balance of the effects of free forms of Bcl-x_L and cytochrome *c* existing in the protein mixture that was added to the cell lysate. The error bars represent standard deviations determined from three independent experiments. Admittedly, these results are primary, and more experiments need to be performed for a conclusive demonstration that Bcl-x_L can arrest the cytosolic fraction of cytochrome *c* leading to the inhibition of caspase activation.

3. Discussion

3.1. Monomeric and associated forms of Bcl-x_L

The Bcl-2 family proteins are known to homodimerize, heterodimerize, and even homo-oligomerize to exert their survival and death effects [23–30]. Cellular Bcl-x_L, irrespective of cytosolic or mitochondrial location, has been shown to form homodimers or oligomers [31] wherein monomers are able to sequester their C-terminal hydrophobic membrane anchors in the partner BH3-binding pockets [23]. Although the function associated with the homodimer (D) is less well understood, the pro-survival virtue of Bcl-x_L is believed to be a consequence of its existence as homodimers. It is then worth considering as to what extent Bcl-x_L may exist as monomer (M). In our experiments, the purified full length Bcl-x_L shows a M ⇌ D equilibrium, where the equilibration between the two forms are very slow compared to the time of size-exclusion chromatography (Fig. 1b). We have observed this equilibrium consistently in all our preparations, as has also been reported previously [32]. To note is that Bcl-x_L migrates as higher molecular weight large complexes, often with no trace of monomers, if nonionic detergents (Tween 20, for example) are included in the developer buffer [32,33]. The dimerization ability of Bcl-x_L is entirely due to its C-terminal hydrophobic tail, a fact consistent with the observation that Bcl-$x_L\Delta$CT is recovered as a monomer [23]. Two additional observations: (1) the Western blots for Bcl-x_L in healthy Cos-7 and HeLa cell cytosolic extracts show a small fraction of endogenous monomeric form, and (2) the equilibrium binding experiments for Bcl-x_L–cytochrome *c* interaction show a 1:1 complex formation (Fig. 4b), indicate the presence of a monomeric fraction in both endogenous and purified Bcl-x_L preparation. Even if there is no monomeric form, it might as well be that cytochrome *c* causes the dimers to dissociate, just as the proapoptotic Bad shifts the endogenous Bcl-x_L homodimer formation, possibly by direct binding [34], causing translocation of Bcl-x_L to mitochondrial membrane. It will be interesting to know if there are other factors that displace the cytosolic M ⇌ D equilibrium in favor of M that will expose the C-terminal membrane anchor tail and subsequent relocalization to mitochondria.

3.2. Binding of Bcl-x_L to cytochrome *c*

The major finding of this study is a tight 1:1 binding of Bcl-x_L and cytochrome *c*, and it is of interest as to how this affinity compares with those for known protein–protein or protein–peptide interactions involved in survival and death. The apparent binding affinities or dissociation constants ($K_{diss}=1/K_{ass}$) for the interaction of Bcl-x_L with other members of the Bcl-2 family have been reported in the 2–6 μM range at pH 7 [32]. In more recent studies, the apparent K_{diss} values for the

interactions of BH3 peptides from pro-apoptotic Bcl-2 family proteins with Bcl-x_L Δ Cx (truncated at the C-tail by x residues) have been found to fall in the 1–90 nM range [35], suggesting tighter binding, while the affinity of BH3 peptides from anti-apoptotic Bcl-2 family proteins with other survival or killer proteins is relatively low, into micromolar range [36]. Thus the binding of Bcl-x_L with cytochrome c (K_{diss}~120 nM at pH 7) is indeed tight, and is fairly comparable to its affinity for BH3 domains from the anti-survival proteins of the Bcl-2 family. Even the bimolecular/second order rate constants for the binding of Bcl-x_L to cytochrome c (k_{bi}=0.24 μM^{-1} s^{-1}, Fig. 5b) and Bcl-x_L to other Bcl-2 family proteins (k_{bi} in the 0.27–0.34 μM^{-1} s^{-1} range [32]) are nearly identical, implying that these interprotein interactions closely match in terms of binding free energy and the activation energy barrier.

3.3. Cytochrome c–Bad BH3 and cytochrome c–Bid interactions

Another interesting finding is individual binding interactions of cytochrome c with Bad BH3 and Bcl-x_L. The idea that such interactions could exist emanated as a corollary of the BH3-mediated interprotein interactions amongst the Bcl-2 family of proteins, and the high-affinity binding of Bcl-x_L with cytochrome c observed in this study. The binding affinity (K_{diss}=1/K_{ass}) of Bad BH3 for cytochrome c, averaged from optical absorption and fluorescence data (Fig. 6), is 538(±295) nm, which is numerically significantly higher than the value of 21.5 nm reported for the Bad BH3–Bcl-x_L interaction [37,26]. The numerical value for the binding affinity of Bid for cytochrome c (373(±126) nM), on the other hand, is rather smaller than the reported value of 1.9 μM for Bcl-x_L–Bid interaction at neutral pH [32]. This suggests that while the affinity of Bad BH3 for cytochrome c is considerably lower, the affinity of Bid for cytochrome c is higher, both compared with the affinity of cytochrome c for Bcl-x_L (Table 1). Nonetheless, it does appear that the cytosolic pool of cytochrome c is capable of interacting with both pro- and antiapoptotic proteins with varying degrees of affinity. For a more definitive statement, we are in the process of a detailed characterization of the interactions of cytochrome c with several other members of the Bcl-2 family of proteins.

3.4. Possible structural factors for Bcl-x_L and cytochrome c interaction

From parametric similarity of interactions between Bcl-x_L and cytochrome c, and Bcl-x_L and other Bcl-2 family proteins, one may naively assume that Bcl-x_L deploys the same surface to bind cytochrome c as it does for binding with other Bcl-2 family members or the BH3 sequences derived from them. The availability of NMR and X-ray structures of Bcl-x_L [23,38] augments deduction of the structural basis of these interprotein interactions. Muchmore et al. have proposed that an elongated hydrophobic cleft, the constituent residues of which are highly conserved in the Bcl-2 family of proteins, is the site of interaction of Bcl-x_L with death-promoting proteins [38]. Structures of BH3 peptide-bound Bcl-x_L show that the alignment of the BH3 helix along the hydrophobic cleft of Bcl-x_L is stabilized by apolar interactions at the base and polar contacts along the sides of the cleft [39]. Cytochrome c is a highly charged protein with 19 lysine residues most of which are surface exposed. It is likely that the polar residues along the side of the same Bcl-x_L cleft supports charged interactions with cytochrome c. The decrease of the binding affinity for the Bcl-x_L–cytochrome c interaction at high NaCl concentration (Fig. 4c) lends support to this view. Strategic high-resolution surface mapping experiments are underway to test this conjecture.

3.5. How relevant is the Bcl-x_L–cytochrome c interaction for upstream regulation of apoptosis?

From the results of this study together with earlier immunochemical results demonstrating that Bcl-x_L interacts with cytochrome c as a part of the cellular response to ionizing radiation and other genotoxic agents [21], it might seem that this interaction is operative *in vivo* as well. If the interaction indeed exists under cellular conditions, then a regulatory role can be established on the basis of the current understanding of upstream interprotein interactions involving cytochrome c. Once translocated to cytosol in response to an apoptotic stimulus [1,10,15], binds Apaf-1 in the presence of dATP or dADP [10]. The binary complex in turn interacts with procaspase-9, and subsequently cleaves the CED-3-like prodomain of the zymogen form of caspase-9 [40]. The ternary cyt-Apaf-1–caspase-9 complex recruits procaspase-3 and possibly procaspase-7 in quick succession to form a functional apoptosome [2]. Thus, the initial ternary complex formed of cytochrome c, Apaf-1, and caspase-9 (the cyt-Apaf-1–caspase-9 complex) appears to be the hallmark of the initiation of the death cascade [41]. The quantitative and conclusive *in vitro* data presented here leads one to wonder if Bcl-x_L competes with Apaf-1 in order to block the formation of the initial Apaf-1–cytochrome c complex, thereby inhibiting caspase activation.

Unfortunately, there is no conclusive evidence for this regulatory response *in vivo*. If a regulatory role of Bcl-x_L–cytochrome c interaction is granted, the effectiveness of the regulation must be considered in the light of possible affinities of cytochrome c for other Bcl-2 family proteins. For example, some data here indicate variable affinity interactions of cytochrome c with Bid and with Bad BH3. In this perspective, the extent to which Bcl-x_L can arrest cytochrome c to exert a regulatory role would depend on the balance of thermodynamics of various interactions involving the pro- and antisurvival proteins, provided these interactions operate *in vivo*. Clearly, more evidence must be obtained that the Bcl-x_L–cytochrome c interaction is indeed relevant for regulation of apoptosis *in vivo*.

Acknowledgments

We thank Professor J. C. Martinou for the kind gift of purified Bid protein, and the anonymous reviewers for encouraging us to incorporate adequate control experiments. We are grateful to Dr.

Apurva Sarin for kindly providing the wild type Bcl-x_L gene. This work is supported by a Swarnajayanti grant (4/1/2003-SF) to AKB from the Department of Science and Technology, Government of India.

References

[1] R.M. Kluck, E. Bossy-Wetzel, D.R. Green, D.D. Newmeyer, The release of cytochrome *c* from mitochondria: a primary site for Bcl-2 regulation of apoptosis, Science 275 (1997) 1132–1136.
[2] Y. Hu, M.A. Benedict, L. Ding, G. Nunez, Role of cytochrome *c* and dATP/ATP hydrolysis in apaf-1-mediated caspase -9 activation and apoptosis, EMBO J. 18 (1999) 3586–3595.
[3] J.C. Goldstein, N.J. Waterhouse, P. Juin, G.I. Evan, D.R. Green, The coordinate release of cytochrome *c* during apoptosis is rapid, complete and kinetically invariant, Nat. Cell Biol. 2 (2000) 156–162.
[4] R. Eskes, B. Antonsson, A. Osen-Sand, S. Montessuit, C. Richter, R. Sadoul, G. Mazzei, A. Nichols, J.C. Martinou, Bax-induced cytochrome *c* release from mitochondria is independent of the permeability transition pore but highly dependent on Mg^{2+} ions, J. Cell Biol. 143 (1998) 217–224.
[5] X. Luo, I. Budihardjo, H. Zou, C. Slaughter, X. Wang, Bid, a Bcl-2 interacting protein, mediates cytochrome *c* release from mitochondria in response to activation of cell surface death receptors, Cell 94 (1998) 481–490.
[6] M. Narita, S. Shinina, T. Ito, T. Chittenden, R.J. Lutz, H. Matsuda, Y. Tsujimoto, Bax interacts with the permeability transition pore to induce permeability transition and cytochrome *c* release in isolated mitochondria, Proc. Natl. Acad. Sci. U. S. A. 95 (1998) 14681–14686.
[7] D.M. Finucane, E. Bossy-Wetzel, N.J. Waterhouse, T.G. Cotter, D.R. Green, Bax-induced caspase activation and apoptosis via cytochrome *c* release from mitochondria is inhibitable by Bcl-xL, J. Biol. Chem. 274 (1999) 2225–2233.
[8] S. Desagher, A. Osen-Sand, A. Nichols, R. Eskes, S. Montessuit, S. Lauper, K. Maundrell, B. Antonsson, J.C. Martinou, Bid-induced conformational change of Bax is responsible for mitochondrial cytochrome *c* release during apoptosis, J. Cell Biol. 144 (1999) 891–901.
[9] G. Basanez, A. Nechushtan, O. Drozhinin, A. Chanturiya, E. Choe, S. Tutt, K.A. Wood, Y.-T. Hsu, J. Zimmerberg, R.J. Youle, Bax, but not Bcl-x_L, decreases the lifetime of planar phospholipid bilayer membranes at subnanomolar concentrations, Proc. Natl. Acad. Sci. U. S. A. 96 (1999) 5492–5497.
[10] X. Liu, C.N. Kim, J. Yang, R. Jemmerson, X. Wang, Induction of apoptotic program in cell-free extracts: requirement for dATP and cytochrome *c*, Cell 86 (1996) 147–157.
[11] M.G. Vander Heiden, N.S. Chandel, E.K. Williamson, P.T. Schumacker, C.B. Thompson, Bcl-x_L regulates the membrane potential and volume homeostasis of mitochondria, Cell 91 (1997) 627–637.
[12] P. Marchetti, M. Castedo, S.A. Susin, N. Zamzami, T. Hirsch, A. Macho, A. Haeffner, F. Hirsch, M. Geuskens, G. Kroemer, Mitochondrial permeability transition is a central coordinating event of apoptosis, J. Exp. Med. 184 (1996) 1155–1160.
[13] J.C. Martinou, D.R. Green, Breaking the mitochondrial barrier, Nat. Rev., Mol. Cell Biol. 2 (2001) 63–67.
[14] N. Zamzami, G. Kroemer, The mitochondria in apoptosis: how Pandora's box opens, Nat. Rev., Mol. Cell Biol. 2 (2001) 67–71.
[15] J. Yang, X. Liu, K. Bhalla, C.N. Kim, A.M. Ibrado, J. Cai, T-I. Peng, D.P. Jones, X. Wang, Prevention of apoptosis by Bcl-2: release of cytochrome *c* from mitochondria blocked, Science 275 (1997) 1129–1132.
[16] D.G. Breckenridge, D. Xue, Regulation of mitochondrial membrane permeabilization by Bcl-2 family proteins and caspases, Curr. Opin. Cell Biol. 16 (2004) 647–652.
[17] M. Lutter, M. Fang, X. Luo, M. Nishijima, X. Xie, X. Wang, Cardiolipin provides specificity for targeting of tBid to mitochondria, Nat. Cell Biol. 2 (2000) 754–761.
[18] X. Wang, J. Zhang, H.P. Kim, Y. Wang, A.M.K. Choi, S.W. Ryter, Bcl-x_L disrupts death-inducing signal complex formation in plasma membrane induced by hypoxia/reoxygenation, FASEB J. 18 (2004) 1826–1833.
[19] G. Pan, K. O'Rourke, V.M. Dixit, Caspase-9, Bcl-xL, and Apaf-1 form a ternary complex, J. Biol. Chem. 273 (1998) 5841–5845.
[20] Y. Hu, M.A Benedict, D. Wu, N. Inohara, G. Nunez, Bcl-x_L interacts with Apaf-1 and inhibits Apaf-1-dependent caspase-9 activation, Proc. Natl. Acad. Sci. U. S. A. 95 (1998) 4386–4391.
[21] S. Kharbanda, P. Pandey, L. Schofield, S. Israels, R. Roncinske, K. Yoshida, A. Bharti, Z.-M. Yuan, S. Saxena, T. Weichselbaum, C. Nalin, D. Kufe, Role for Bcl-x_L as an inhibitor of cytosolic cytochrome *c* accumulation in DNA damage-induced apoptosis, Proc. Natl. Acad. Sci. U. S. A. 94 (1997) 6939–6942.
[22] E.B. Wetzel, D.D. Newmeyer, D.R. Green, Mitochondrial cytochrome *c* release in apoptosis occurs upstream of DEVD-specific caspase activation and independently of mitochondrial transmembrane depolarization, EMBO J. 17 (1998) 37–49.
[23] J.W. O'Neill, M.K. Manion, B. Maguire, D.M. Hockenbery, Bcl-x_L dimerization by three-dimensional domain swapping, J. Mol. Biol. 356 (2006) 367–381.
[24] J.C. Reed, Bcl-2 and the regulation of programmed cell death, J. Cell Biol. 124 (1994) 1–6.
[25] M.C. Wei, W.Z. Zong, E.H.Y. Cheng, T. Lindsten, V. Panoutsakopoulou, A.J. Ross, K.A. Roth, G.R. MacGregor, C.B. Thompson, S.J. Korsmeyer, Proapoptotic Bax and Bak: a requisite gateway to mitochondrial dysfunction and death, Science 292 (2001) 727–730.
[26] A. Kelekar, B.S. Chang, J.E. Harlan, S.W. Fesik, C.B. Thompson, Bad is a BH3 domain-containing protein that forms an inactivating dimmer with Bcl-x_L, Mol. Cell. Biol. 17 (1997) 7040–7046.
[27] R. Eskes, S. Desagher, B. Antonsson, J.C. Martinou, Bid induces the oligomerization and insertion of Bax into the outer mitochondrial membrane, Mol. Cell. Biol. 20 (2000) 929–935.
[28] M.C. Wei, T. Lindsten, V.K. Mootha, S. Weiler, A. Gross, M. Ashiya, C.B. Thompson, S.J. Korsmeyer, tBid, a membrane targeted death ligand, oligomerizes Bak to release cytochrome *c*, Genes Dev. 14 (2000) 2060–2071.
[29] E.H. Cheng, M.C. Wei, S. Weiler, R.A. Flavell, T.W. Mak, T. Lindsten, S.J. Korsmeyer, Bcl-2, Bcl-x_L sequester BH3 domain-only molecules preventing Bax- and Bak-mediated mitochondrial apoptosis, Mol. Cell 8 (2001) 705–711.
[30] S.C. Ruffolo, G.C. Shore, Bcl-2 selectively interacts with the Bid-induced open conformer of Bak, inhibiting Bak auto-oligomerization, J. Biol. Chem. 278 (2003) 25039–25045.
[31] B. Antonsson, S. Montessuit, B. Sanchez, J.C. Martinou, Bax is present as a high molecular weight oligomer/complex in the mitochondrial membrane of apoptotic cells, J. Biol. Chem. 276 (2001) 11615–11623.
[32] Z. Xie, S. Schendel, S. Matsuyama, J.C. Reed, Acidic pH promotes dimerization of Bcl-2 family proteins, Biochemistry 37 (1998) 6410–6418.
[33] G. Basanez, J. Zhang, B.N. Chau, G.I. Maksaev, V.A. Frolov, T.A. Brandt, J. Burch, J.M. Hardwick, J. Zimmerberg, Pro-apoptotic cleavage products of Bcl-xL form cytochrome *c*-conducting pores in pure lipid membranes, J. Biol. Chem. 276 (2004) 31083–31091.
[34] A.M. Petros, D.G. Nettesheim, Y. Wang, E.T. Olejniczak, R.P. Meadows, J. Mack, K. Swift, E.D. Matayoshi, H. Zhang, C.B. Thompson, S.W. Fesik, Rationale for Bcl-xL/Bad peptide complex formation from structure, mutagenesis, and biophysical studies, Protein Sci. 9 (2000) 2528–2534.
[35] L. Chen, S.N. Willis, A. Wei, B.J. Smith, J.I. Fletcher, M.G. Hinds, P.M. Colman, C.L. Day, J.M. Adams, D.C.S. Huang, Differential targeting of prosurvival Bcl-2 proteins by their BH3-only ligands allows complementary apoptotic function, Mol. Cell 17 (2005) 393–403.
[36] A. Letai, M.C. Bassik, L.D. Walensky, M.D. Sorcinelli, S. Weiler, S.J. Korsmeyer, Distinct BH3 domains either sensitize or activate mitochondrial apoptosis, serving as prototype cancer therapeutics, Cancer Cells 2 (2002) 183–192.
[37] H. Zhang, P. Nimmer, S.H. Rosenberg, S-C. Ng, M. Joseph, Development of a high-throughput fluorescence polarization assay for Bcl-x_L, Anal. Biochem. 307 (2002) 70–75.
[38] S.W. Muchmore, M. Sattler, H. Liang, R.P. Meadows, J.E. Harlan, H.S. Yoon, D. Nettesheim, B.S. Chang, C.B. Thompson, S.-L. Wong, S.C. Ng, S.W. Fesik, X-ray and NMR structure of human Bcl-x_L, an inhibitor of programmed cell death, Nature 381 (1996) 335–341.

[39] M. Sattler, H. Liang, D. Nettesheim, R.P. Meadows, J.E. Harlan, M. Eberstadt, H.S. Yoon, S.B. Shuker, B.S. Chang, A.J. Minn, C.B. Thompson, S.W. Fesik, Structure of Bcl-x_L–Bak peptide complex: recognition between regulators of apoptosis, Science 275 (1997) 983–986.
[40] P. Li, D. Nijhawen, I. Budihardjo, S.M. Srinivasula, M. Ahmad, E.S. Alnemri, X. Wang, Cytochrome c and dATP-dependent formation of Apaf-1/caspase-9 complex initiates an apoptotic protease cascade, Cell 91 (1997) 479–489.
[41] Q. Bao, Y. Shi, Apoptosome: a platform for the activation of initiator caspases, Cell Death Differ. 14 (2007) 56–65.

Glassy Dynamics in the Folding Landscape of Cytochrome *c* Detected by Laser Photolysis†

M. Yadaiah, Rajesh Kumar, and Abani K. Bhuyan*

School of Chemistry, University of Hyderabad, Hyderabad 500046, India

Received October 22, 2006; Revised Manuscript Received December 12, 2006

ABSTRACT: Ferrocytochrome *c* liganded with CO refolds to a nativelike compact state, called the M state, where the non-native Fe^{2+}—CO contact persists. The M state resembles the generic molten globule-like states and can be driven to the native state by pulsed laser photolysis of the CO ligand. The microsecond kinetics measured all across the guanidine hydrochloride unfolding transition of the protein produce a chevron plot with accentuated rollover in the folding limb, suggesting a glass transition of M en route to N. The rate of exit of the folding structure from the kinetic trap(s) limits the overall rate of folding of M to N. Sulfate-induced deceleration of the observed folding rate suggests that the folding structure indeed is transiently frozen in glassy traps. The results connect the post-transition features of the funnel paradigm.

The emergence of theoretical models inspired by the folding of lattice polymers (*1*−*10*) has fuelled the excitement in protein folding research very significantly. These studies have unraveled the complexity of the folding process within the framework of the sequence-based organization of conformational energies into a funnel landscape (*11*). Remarkably, the organization of the energy landscape appears to offer a variety of mechanisms for approaching the folding problem from thermodynamic, kinetic, evolutionary, and sequence-selection viewpoints (*9*). Such developments most definitely invite intense collaboration between theory and experiments. Several theoretical studies already appear to agree closely with experiments regarding the rate-limiting structures, folding intermediates, and speed limit of real proteins (*10*, *12*−*18*). Experimental studies, especially those engaging laser-based kinetic methods (*19*−*22*) and protein engineering approaches (*23*, *24*), have also begun to reciprocate (*25*). A nice illustration of such studies is the recent demonstration of downhill (type 0) folding under native-biased conditions (*26*).

A basic finding of theory is that discrete kinetic intermediates appear very late in folding (*11*). Post-transition late intermediates that are structurally nativelike have been detected independently by native-state hydrogen exchange experiments using cytochrome *c* (*27*−*29*). Even though the modified classical pathway that fits these experimental data is conceptually different from the landscape funnel regarding at least the "barrier mechanism", both enumerate nativelike intermediates. Accordingly, even for an apparently two-state protein like cytochrome *c*, the energy landscape can be rough everywhere along the reaction coordinate, not just near the unfolded state.

Another fundamental element of the funneling process is that folding is dominated by glassy dynamics once the folding ensemble has passed from the compact molten globule-like band over the transition-state region of the funnel. Folding is blocked as long as the protein stays frozen in the kinetic traps, and a reorganization of the misconfigured interactions is required for descending to the native well (*7*, *11*). In the effort of connecting this prediction of the theory, experimental work has focused on the nature of the exponential relaxation during folding, since glass transitions are characterized by stretched exponentials (*30*). Earlier observations of the non-single-exponential nature of folding (*31*, *32*) appeared to indicate glassy dynamics. In more recent ultrafast experiments, helix formation kinetics has been found to be stretched exponential (*33*). On the other hand, single-exponential, and hence nonglassy, kinetics for the folding of protein L at low temperatures has also been reported (*34*). However, simple single-exponential kinetics can often produce rate rollover due to kinetic trapping and glassy dynamics (see below).

This work shows how a molten globule-like late intermediate enters glassy dynamics as the protein runs down the folding funnel. We have used ferrocytochrome *c*, the paradigmatic fast folding, two-state protein that preserves the folding speed even when the native Fe^{2+}—M80 link is replaced with a Fe^{2+}—CO link by using extrinsic CO ligand (*35*, *36*). In the stopped-flow experiment, the CO-liganded protein (carbonmonoxycyt *c*)[1] refolds rapidly with the Fe^{2+}—CO interaction intact. This natively folded species, labeled the M state, exhibits the generic properties of molten globule-like states and was first used in this laboratory to study the protein stiffening effect of subdenaturing concentrations of

† This work was supported by grants from the Department of Biotechnology (BRB/15/227/2001), the Department of Science and Technology (4/1/2003-SF), and the University Grants Commission (UPE Funding), Government of India. A.K.B. is the recipient of a Swarnajayanti Fellowship from the Department of Science and Technology.

* To whom correspondence should be addressed. E-mail: akbsc@uohyd.ernet.in. Phone: 91-40-2313-4810. Fax: 91-40-2301-2460.

[1] Abbreviations: GdnHCl, guanidinium chloride; cyt, cytochrome; ferrocyt, ferrocytochrome; cyt-CO, carbonmonoxide-liganded ferrocytochrome *c*; MG, molten globule.

10.1021/bi062193u CCC: $37.00
Published on Web 02/09/2007

denaturants (*37*, *38*). Pabit et al. (*39*) have elegantly subjected the M state to laser photolysis to investigate the role of internal friction in protein folding. Along the same line, we have employed a nanosecond laser pulse to photodissociate the CO ligand over the entire range of aqueous solubilities of guanidinium hydrochloride (GdnHCl). In the effort to establish the folding dynamics of the molten globule-like state, we treat the kinetic data as a chevron. Analyses indicate that the M ⟶ N folding proceeds via at least one glassy state that gives rise to rate rollover in the chevron plot. For simplicity, we liken this process to the phenomenological M ⟶ I ⟶ N folding, where the I state belongs to a set of trapped intermediates. Further, we show that the misorganized interactions in the I state must be reorganized to achieve the native state and that the energy barrier for the exit from the kinetic trap is fairly high. Overall, the paper highlights the connection between "classic" kinetic models and landscape models.

MATERIALS AND METHODS

Cyt *c* was from Sigma (type VI). Experiments were performed in a strictly anaerobic atmosphere, at 22 °C, in 0.1 M sodium phosphate buffer (pH 7) containing 0.5−3 mM freshly prepared sodium dithionite. The concentration of GdnHCl was determined by refractive indices.

Equilibrium Unfolding. Samples of cytochrome *c* (10−15 μM protein) were prepared in the range of 0−7 M GdnHCl. The solutions were deaerated and reduced under nitrogen with 0.5−1 mM sodium dithionite. The samples were saturated with CO by passing a slow stream of the dry gas into the solutions for 1 min. The tubes were then capped with sleeved rubber stoppers and incubated for ∼45 min. The tryptophan fluorescence excited at 280 nm was measured at 358 nm using a photon counting instrument.

Preparation of the M State (*the CO-liganded nativelike ferrocytochrome c*). Cytochrome *c* (0.6 mM), initially dissolved in 6.35 M GdnHCl and 0.1 M phosphate (pH 7), was deaerated, reduced, and liganded with CO. Ferrocyt *c* thus obtained (called UCO) is completely unfolded. UCO was then diluted at least 20-fold by transferring a required volume of the solution into a cuvette containing 2 mL of the degassed and dithionite-reduced CO-free refolding buffer [0.1 M phosphate (pH 7) at 22 °C containing the desired solvent additive]. This procedure allows complete refolding of ferrocyt *c* to the M state. The M-state preparation was used up as quickly as possible, usually within 5 min.

Stopped-Flow Kinetics of the UCO ⇌ M Reaction. Cytochrome *c* (318 μM), initially unfolded in 6.35 M GdnHCl (pH 7) and reduced under nitrogen with 3.2 mM sodium dithionite, was reacted with CO. The CO-saturated unfolded protein solution contained in a gastight syringe was mounted on the stopped-flow mixing module and equilibrated at 22 °C for ∼20 min. Similarly, the dithionite-reduced refolding buffer that did not contain CO was also mounted and equilibrated at the same temperature. Folding was initiated by two-syringe mixing (1:7 protein:buffer ratio) with a total flow rate of 8 mL/s. This procedure ensures minimal air oxidation of the protein. The final protein concentration in the refolding mixture was 39 μM.

The same procedure was used for unfolding experiments. The M state was prepared by 45-fold dilution of the UCO solution following the procedure described above. The final protein concentration was ∼3 μM. A Bio-Logic SFM 400 instrument was used.

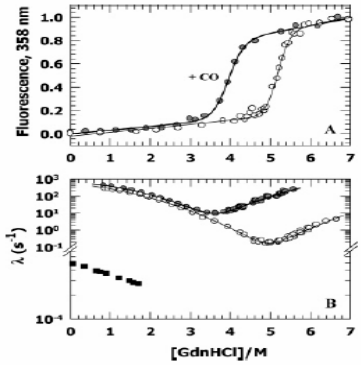

FIGURE 1: (A) Equilibrium unfolding of ferrocyt *c* illustrating the mass action effect of CO. Values of ΔG° (kilocalories per mole) and m_g (kilocalories per mole per molar) obtained from standard two-state analysis are 11 ± 1 and 2.95 ± 0.2 in the presence of CO and 19 ± 0.5 and 3.6 ± 0.2 in the absence of CO, respectively. (B) Effect of the Fe^{2+}−CO interaction on the millisecond folding chevron. In the presence of CO, the chevron is shifted both horizontally and vertically. The refolding rate is only marginally affected. To account for curvatures in the chevron limb, the data were fitted assuming a quadratic dependence of rates on the denaturant. Also shown is the denaturant dependence of the rate of thermal dissociation of CO from the NCO or M state (■).

Laser Photolysis and Microsecond Kinetics of the M ⟶ N Reaction. The M-state preparation contained in a tightly capped quartz cuvette was equilibrated for 3 min at the desired temperature in the spectrometer cuvette holder. CO photolysis was achieved by irradiation with 90 ± 10 mJ pulses of the 532 nm second-harmonic output of a Spectra Physics Q-switched Nd/YAG laser (10 Hz). Spectral changes at 550 nm following the photolysis pulse were recorded with a pulsed Xe lamp. Photolysis was nearly complete, since another laser shot pulsed immediately afterward produced insignificant spectral changes. A fresh sample was used for each single-pulse kinetic trace. For each concentration of GdnHCl, four or five kinetic traces were taken. The basic configuration of the instrument is based on the Applied Photophysics laser-flash photolysis spectrometer. The temperature of the cuvette holder was maintained by using an external circulating water bath.

RESULTS AND DISCUSSION

Routing Ferrocytochrome c to a Molten Globule-like M State. The Fe^{2+}−M80 covalent link of ferrocyt *c*, which is very stable under physiological conditions, weakens when the protein is destabilized, thereby allowing the binding of exogenous ligands such as CO and NO to the heme iron. Figure 1a illustrates the effect of preferential binding of CO to the unfolded state on the GdnHCl-induced transition of ferrocyt *c* at 22 °C. CO binds tightly to the unfolded protein

($K_a \sim 21\ \mu M^{-1}$) and lowers the folding free energy by ~8.1 kcal/mol.

When the unfolded protein solution liganded with CO (UCO) is diluted into a refolding medium, the protein collapses and forms a nativelike "intermediate" state (NCO or M) in which the Fe^{2+}—CO interaction persists for a considerably long time. The NCO state can also be driven to unfold when the solution is transferred to the unfolding buffer. Figure 1b shows that the millisecond rates for the refolding of UCO are only marginally faster than those for the unfolded protein without CO (U). The unfolding rates of NCO are, however, much faster. Because the concentration of CO in the final refolding medium is substantially low and the Fe^{2+}—M80 interaction is preferred over the Fe^{2+}—CO interaction, the trapped CO escapes as thermal motions facilitate the dissociation of the Fe^{2+}—CO bond. The time constant for this thermal process (NCO → N + CO) measured by changes in optical absorbance at 550 nm is ~45 min (Figure 1b and refs *37* and *38*). The thermally activated CO dissociation limits the overall UCO → N refolding and thus renders the NCO → N part of the refolding reaction invisible. The NCO → N process can, however, be captured by recording the kinetics of conformational changes following photodissociation of CO.

The differences in kinetics of the UCO ⇌ NCO and U ⇌ N reactions suggest that NCO and N are energetically and structurally somewhat disparate. From simple thermodynamic calculations using the data shown in Figure 1a, and the comparison of spectral signatures of N and NCO, provided as Supporting Information, it can be shown that (i) NCO is less stable than N by ~2 kcal/mol (*35*) and (ii) it fairly fits into the molecular organizational definition of the classic molten globule (MG) state (*40*, *41*). The fluorescence and far-UV CD spectra of NCO are nearly identical to those for N. The near-UV CD absorption of NCO is, however, substantially weaker than that for N. Also, the ^1H NMR spectra of NCO and the alkali MG state of ferrocytochronme *c* match very closely (data provided as Supporting Information). These observations suggest that NCO represents a compact and largely mobile molecular state containing nativelike secondary structure and hydrodynamic radius, but without rigid tertiary structure. To emphasize such similarities of NCO and MG states, we call NCO the M state. Thus, the study reports on the reaction kinetics of the late molten globule-like M state (M → N) and relates the observed behavior to the predictions of the funnel paradigm.

M → N Kinetics Observed by Laser Photolysis. As mentioned above, the M → N process is difficult to study, because the folding kinetics are rate-limited by very slow thermal dissociation of the Fe^{2+}—CO bond. In the photodissociation protocol, the CO dissociation occurs in the subpicosecond regime so that the slower relaxations associated with the dynamics of side chain folding can be conveniently monitored. Figure 2a shows the microsecond kinetics of the M → N transition in 0.85 M GdnHCl initiated by a single-pulse laser photolysis. The time evolution of the optical absorbance of N is adequately described by a single exponential with a rate constant (k_f) of $1.7 \times 10^5\ s^{-1}$ ($\tau = 5.9\ \mu s$). Rates measured at several concentrations of GdnHCl all across the unfolding transition of ferrocyt *c* are plotted in Figure 2b. Clearly, k_f rolls over in the pretransition region (<2.6 M GdnHCl) where ferrocyt *c* is most stable but

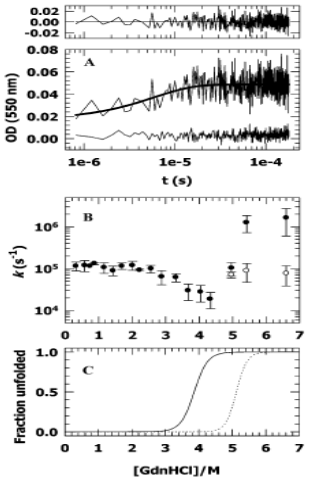

FIGURE 2: Microsecond kinetics for the folding of M. (A) Single-pulse laser photolysis of CO from the M state in the presence of 0.85 M GdnHCl. Subsequent laser shots produce no change in absorbance (bottom trace), indicating that the folded protein does not rebind CO under the conditions of low gas pressure and strongly refolding solvent. The residual in the top panel indicates that the relaxation is adequately monophasic ($k_f = 1.7 \times 10^5\ s^{-1}$; $\tau = 5.9\ \mu s$). (B) Chevron plot for the folding of the M state. As described in the text, the biphasic relaxations under the unfolding conditions (>4.5 M GdnHCl) correspond to ligand exchange dynamics reported previously (*39*—*41*). That the rates measured in <4.5 M GdnHCl correspond to refolding relaxations is consistent with the CO-induced shift in the unfolding transition of ferrocyt *c* (C).

decreases rapidly as progressively destabilizing conditions are employed. The decrease continues to the region where the CO-liganded protein is unfolded, but the unliganded protein is not. Passing this, the transition region of ferrocyt *c* is approached (>4.4 M GdnHCl) where the postphotolysis kinetics begins to accelerate in two distinct phases. These two phases are assigned to, in decreasing order of rate coefficient, transient bindings of methionines (M65 and M80) and histidines (H18 and H33) to the heme iron, consistent with earlier studies of postphotolysis chain dynamics (*19*, *42*—*44*). The biphasic relaxation following CO photolysis is the hallmark of heme—polypeptide dynamics in the unfolded state of ferrocyt *c*. Thus, the rates in the range of 0—4.4 M GdnHCl contain the information relevant to the M → N conformational transition. We note that the rate constant for this transition extracted by linear extrapolation of the rate data from the transition region to the ordinate is $\approx 1 \times 10^6\ s^{-1}$ for k^o_{MI} ($\tau = 1\ \mu s$). This is the fastest achievable rate for the M → N transition in the absence of a trapped intermediate and is within the range set for limited structural events, including local hydrophobic collapse (*45*), and the folding of the model peptide α-helix (*46*—*48*) and β-hairpin fragment (*49*). It also closely matches the rate of

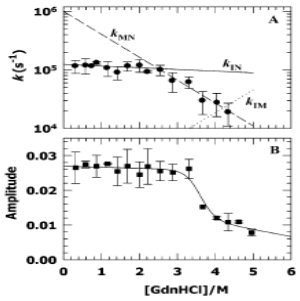

FIGURE 3: (A) Rate rollover in the folding limb can be explained on the basis of glassy dynamics. The exit of the frozen folding structures from kinetic traps limits the overall folding rate, giving rise to rate rollover. Within the framework of classical chemical kinetics, the phenomenon is illustrated with the minimal M ⇌ I ⇌ N scheme. From the denaturant dependencies of the microscopic rate constants, calculated by diagonalizing the rate matrix, the rate constants in water (inverse seconds) and $m^{\ddagger}$ values (kilocalories per mole per molar) for the four processes are as follows: $k^{\circ}_{MI} = 1 \times 10^{6}$, $m^{\ddagger}_{MI} = -0.5$, $k^{\circ}_{IM} = 500$, $m^{\ddagger}_{IM} = 0.5$, $k^{\circ}_{IN} = 1.24 \times 10^{5}$, $m^{\ddagger}_{IN} = -0.037$, $k^{\circ}_{NI} = 10$, and $m^{\ddagger}_{NI} = 0.037$. (B) Dependence of the amplitude of the microsecond relaxation process fits to the equilibrium unfolding transition of CO-liganded ferrocyt *c* (ΔG°=10.34 kcal mol^{-1}, and m_g=2.92 kcal mol^{-1} M^{-1}. This analysis would appear inconsistent, from the viewpoint of traditional analysis, with transient trapping of the intermediate I (but see the text).

local tertiary conformational changes following laser photolysis of carbonmonoxyhemoglobin (*50*).

Rate Rollover and Accumulation of Kinetic Intermediates. The thermodynamically distinct molten globule-like nature of the M state facilitates analysis of the rate−stability data within the formalism of a folding chevron. The rate rollover under strongly nativelike conditions is a distinctive feature of the chevron plot for the M → N transition (Figure 3a). Rollover to varying extents has been observed for numerous proteins, as illustrated in Figure 1b for ferrocyt *c* and carbonmonoxycyt *c*, although the refolding limb of nitrosylcyt *c* does not exhibit this phenomenon (*36*). Unfortunately, a clear understanding of curvatures in the plot of the logarithm of folding rates versus denaturant concentration is lacking. A number of factors, individually or in combination, may be associated with rollover in a case specific manner. In the funnel paradigm, a protein whose energy landscape in the absence of denaturant is sufficiently smooth should not exhibit a rollover, as observed for nitrosylcyt *c* (*36*), CspB (*51*), and CI2 (*52*). Analyses of coarse-grained protein chain models indicate that rollover may result from an internal frictional effect that impedes chain motions under strongly nativelike conditions (*53*−*55*). Using the principles of classical kinetics, the rollover has been explained by invoking the accumulation of at least one structural intermediate whose slower rate of folding limits the observed folding rate (*56*). Yet another possible cause for rollover is a broad energy barrier that separates the native state from the initial state. The rate-limiting transition-state ensemble which is the highest point on the barrier energy profile moves toward the unfolded state when nativelike conditions are approached, giving rise to rate rollover in the refolding limb of the chevron. This model was used to explain chevron curvature for the two-state protein U1A (*57*). Indeed, these subtly different explanations convey the same general picture that folding decelerates because of roughness toward the bottom of the funnel. A contribution to the roughness may come from one or more stable intermediates as exemplified by extensive native-state hydrogen exchange data on ferricyt *c* (*27*, *29*), kinetic traps set up by non-native interactions that may originate from nonspecific collapse of the initial unfolded state or from proline isomerization, and internal frictional effects that are intensified by frustrating interactions causing the traps to deepen. From this synthesis, we attribute the accentuated rollover in the folding chevron of the M → N transition to at least one kinetic trap, the structural nature and the causative interactions of which stand to scrutiny. In phenomenological terms, the minimalist scheme is then M ⇌ I ⇌ N, where I is a trapped intermediate that occupies an energy well. The microscopic rate constants shown in Figure 3a represent one of the eigenvalue solutions of the kinetic model. At higher denaturant concentrations where the intermediate is destabilized, the denaturant function of the observed rate is linear, and the rate constant measured is that for the two-state M → N transition, k_{MN}. Linear extrapolation of k_{MN} values to the ordinate provides the fastest rate for the folding of ferrocytochrome *c*. The phenomenological three-state nature of the M → N transition becomes visible only when the glassy trap deepens under strongly nativelike conditions reflected by the chevron rollover.

The amplitude of the single-phase microsecond spectral change as a function of GdnHCl is shown in Figure 3b. In this time regime, we do not observe denaturant-dependent missing amplitude. Any ultrafast signal decay, which is beyond the resolution of our spectrometer, can be attributed to heme-associated electronic structural changes immediately after photodissociation of CO. The denaturant-dependent changes in the observed amplitude (Figure 3b) are as expected from the observed mass action effect of CO on the unfolding transition of ferrocyt *c* (Figure 2c). The denaturant−amplitude data best fit a two-state M → N transition (Figure 3b), the iterated fit parameters for which are within 12% of the values obtained from independently measured data. Clearly, this is not a fit to the M ⇌ I ⇌ N model, nor is it consistent with the missing amplitude analysis for accumulation of intermediates (*56*, *58*). The observation of chevron rollover with no missing amplitude might appear to make the existence of I doubtful. While the rollover in the rate-denaturant data suggests the intermediate state, the denaturant distribution of the decay amplitude does not. However, the visible optical probe employed here (550 nm) may be silent to a possible tertiary structural change associated with the formation of I that leads the M80 ligation event. An illustration of this point is found in the recent "downhill folding" experiments with the λ_{6-85} protein (*26*). Also, spectra of deligated or five-coordinate hemes could be quite complex (*59*), and optical changes as a result of local tertiary structural adjustments in the photoproduct are not assured. Further, missing amplitude is not a necessary and sufficient criterion for chevron rollover. Simple single-exponential folding kinetics, which become increasingly insensitive to denaturant as strongly nativelike conditions are approached, can often produce rate rollover and reveal kinetic

trapping and glassy dynamics (*53*). The data presented in panels a and b of Figure 3 are consistent with this interpretation of the folding transition.

Although the data available at this point are not quite adequate to provide mechanistic insights into the M → N transition, a simple model may be contemplated on the basis of what is expected to happen in the photoproduct. As established by a number of seminal photodissociation studies of CO-bound heme proteins (*60*−*64*), protein tertiary conformational changes emerge only in nanoseconds or longer. This time is well within the range expected for local structural organization (*45*), or for fast folding of short loops, helices, and side chains (*33*, *65*). The time range of ∼10−500 ns has been associated with an adjustment of the local tertiary structure into the void created by the departing CO ligand in hemoglobin (*50*). It is likely that such a structural rearrangement that is perhaps spectrally silent occurs in the photolyzed product of the M state, leading to transient accumulation of the species labeled I. Further folding involves the native-state M80 ligation to the heme iron and is limited by reorganization of presumably misfolded side chain elements to facilitate the formation of a contact between Fe^{2+} and the sulfur of M80. This speculative model must be treated cautiously before a more complete picture of postphotolysis dynamics is obtained.

The Reverse Sodium Sulfate Effect for I → N Folding Suggests that I Is a Trapped Misfolded Intermediate. To understand the nature of the tertiary interactions in I, we measured the folding rate as a function of the stabilizing salt, Na_2SO_4. The rationale was that Na_2SO_4, which is known to stabilize intermediate species (*66*), would retard the rate of I → N conversion if I contained tertiary interactions that were not nativelike. In a folding scenario in which the interactions become increasingly nativelike (Q) as the protein runs down the funnel, Na_2SO_4 will stabilize a transition state with a higher Q value more than a state that is less compact. Consequently, the rate will increase with an increase in the Na_2SO_4 concentration. As Figure 4a shows, at a constant GdnHCl concentration (0.3 M), the measured I → N folding rate decreases monotonously with an increase in the concentration of Na_2SO_4, suggesting that the transition state (TS) for the I → N segment exposes more surface area than the I state. The addition of sulfate stabilizes the I state with respect to the TS because I is the more compact state, the consequence being a decrease in the observed folding rate. By this explanation, to achieve the correct conformation with respect to the N state, an unfolding event that would disperse the incorrect organization in the I state is necessary. Accordingly, the intermediate could be regarded as a trapped misfolded structure, a prototype of dynamically frozen late intermediates predicted by the funnel theory (*11*). The emerging picture then is that in response to the exit of the photolyzed CO ligand, the tertiary structure of the M state configures nonspecifically to give rise to the I state. One or more interactions in I are geometrically and (or) energetically frustrated; they act as kinetic traps, and the rate of their reorganization into the correct state limits the formation of the native Fe^{2+}−M80 bond.

Fairly Sizable Energy Barrier for I → N Folding. To estimate the energy scale for the interactions that must be reconfigured to establish the N state, we looked at the temperature dependence of I → N folding (Figure 4b).

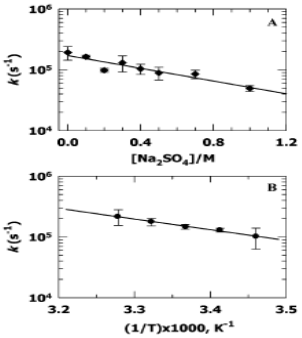

FIGURE 4: (A) Monotony of the decrease in the I → N folding rate with increments of Na_2SO_4 in the folding milieu which suggests that I is indeed misfolded. The transition state from I to N thus exposes relatively more surface area, with the consequence that it is stabilized less by sulfate. (B) Barrier for the I → N transition is substantial ($E_a = 8 \pm 1$ kcal/mol), consistent with the observation that the transition state is weakly stabilized by sulfate.

Assuming the applicability of the thermally activated rate law, the derived activation energy $E_a = 8 \pm 1$ kcal/mol and the prefactor $A_o \sim 1.2 \times 10^{11}$ s^{-1}. Such a strong temperature dependence is conceivable at very late stages of folding where intrachain reorganizations of the kind pondered here are necessary. The conformational energy difference between I and N is just approximately a few k_BT; I is less mobile and is as compact as N, implying no significant enthalpic and entropic mismatch in I. The observed barrier energy then is likely to originate from substantial reorganization of nonnative interactions in I. The TS is thus relatively more unfolded, little stabilized by sulfate, and is sizable in energy. Similar strong thermal activation and a large Arrhenius prefactor have been reported for α-helix formation in a photoswitchable peptide that displays stretched exponential, and the authors relate the observed thermal activation to multiple local barriers between misfolded microstates or, equivalently, to activated diffusion on a rugged energy landscape (*33*).

Glassy Folding of the M State of Ferrocyt c. The conclusions reached here are consistent with at least two earlier studies. Theoretical studies of Chan and co-workers (*53*, *54*, *67*) show that rollover in the folding chevron may often be a consequence of kinetic traps, and hence glassy dynamics under nativelike conditions. The role of internal friction effect under nativelike conditions is also documented by the experiments of Hagen and co-workers (*39*). While the results of this study agree with theirs, it is also shown here that chain misconfiguration at very late stages of folding intensifies the frictional effects producing rate rollovers and glassy dynamics for cytochrome *c*. Misconfiguration and the consequent geometric frustration deepen the energy minima and obviously produce more drag forces. Kinetic traps and internal friction are related phenomena. Internal friction could be considered a kinetic trap because it decelerates folding, but kinetic traps are more direct manifests of chain misorganization. They make the landscape rugged because energy

barriers to chain reorganization giving rise to drag forces exist. It is interesting to note that varying degrees of internal friction persist at all stages of folding. Even the native state experiences internal friction, because the protein structure in solution is dynamic. Thus, a perfectly smooth folding funnel should not exist. The energy landscape theory does find that the folding funnel is generally rugged toward the bottom where molten globule-like states have already crossed over the glass transition-state region (*1*, *3*, *11*). In a highly rugged funnel where the minima are deeper than a few k_BT, folding becomes glassy and decelerates because of transient trapping of structures in the local minima. Folding of these structures containing non-native interactions will be dominated by the rate of their exit from the kinetic traps. The data for the folding of the molten globule-like M state corroborate these predictions, although we still do not have complete information about the structural changes involved in the M ⟶ I transition. The frustrated interactions that trap the I-like microstates and whose reorganization limits the folding within this segment of the folding coordinate remain to be investigated. Finally, the overall folding rate of a protein could be limited by such late glass transitions only if the earlier folding events are faster than the rate of exit from the glassy traps.

SUPPORTING INFORMATION AVAILABLE

Basic spectral data, including one-dimensional proton NMR spectra, for the NCO or M state. This material is available free of charge via the Internet at http://pubs.acs.org.

REFERENCES

1. Bryngelson, J. D., and Wolynes, P. G. (1987) Spin-glasses and the statistical mechanics of protein folding, *Proc. Natl. Acad. Sci. U.S.A. 84*, 7524−7528.
2. Onuchic, J. N., Wolynes, P. G., Luthey-Schulten, Z., and Socci, N. D. (1995) Toward an outline of the topography of a realistic protein-folding funnel, *Proc. Natl. Acad. Sci. U.S.A. 92*, 3626−3630.
3. Bryngelson, J. D., Onuchic, J. N., Socci, N. D., and Wolynes, P. G. (1995) Funnels, pathways and the energy landscape of protein folding: A synthesis, *Proteins 21*, 167−195.
4. Thirumalai, D., Ashwin, V., and Bhattacharjee, J. K. (1996) Dynamics of random hydrophobic-hydrophilic copolymers, *Phys. Rev. Lett. 77*, 5385−5388.
5. Dill, K. A., and Chan, H. S. (1997) From Levinthal to pathways to funnels, *Nat. Struct. Biol. 4*, 10−19.
6. Nymeyer, H., Garcia, A. E., and Onuchic, J. N. (1998) Folding funnels and frustration in off-lattice minimalist protein landscapes, *Proc. Natl. Acad. Sci. U.S.A. 95*, 5921−5928.
7. Socci, N. D., Onuchic, J. N., and Wolynes, P. G. (1998) Protein folding mechanisms and the multidimensional folding funnel, *Proteins 32*, 136−158.
8. Schonbrun, J., and Dill, K. A. (2003) Fast protein folding kinetics, *Proc. Natl. Acad. Sci. U.S.A. 100*, 12678−12682.
9. Onuchic, J. N., and Wolynes, P. G. (2004) Theory of protein folding, *Curr. Opin. Struct. Biol. 14*, 70−75.
10. Wolynes, P. G. (2005) Energy landscapes and solved protein-folding problems, *Philos. Trans. R. Soc. London, Ser. A 363*, 453−467.
11. Wolynes, P. G., Onuchic, J. N., and Thirumalai, D. (1995) Navigating the folding routes, *Science 267*, 1619−1620.
12. Lazaridis, T., and Karplus, M. (1997) "New view" of protein folding reconciled with the old through multiple unfolding simulations, *Science 278*, 1928−1931.
13. Dobson, C. M., Sali, A., and Karplus, M. (1998) Protein folding: A perspective from theory and experiments, *Angew. Chem., Int. Ed. 37*, 868−893.
14. Nymeyer, H., Socci, N. D., and Onuchic, J. N. (2000) Landscape approaches for determining the ensemble of folding transition states: Success and failure hinge on the degree of frustration, *Proc. Natl. Acad. Sci. U.S.A. 97*, 634−639.
15. Clementi, C., Jennings, P. A., and Onuchic, J. N. (2000) How native-state topology affects the folding of dihydrofolate reductase and interleukin-β, *Proc. Natl. Acad. Sci. U.S.A. 97*, 5871−5876.
16. Koga, N., and Takada, S. (2001) Roles of native topology and chain-length scaling in protein folding: A simulation study with a Go-like model, *J. Mol. Biol. 313*, 171−180.
17. Garcia, A. E., and Onuchic, J. N. (2003) Folding a protein in a computer: An atomic description of the folding/unfolding of protein A, *Proc. Natl. Acad. Sci. U.S.A. 100*, 13898−13903.
18. Pogorelov, T. V., and Luthey-Shulten, Z. (2004) Variations in the fast folding rates of the λ-repressor: A hybrid molecular dynamics study, *Biophys. J. 87*, 207−214.
19. Jones, C. M., Henry, E. R., Hu, Y., Chan, C. K., Luck, S., Bhuyan, A., Roder, H., Hofrichter, J., and Eaton, W. A. (1993) Fast events in protein folding initiated by nanosecond laser photolysis, *Proc. Natl. Acad. Sci. U.S.A. 90*, 11860−11864.
20. Williams, S., Causgrove, T. P., Gilmanshin, R., Fang, K. S., Callender, R. H., Woodruff, W. H., and Dyer, R. B. (1996) Fast events in protein folding: Helix melting and formation in a small peptide, *Biochemistry 35*, 691−697.
21. Goldbeck, R. A., Thomas, Y. G., Chen, E., Esquerra, R. M., and Kliger, D. S. (1999) Multiple pathways on a protein-folding energy landscape: Kinetic evidence, *Proc. Natl. Acad. Sci. U.S.A. 96*, 2782−2787.
22. Snow, C. D., Nguyen, N., Pande, V. S., and Gruebele, M. (2002) Absolute comparison of simulated and experimental protein-folding dynamics, *Nature 420*, 102−106.
23. Matouschek, A., Kellis, J. T., Serrano, L., and Fersht, A. R. (1989) Mapping the transition state and pathway of protein folding by protein engineering, *Nature 340*, 122−126.
24. Fersht, A. R. (1997) Nucleation mechanism in protein folding, *Curr. Opin. Struct. Biol. 7*, 3−9.
25. Zong, C., Wilson, C. J., Shen, T., Wolynes, P. G., and Wittung-Stafshede, P. (2006) ϕ-Value analysis of apo-azurin folding: Comparison between experiment and theory, *Biochemistry 45*, 6458−6466.
26. Ma, H., and Gruebele, M. (2005) Kinetics are probe-dependent during downhill folding of an engineered λ_{6-85} protein, *Proc. Natl. Acad. Sci. U.S.A. 102*, 2283−2287.
27. Bai, Y., Sosnick, T. R., Mayne, L., and Englander, S. W. (1995) Protein folding intermediates: Native-state hydrogen exchange, *Science 269*, 192−197.
28. Englander, S. W., Sosnick, T. R., Mayne, L. C., Shtilerman, M., Qi, P. X., and Bai, Y. (1998) Fast and slow folding in cytochrome c, *Acc. Chem. Res. 31*, 737−744.
29. Hoang, L., Bédard, S., Krishna, M. M. G., Lin, Y., and Englander, S. W. (2002) Cytochrome c folding pathway: Kinetic native-state hydrogen exchange, *Proc. Natl. Acad. Sci. U.S.A. 99*, 12173−12178.
30. Angell, C. A. (1995) Formation of glasses from liquids and biopolymers, *Science 267*, 1924−1935.
31. Morozova-Roche, L. A., Jones, J. A., Noppe, W., and Dobson, C. M. (1999) Independent nucleation and heterogeneous assembly of structure during folding of equine lysozyme, *J. Mol. Biol. 289*, 1055−1073.
32. Leeson, D. T., Gai, F., Rodrigues, H. M., Gregoret, L. M., and Dyer, R. B. (2000) Protein folding and unfolding on a complex energy landscape, *Proc. Natl. Acad. Sci. U.S.A. 97*, 2527−2532.
33. Bredenbeck, J., Helbing, J., Kumita, J. R., Wooley, G. A., and Hamm, P. (2005) α-Helix formation in a photoswitchable peptide tracked from picoseconds to microseconds by IR spectroscopy, *Proc. Natl. Acad. Sci. U.S.A. 102*, 2379−2384.
34. Gillespie, B., and Plaxco, K. W. (2000) Nonglassy kinetics in the folding of a simple single-domain protein, *Proc. Natl. Acad. Sci. U.S.A. 97*, 12014−12019.
35. Bhuyan, A. K., and Kumar, R. (2002) Kinetic barriers to the folding of horse cytochrome c in the reduced state, *Biochemistry 41*, 12821−12834.
36. Prabhu, N. P., Kumar, R., and Bhuyan, A. K. (2004) Folding barrier in horse cytochrome c: Support for a classical folding pathway, *J. Mol. Biol. 337*, 195−208.
37. Bhuyan, A. K. (2002) Protein stabilization by urea and guanidine hydrochloride, *Biochemistry 41*, 13386−13394.
38. Kumar, R., Prabhu, N. P., Yadaiah, M., and Bhuyan, A. K. (2004) Protein stiffening and entropic stabilization in the subdenaturing limit of guanidine hydrochloride, *Biophys. J. 87*, 2656−2662.

39. Pabit, S. A., Roder, H., and Hagen, S. J. (2004) Internal friction controls the speed of protein folding from a compact configuration, *Biochemistry 43*, 12532−12538.
40. Ptitsyn, O. B. (1995) Molten globule and protein folding, *Adv. Protein Chem. 47*, 83−229.
41. Rao, D. K., Kumar, R., Yadaiah, M., and Bhuyan, A. K. (2006) The alkali molten globule state of ferrocytochrome c: Extraordinary stability, persistent structure, and constrained overall dynamics, *Biochemistry 45*, 3412−3420.
42. Hagen, S. J., Carswell, C. W., and Sjolander, E. W. (2001) Rate of intrachain contact formation in an unfolded protein: Temperature and denaturant effects, *J. Mol. Biol. 305*, 1161−1171.
43. Hagen, S. J., Latypov, R. F., Dolgikh, D. A., and Roder, H. (2002) Rapid intrachain binding of histidine-26 and histidine-33 to heme in unfolded ferrocytochrome *c*, *Biochemistry 41*, 1372−1380.
44. Kumar, R., Prabhu, N. P., and Bhuyan, A. K. (2005) Ultrafast events in the folding of ferrocytochrome *c*, *Biochemistry 44*, 9359−9367.
45. Ballew, R. M., Sabelko, J., and Gruebele, M. (1996) Observation of distinct nanosecond and microsecond protein folding events, *Nat. Struct. Biol. 3*, 923−926.
46. Hammes, G. G., and Roberts, P. B. (1969) Dynamics of the helix-coil transition in poly-L-ornithine, *J. Am. Chem. Soc. 91*, 1812−1816.
47. Thompson, P. A., Eaton, W. A., and Hofrichter, J. (1997) Laser temperature jump study of the helix-coil kinetics of an alanine peptide interpreted with a 'kinetic zipper' model, *Biochemistry 36*, 9200−9210.
48. Lednev, I. K., Karnoup, A. S., Sparrow, M. C., and Asher, S. A. (1999) α-Helix peptide folding and unfolding activation barriers: A nanosecond UV resonance Raman study, *J. Am. Chem. Soc. 121*, 8074−8086.
49. Eaton, W. A., Muñoz, V., Thompson, P. A., Henry, E. R., and Hofrichter, J. (1998) Kinetics and dynamics of loops, α-helices, β-hairpins, and fast-folding proteins, *Acc. Chem. Res. 31*, 745−753.
50. Murray, L. P., Hofrichter, J., Henry, E. R., and Eaton, W. A. (1988) Time-resolved optical spectroscopy and structural dynamics following photodissociation of carbonmonoxyhemoglobin, *Biophys. Chem. 29*, 63−76.
51. Schindler, T., Herrler, M., Marahiel, M. A., and Schmid, F. X. (1995) Extremely rapid protein folding in the absence of intermediates, *Nat. Struct. Biol. 2*, 663−673.
52. Jackson, S. E., and Fersht, A. R. (1991) Folding of chymotrypsin inhibitor-2. 1. Evidence for a two-state transition, *Biochemistry 30*, 10428−10435.
53. Kaya, H., and Chan, H. S. (2002) Towards a consistent modeling of protein thermodynamics and kinetic cooperativity: How applicable is the transition state picture to folding and unfolding, *J. Mol. Biol. 315*, 899−909.
54. Kaya, H., and Chan, H. S. (2002) Solvation effects and driving forces for protein thermodynamic and kinetic cooperativity: How adequate is native-centric topological modeling, *J. Mol. Biol. 326*, 911−931.
55. Chan, H. S., Shimizu, S., and Kaya, H. (2004) Cooperativity principles in protein folding, *Methods Enzymol. 380*, 350−379.
56. Khorasanizadeh, S., Peters, I. D., and Roder, H. (1996) Evidence for a three-state model of protein folding from kinetic analysis of ubiquitin variants with alterd core residues, *Nat. Struct. Biol. 3*, 193−205.
57. Otzen, D. E., Kristensen, O., Proctor, M., and Oliveberg, M. (1999) Structural changes in the transition state of protein folding: Alternative interpretations of curved chevron plots, *Biochemistry 38*, 6499−6511.
58. Ikeguchi, M., Kuwajima, K., Mitani, M., and Sugai, S. (1986) Evidence for identity between the equilibrium unfolding intermediate and a transient folding intermediate: A comparative study of the folding reactions of α-lactalbumin and lysozyme, *Biochemistry 25*, 6965−6972.
59. Eaton, W. A., and Hofrichter, J. (1981) Polarized absorption and linear dichroism spectroscopy of hemoglobin, *Methods Enzymol. 76*, 175−261.
60. Greene, B. I., Hochstrasser, R. M., Weisman, R. B., and Eaton, W. A. (1978) Spectroscopic studies of oxy- and carbonmonoxy-hemoglobin after pulsed optical excitation, *Proc. Natl. Acad. Sci. U.S.A. 75*, 5255−5259.
61. Chernoff, D. A., Hochstrasser, R. M., and Steele, A. W. (1980) Geminate recombination of O_2 and hemoglobin, *Proc. Natl. Acad. Sci. U.S.A. 77*, 5606−5610.
62. Terner, J., Stong, J. D., Spiro, T. G., Nagumo, M., Nicol, M., and El-Sayed, M. A. (1981) Picosecond resonance Raman spectroscopic evidence for excited-state spin conversion in carbonmonoxy-hemoglobin photolysis, *Proc. Natl. Acad. Sci. U.S.A. 78*, 1313−1317.
63. Terner, J., Spiro, T. G., Nagumo, M., Nicol, M. F., and El-Sayed, M. A. (1980) Resonance Raman spectroscopy in the picosecond time scale: The carbonmonoxy photointermdeiate, *J. Am. Chem. Soc. 102*, 3238−3239.
64. Findsen, E. W., Friedman, J. M., Ondrias, M. R., and Simon, S. R. (1985) Picosecond time-resolved resonance Raman studies of hemoglobin: Implications for reactivity, *Science 229*, 661−665.
65. Krieger, F., Fierz, B., Bieri, O., Drewello, M., and Kiefhaber, T. (2003) Dynamics of unfolded polypeptide chains as model for the earliest steps in protein folding, *J. Mol. Biol. 332*, 265−274.
66. von Hippel, P. H., and Wong, K.-Y. (1965) On the conformational stability of globular proteins. The effect of various electrolytes and nonelectrolytes on the thermal ribonuclease transition, *J. Biol. Chem. 240*, 3909−3923.
67. Portman, J. J., Takada, S., and Wolynes, P. G. (2001) Microscopic theory of protein folding rates. II. Local reaction coordinate and chain dynamics, *J. Chem. Phys. 114*, 5082−5096.

BI062193U